Quantum interface between light and atomic ensembles

Klemens Hammerer

Institute for Theoretical Physics, University of Innsbruck, and Institute for Quantum Optics and Quantum Information, Austrian Academy of Science, Technikerstrasse 25, 6020 Innsbruck, Austria

Anders S. Sørensen and Eugene S. Polzik

Niels Bohr Institute, Copenhagen University, Blegdamsvej 17, Copenhagen 2100, Denmark

(Published 5 April 2010)

During the past decade the interaction of light with multiatom ensembles has attracted much attention as a basic building block for quantum information processing and quantum state engineering. The field started with the realization that *optically thick* free space ensembles can be efficiently interfaced with quantum optical fields. By now the atomic ensemble-light interfaces have become a powerful alternative to the cavity-enhanced interaction of light with single atoms. Various mechanisms used for the quantum interface are discussed, including quantum nondemolition or Faraday interaction, quantum measurement and feedback, Raman interaction, photon echo, and electromagnetically induced transparency. This review provides a common theoretical frame for these processes, describes basic experimental techniques and media used for quantum interfaces, and reviews several key experiments on quantum memory for light, quantum entanglement between atomic ensembles and light, and quantum teleportation with atomic ensembles. The two types of quantum measurements which are most important for the interface are discussed: homodyne detection and photon counting. This review concludes with an outlook on the future of atomic ensembles as an enabling technology in quantum information processing.

DOI: 10.1103/RevModPhys.82.1041 PACS number(s): 03.67.Ac, 03.67.Hk, 42.50.Ct

CONTENTS

 ©2010 The American Physical Society

I. INTRODUCTION

A. History and motivation

Quantum features of atom-light interaction have been among the central issues in physics since the early days of quantum mechanics. Starting in the 1960s with the development of quantum optics—the field where second quantization of light is central—quantum electrodynamics (QED) became part of optical and atomic physics. For decades after that the inherently quantum features of atom-light interaction have been studied primarily within the framework of cavity QED where light can be efficiently coupled to a few atoms or even to a single atom. Despite the spectacular progress achieved in this direction, the complexity and technical challenges associated with an atom strongly coupled to a high-finesse cavity were calling for alternative approaches.

A new approach to the matter-light quantum interface came with the realization of the fact that a large collection of atoms, an atomic ensemble, can be efficiently coupled to quantum light if a collective superposition state of many atoms can be utilized for the coupling. The simplest example of such coupling is shown in Fig. 1(a). A collection of atoms in the ground state is illuminated with two modes of light a_+ and a_-. As shown by Kuzmich *et al.* (1997), if the modes possess quantum correlations (entanglement) and light is absorbed by the atomic ensemble, the quantum correlations can be mapped on the collective superposition of the two final states of the atoms. The strong coupling condition in this case amounts to the requirement of large resonant optical depth d of the atomic ensemble. It later turned out that the requirement $d \gg 1$ is the most significant requirement for all types of the quantum interface between atomic ensembles and light known up to now. The experiment demonstrating that a quantum feature of radiation (squeezing) can be transferred onto atoms via the process shown in Fig. 1(a) was performed by Hald *et al.* (1999). This approach has been further developed using photon echo ideas (Moiseev, 2003).

A natural next step was to utilize long-lived atomic ground states for the interface via a Raman interaction in a Λ scheme, as proposed by Kozhekin *et al.* (2000) for storage of squeezed states. The Raman process together with electromagnetically induced transparency (EIT) (Boller *et al.*, 1991; Lukin, 2003; Fleischhauer *et al.*, 2005)

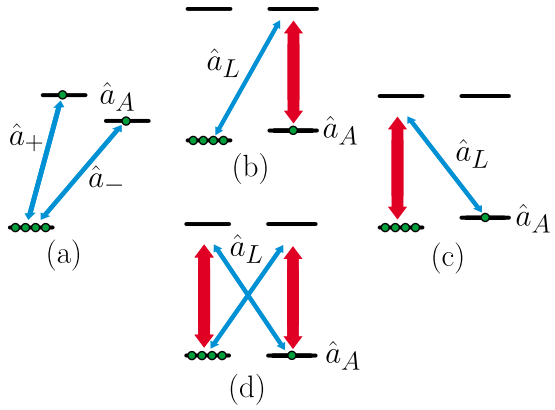

FIG. 1. (Color online) Elementary level schemes: (a) A simple absorption scheme with the quantum fields $a_\pm$ mapped onto the atomic states a_A. (b) Beam-splitter-type interaction—basis for Raman and EIT memory schemes. (c) Parametric-gain-type interaction—basis for entanglement schemes. (d) Quantum nondemolition (or Faraday) interaction—basis for entanglement, memory, and teleportation schemes.

have soon become important routines for quantum interfaces. After Hau *et al.* (1999) demonstrated that EIT allows for very slow propagation of light through an atomic ensemble, it was quickly realized that reducing the group velocity to zero would enable an atomic memory for light (Fleischhauer and Lukin, 2000; Lukin *et al.*, 2000) and the first experimental demonstrations of this for classical pulses have been presented by Liu *et al.* (2001) and Phillips *et al.* (2001).

Quantum nondemolition (QND) measurement (Braginsky and Khalili, 1996) based on light-matter interaction has emerged as a powerful tool for quantum state engineering, first in the cavity QED setting and then in the atomic ensemble context as an efficient method for generation of spin squeezing (Kuzmich *et al.*, 1998). Shortly thereafter QND interaction with atomic ensembles has become one of the main instruments for the quantum interface.

The process shown in Fig. 1(a) is a rudimentary example of one of the main routines for atoms-light quantum interface: the quantum state transfer from light to atoms, or the quantum memory for light. The ability for mapping, storing, and retrieving quantum states of light—the natural long-distance carrier of information—onto the material storage medium is one of the major enabling procedures in quantum information processing. In this review we cover various approaches to the quantum memory, including the Raman process, EIT, photon echo, and the QND measurement and feedback. We review methods which provide a long-term quantum memory with the fidelity better than any classical procedure can achieve, as well as approaches which allow one to preserve entanglement in the process of storage and retrieval. The interface can be implemented either via interaction only or by the teleportationlike procedure involving generation of entanglement, Bell measurement on light, and quantum feedback onto atoms. In this article we discuss both approaches.

The second most important routine for the quantum interface is generation of entanglement between light and atoms. The light-atom entanglement in turn enables generation of entanglement between remote atomic ensembles, as well as atomic teleportation and entanglement swapping protocols. Furthermore the light-atom entanglement also allows for quantum memory through light-atom teleportation.

The quantum interface can be formulated either in the Schrödinger or in the Heisenberg picture. For example, the transformation of a quantum state of light into a quantum state of atoms in the Schrödinger picture $\hat{U}|\Psi_L 0_A\rangle \rightarrow |0_L \Psi_A\rangle$ corresponds to the operator transformation $\hat{U}^\dagger \hat{a}_A \hat{U} = a_L$ in the Heisenberg picture. The two pictures are equivalent, and we mostly use the Heisenberg picture throughout this review.

In this review we discuss protocols based on both homodyning of light and photon counting. The most dramatic difference between the two approaches is that a single homodyne measurement does not necessarily distinguish between a vacuum and a nonvacuum state, whereas an ideal photon counter does. This makes ideal photon counting insensitive to losses if the protocol is conditioned on a click of the detector. This feature is important as an elementary purification mechanism, but it also makes protocols which use it probabilistic. On the other hand, homodyning always yields a measurement result and is thus deterministic. Another difference between the two measurements is that photon counting yields a discrete variable result, whereas homodyning yields a continuous variable outcome. From a practical perspective detectors used for homodyning are almost perfect in their quantum efficiency and dark current, whereas photon counters usually are less than perfect (although the progress in their development driven by quantum information applications is remarkable). The distinction between the two approaches is, however, not strict. For example, photon counting can be used as a deterministic characterization of a protocol if the absence of a photon count (the vacuum contribution) is included in the analysis. Continuous variable outcome of a homodyne measurement can be "digitized" if suitable superposition states are employed. Various figures of merit are used for characterization of quantum interfaces, as discussed in Sec. V.A.

Probabilistic protocols based on generation of a single collective atomic excitation of an atomic ensemble following detection of a photon emitted by the ensemble have been actively developed in recent years (Kuzmich *et al.*, 2003; van der Wal *et al.*, 2003; Chou *et al.*, 2004, 2007; Matsukevich and Kuzmich, 2004; Chen *et al.*, 2006; Matsukevich *et al.*, 2006; Chaneliere *et al.*, 2007). This approach has been motivated by a proposal for a quantum repeater with atomic ensembles (Duan *et al.*, 2001). The research on quantum repeaters deserves a separate review paper and will only be briefly discussed here.

The requirements for the atomic memory may differ depending on the particular application. A distributed quantum computer network requires the complete set of memory capabilities: mapping of the light state onto memory, storage and operations on the memory state, and retrieval of the memory state back onto light for further processing. Applications in quantum communications, which involve local operations on stored states and classical communications between partners, often only require a measurement of the memory state in a specific basis, i.e., no full retrieval of the quantum state of the memory back onto light is necessary. Yet other proposals, such as linear optics quantum computing which uses offline entanglement resources, require only the retrieval of the atomic state onto light but it has to be rather efficient and with high fidelity (Menicucci *et al.*, 2006).

B. Elementary level schemes

Naturally, the atomic levels used for storage of a quantum state should be long lived, with particular requirements for the lifetime depending on applications. For example, for a memory used in a long-distance communication protocol, the memory lifetime usually should be longer than the time required for classical communication over this distance. For a few hundred kilometers this time is of the order of 10^{-3} sec. Short-distance applications may require shorter memory time but one should keep in mind that a low-loss fiber loop can be a strong competitor for a short term atomic quantum memory for light (Pittman and Franson, 2002). A 5 km fiber loop can, in principle, store a photon for 25 μsec with only 20% losses at the telecom wavelength. However, even for short storage times atoms have the important advantage of being able to provide on-demand retrieval and may in addition be advantageous if a nontrivial operation has to be performed on the stored quantum states.

The optical atomic transitions used for coupling light to the storage ground states of the atoms should be preferably strong in order to have a large bandwidth of the memory. Therefore strong dipole allowed transitions are typically used for the interaction, but some experiments, in particular in solid-state systems, compensate for weak optical transition by having a large number of atoms. Figures 1(b)–1(d) present the atomic level schemes typically used for the interface. Figures 1(b) and 1(c) present the Λ scheme used in the Raman and EIT memory schemes as well for entanglement generation. Figure 1(d) shows the so-called Faraday interaction which is sometimes also referred to as QND interaction for reasons discussed below.

In Fig. 1(b) the atoms are prepared in the ground state coupled to the quantum field $\hat{a}_L$ (thin line), with the bold line showing a strong coupling field. With a large detuning from the optically excited states, the interaction Hamiltonian for such a system, after adiabatic elimination of the excited state, can be cast in the form $\hat{H} = \chi_{BS} \hat{a}_L \hat{a}_A^\dagger + \text{H.c.}$ In quantum optics this Hamiltonian is often referred to as the beam-splitter Hamiltonian Leonhardt (2003). The interface mixes the input atom and

light states as a "beam splitter" and the "reflection coefficient" of unity corresponds to a perfect state swapping between light and atoms. The detailed derivation of this Hamiltonian for the light-atom interaction is given later, but the intuitive picture is obvious—if a single photonic excitation is removed (annihilated) from the field $\hat{a}_L$, a single collective atomic excitation $\hat{a}_A^\dagger$ is created. If this process is efficient, it works as the Raman-type quantum memory for light introduced for atomic ensembles by Kozhekin *et al.* (2000) and described in Sec. V.D. The same level scheme can be used for the EIT-based memory where the fields are resonant with the optical transition (Fleischhauer and Lukin, 2000; Lukin *et al.*, 2000), although in this limit it is essential to account for spontaneous emission and the effective beam-splitter Hamiltonian is less applicable (see Secs. II). EIT-based quantum memory experiments are also described in Sec. V.D.

Figure 1(c) shows the same atomic structure but now the fields are arranged in a way which can be used for the atom-light entangling interaction with the Hamiltonian $\hat{H}=\chi_P\hat{a}_L\hat{a}_A+\text{H.c.}$ The Hamiltonian is formally identical to the parametric-gain interaction Hamiltonian Leonhardt (2003), which has been a workhorse for studies of entangled and nonclassical states of light since the 1960s. The important new feature in the present case is that two entangled operators belong to a light mode and an atomic mode, respectively. This kind of entanglement has been used for unconditional light-to-atom teleportation experiment described in Sec. VI and its probabilistic version discussed in Sec. IV.C is the basis for the repeater protocol of Duan *et al.* (2001).

To complete the discussion of elementary level schemes used for basic interface routines, we consider the four-level scheme shown in Fig. 1(d). The Hamiltonian for this interaction can be obtained by combining the beam-splitter Hamiltonian [Fig. 1(b)] and the parametric entangling Hamiltonian with equal coupling constants, $\chi_{\text{BS}}=\chi_P$ [Fig. 1(c)] provided that the two quantum fields (thin lines) belong to the same mode: $\hat{H}\sim\chi\hat{P}_L\hat{P}_A$, where the canonical operators for light and atoms which obey the canonical commutation relation $[\hat{X},\hat{P}]=i$ have been introduced. This interaction allows for a QND measurement of the atomic operator P_A by means of detection of the light operator X_L. As discussed in Secs. IV.A and IV.B, the QND measurement projects atoms into an entangled state. The same interaction is often called the quantum Faraday interaction because in the case of magnetic levels it leads to polarization rotation of light. The QND-Faraday interaction of atoms and light followed by the measurement on the light and the feedback conditioned on the measurement applied onto atoms was used to demonstrate quantum memory for light as described in Sec. V. As shown theoretically and experimentally by Wasilewski *et al.* (2009), a more general combination of the beam-splitter Hamiltonian and the parametric entangling Hamiltonian with *unequal* weights performs both those operations simultaneously.

To summarize, the basic features of most quantum interface protocols to date can be understood by analyzing simple three- or four-level atoms. Besides the condition $d\gg1$ mentioned above, another unifying feature for all approaches which use multiatom ensembles is the possibility to initialize the ensemble, e.g., by optical pumping, in one of the ground substates. Choosing suitable atomic transitions, and polarizations and frequencies of the quantum and classical coupling fields, one can choose between various routines, such as memory, entanglement, and Faraday interaction, as shown in Fig. 1. In the following theoretical description we provide a unified approach to all these types of interfaces.

In the literature the interface protocols are often divided into those for states of continuous variables and those for discrete variables, or qubits. The former are usually based on the Faraday interaction and are described most conveniently in terms of X,P operators measured by homodyne detection, while the latter are commonly based on the Λ-type interactions in combination with counting of single photons and are most easily described in terms of $a,a^\dagger$ representations. One of the goals of this review is to show that continuous and discrete variable protocols can in many aspects be treated on equal footing, and that the choice of variables is defined by the convenience of description and the type of measurements involved, e.g., in the ideal limit a memory protocol which is most conveniently described by X,P operators could be used to store a single photon with perfect fidelity. On the other hand, the state of the atomic memory in protocols which use $a,a^\dagger$ representation can be conveniently analyzed by atomic tomography in the X,P basis (Sherson, Julsgaard, and Polzik, 2006; Fernholz *et al.*, 2008) [for a review on quantum tomography see Lvovsky and Raymer (2009)]. The type of errors which appear under nonideal conditions is of course different for different protocols, but irrespectively of the specific protocol the condition $d\gg1$ leads to fewer errors. Which protocol to use, for a given optical density, therefore depends on the specific application and a detailed analysis of the imperfections should be made in each situation.

This review provides a coherent picture of the work on the quantum interface between light and atomic ensembles using various approaches, atomic media, and protocols. It includes the discussion of major experimental achievements to date and concludes with the analysis of the current limitations and future goals.

II. THEORETICAL BACKGROUND

A. Description of light and atoms

1. Harmonic oscillators

Throughout this review we deal with single modes of the electromagnetic field and collective spin excitations of atomic ensembles, which can be well approximated by harmonic oscillators with canonical position and momentum operators X_n and P_n, where n refers to the

mode number. In most cases we shall omit the hats on the operators in what follows. These canonical operators are dimensionless with the standard commutator

$$[X_n, P_m] = i\delta_{mn}. \tag{1}$$

The harmonic oscillators can also be described in terms of the annihilation operators

$$a_n = (1/\sqrt{2})(X_n + iP_n), \tag{2}$$

which have commutation relation $[a_n, a_m^\dagger] = \delta_{nm}$.

Instead of labeling by a discrete number n the modes can be denoted by a continuous parameter, e.g., the position vector $\vec{r}$ with the commutation relations

$$[X(\vec{r}), P(\vec{r}')] = i\delta(\vec{r} - \vec{r}'), \tag{3}$$

$$[a(\vec{r}), a^\dagger(\vec{r}')] = \delta(\vec{r} - \vec{r}'). \tag{4}$$

In some cases we deal with the storage or transfer of a set of n modes. Such discrete modes can be constructed from the continuous modes by introducing a complete orthogonal set of mode functions $\{u_m(\vec{r})\}$ satisfying

$$\int d\vec{r}\, u_m^*(\vec{r}) u_n(\vec{r}) = \delta_{mn}, \tag{5}$$

$$\sum_m u_m^*(\vec{r}) u_m(\vec{r}') = \delta(\vec{r} - \vec{r}'). \tag{6}$$

If we now define the discrete annihilation operators

$$a_m = \int d\vec{r}\, u_m^*(\vec{r}) a(\vec{r}), \tag{7}$$

they have the appropriate commutator $[a_n, a_m^\dagger] = \delta_{mn}$.

2. Light

Light beams traveling in the z direction can be described (in c.g.s. units) in the paraxial approximation by a quantized electric field

$$\vec{E}(\vec{r}) = \sum_{m,\sigma,k} \sqrt{\frac{2\pi\omega_0}{l}} \vec{e}_\sigma u_m(\vec{r}_\perp; z) e^{ikz} a_{L,m\sigma k} + \text{H.c.} \tag{8}$$

Throughout this review we set $\hbar = 1$. l is the length of the quantization volume, and the sum is over the polarization σ and the transverse mode number m, as well as the longitudinal wave vector k. The mode functions $u_m(\vec{r}_\perp; z)$, where $\vec{r}_\perp = (x, y)$ describes the transverse profile of the beam, form a complete orthogonal set in the plane transverse to the propagation direction

$$\int d^2\vec{r}_\perp u_m^*(\vec{r}_\perp; z) u_{m'}(\vec{r}_\perp; z) = \delta_{m,m'}. \tag{9}$$

In the above we have assumed that the fields belong to a narrow frequency band such that for all modes the frequency under the square root is ω_0. Second, the field should in general be expanded into a complete set of modes $\vec{u}_k(\vec{r})$, but in the paraxial approximation we have assumed that we can factor out a polarization vector $\vec{e}_\sigma$ as well as ignore the k dependence of the transverse mode function $u_m(\vec{r}_\perp; z)$.

Instead of using longitudinal wave vectors we use a slowly varying position space annihilation operator defined by

$$a_{L,m\sigma}(z) = \sqrt{\frac{c}{l}} \sum_k e^{i(k-k_0)z + i\omega_0 t} a_{L,m\sigma k}, \tag{10}$$

where c is the speed of light and $k_0 = \omega_0/c$. In the continuum limit $l \to \infty$ this operator has the commutation relation

$$[a_{L,m\sigma}(z), a_{L,m'\sigma'}^\dagger(z')] = c\,\delta_{m,m'}\delta_{\sigma,\sigma'}\delta(z - z'). \tag{11}$$

Note that we have chosen here a normalization with c appearing in the commutator. With this normalization (i) the traveling fields $a_{L,m\sigma}(z,t) = a_{L,m\sigma}(z - ct)$ considered below have the commutation relation appropriate for operators, which are a function of t ($[a_{L,m\sigma}(z,t), a_{L,m'\sigma'}^\dagger(z,t')] = \delta_{m,m'}\delta_{\sigma,\sigma'}\delta(t - t')$), and (ii) with this normalization $a_{L,m\sigma}(z)^\dagger a_{L,m\sigma}(z)$ describes the flux of photons in mode m with polarization σ at position z.

In terms of this operator the electric field is given by

$$\vec{E}(\vec{r}) = \sqrt{\frac{2\pi\omega_0}{c}} \sum_{m,\sigma} \vec{e}_\sigma u_m(\vec{r}_\perp; z) e^{i(k_0 z - \omega_0 t)} a_{L,m\sigma}(z) + \text{H.c.} \tag{12}$$

We mainly deal with a single transverse field mode and a single polarization, so that the sum in the expression above can be omitted. For an introductory textbook to continuous mode quantum optics see Loudon (2004).

3. Atoms

We first discuss the theory for atoms with two stable ground states $|0\rangle$ and $|1\rangle$. In Sec. II.D we show how one can in many cases reduce the description for multilevel atoms to two state atoms. The two ground states are conveniently described in terms of angular momentum operators. We use here the x as the quantization axis for consistency with Julsgaard *et al.* (2001), Julsgaard, Sherson, Rensen, and Polzik (2004), and Sherson, Krauter, *et al.* (2006). The angular momentum operators describing the mth atom are

$$j_{x,m} = \tfrac{1}{2}(|0\rangle_m\langle 0| - |1\rangle_m\langle 1|), \tag{13}$$

$$j_{+,m} = j_{y,m} + ij_{z,m} = |0\rangle_m\langle 1|, \tag{14}$$

where $j_{+,m}$ is the operator which raises $j_{x,m}$ by unity.

We are interested here in collective variables for an ensemble containing many atoms. In the simplest case such collective operators are given by the total angular momentum operators $J_l = \Sigma_m j_{l,m}$ (with $l = x, y, z$), which fulfill the standard angular momentum commutation relation

$$[J_y, J_z] = iJ_x. \tag{15}$$

The collective state with all atoms in state $|0\rangle$, then corresponds to the state $|J = N_A/2, M_x = N_A/2\rangle$ with total angular momentum quantum number $J = N_A/2$ and an ei-

genvalue of J_x equal to $N_A/2$, where N_A is the number of atoms. If we consider a large number of atoms and only weakly perturb the system (only change the state of a few atoms), we can approximate the J_x operator by its expectation value $J_x \approx \langle J_x \rangle$. For those who feel uneasy about replacing an operator by its mean value, a more rigorous formulation can be made using the so-called Holstein-Primakoff transformation (Holstein and Primakoff, 1940; Kittel, 1987) or in terms of a Wigner group contraction (Arecchi *et al.*, 1972). Without loss of generality we can assume the expectation value $\langle J_x \rangle$ to be positive and we can then introduce new canonical position and momentum operators by

$$X_A = J_y / \sqrt{\langle J_x \rangle}, \quad P_A = J_z / \sqrt{\langle J_x \rangle}. \tag{16}$$

From Eq. (15) we immediately see that these operators satisfy the standard commutation relation for position and momentum (1). The collective annihilation operator is then

$$a_A = \frac{X_A + iP_A}{\sqrt{2}} = \frac{\sum_m j_{+,m}}{\sqrt{2\langle J_x \rangle}} = \frac{\sum_m |0\rangle_m \langle 1|}{\sqrt{2\langle J_x \rangle}}. \tag{17}$$

To get a feeling for this operator, consider the action of the creation operator $a_A^\dagger$. If we apply this operator to the initial state, where all atoms are in state $|0\rangle$, we create a symmetric superposition of one atom being flipped

$$a_A^\dagger |0,0,0,\ldots,0\rangle = \frac{1}{\sqrt{N_A}} \sum_m |0,0,\ldots,0,1_m,0,\ldots,0\rangle. \tag{18}$$

Here $|0,0,\ldots,0,1_m,0,\ldots,0\rangle$ is the state where all atoms except the mth atom are in state $|0\rangle$.

The collective operators introduced above are convenient for describing the entire ensemble. We, however, also be dealing with situations where we need to consider collective operators which do not involve all atoms with an equal weight (Kuzmich and Kennedy, 2004). In the literature such situations are often described by dividing the ensemble into small boxes and constructing collective operators for each box (Raymer and Mostowski, 1981; Fleischhauer and Richter, 1995).

Here we use a slightly different formalism (Sørensen and Sørensen, 2008). For a collection of atoms at positions $\vec{r}_1, \vec{r}_2, \ldots, \vec{r}_{N_A}$ we define the density distribution function

$$n(\vec{r}) = \sum_m \delta(\vec{r} - \vec{r}_m). \tag{19}$$

In condensed matter physics this density distribution function may be used to describe scattering from structures (Chaikin and Lubensky, 1995): averaging this density distribution over the random positions of the atoms gives the average number density of the atoms $\bar{n}(\vec{r}) = \langle n(\vec{r}) \rangle$, whereas higher-order correlations like $\langle n(\vec{r}) n(\vec{r}) \rangle$ describe the correlation responsible for Bragg scattering [in this context the classical function (19) is sometimes referred to as the density operator (Chaikin and Lubensky, 1995), but to avoid confusion with quantum mechanical operators we avoid this terminology]. Similarly we may introduce continuous atomic spin operators by

$$j_k(\vec{r}) = \sum_m \delta(\vec{r} - \vec{r}_m) j_{k,m}, \tag{20}$$

where $k = x, y, z, +, -$. A position dependent atomic annihilation operator can then be introduced by

$$a_A(\vec{r}) = j_+(\vec{r}) / \sqrt{2\langle j_x(\vec{r}) \rangle}, \tag{21}$$

where the average spin density $\langle j_x(\vec{r}) \rangle$, which we assume to be positive, is the quantum mechanical expectation value with respect to the internal state averaged over the random (classical) position of the atoms. The annihilation operator has the commutation relation

$$[a_A(\vec{r}), a_A^\dagger(\vec{r}')] = \delta(\vec{r} - \vec{r}') j_x(\vec{r}) / \langle j_x(\vec{r}) \rangle \approx \delta(\vec{r} - \vec{r}'), \tag{22}$$

where we in the last step have assumed that the fluctuations in the mean spin are much smaller than its average. We use this approximation throughout this article.

The operators (21) will be convenient for describing the spatial dependence of various operators. To relate them to single mode operators such as Eq. (17), we can introduce a normalized set of mode functions $u_n(\vec{r})$ fulfilling the orthogonality and completeness relations in Eq. (6).

We can then construct single mode operators as in Eq. (7). In particular, consider the normalized mode $u_{\mathrm{sym}}(\vec{r}) = \sqrt{\langle j_x(\vec{r}) \rangle / \langle J_x \rangle}$. If we use this mode to construct a collective operator, we see from Eq. (21) that this produces the symmetric operator defined in Eq. (17).

The $j_x(\vec{r})$ operator will appear in the Hamiltonians below; although sometimes it is more convenient to have expressions which only involve the annihilation operator $a_A(\vec{r})$. To find the equations of motion we need to take the commutator of $a_A(\vec{r})$ with the Hamiltonian, but from the commutation relation

$$\begin{aligned}[a_A(\vec{r}), j_x(\vec{r}')] &= -\frac{\delta(\vec{r} - \vec{r}')}{\sqrt{2\langle j_x(\vec{r}) \rangle}} \sum_m \delta(\vec{r} - \vec{r}_m) j_{+,m} \\ &= -\delta(\vec{r} - \vec{r}') a_A(\vec{r}),\end{aligned} \tag{23}$$

we see that we get the same result if we make the replacement

$$j_x(\vec{r}) \to n/2 - a_A^\dagger(\vec{r}) a_A(\vec{r}) \tag{24}$$

and use the commutation relation in Eq. (22) (the first term is included to ensure that j_x has the right value in the vacuum state of a_A, where all atoms are in state $|0\rangle$). This replacement holds even as an exact operator identity in the framework of the Holstein-Primakoff transformation (Holstein and Primakoff, 1940).

B. Interaction of light with model atoms

We consider atoms with stable ground states denoted by $|g_m\rangle$ and excited states denoted by $|e_m\rangle$. The Hamiltonian $H = H_L + H_A + H_{\mathrm{int}}$ describing this system is the sum of the field energy H_L, the atomic energy H_A, and

the interaction Hamiltonian $H_{\rm int}$. We first consider the atomic and interaction parts of the Hamiltonian and derive an effective interaction Hamiltonian involving only the ground states of the atoms. We then include the Hamiltonian H_L responsible for the propagation of the light field, and derive coupled equations of motion for the light and atomic operators.

1. Interaction with a single atom

To describe the atomic part and the interaction let us first consider only a single atom at location $\vec{r}$. In a rotating frame with respect to the laser frequency the atomic Hamiltonian is given by $H_{\rm A}=\Sigma_m \Delta_m |e_m\rangle\langle e_m|$, where Δ_m is the detuning of the mth excited state with respect to the laser frequency.

In the dipole approximation the interaction between light and atoms is described by the Hamiltonian $H_{\rm int}=-\vec{E}\cdot\vec{D}$, where $\vec{D}$ is the electric dipole operator for the atom. In Appendix A we describe the adiabatic elimination of the excited state and derive an effective ground-state Hamiltonian

$$H'_{\rm int}=\sum_{m,m'} V_{m',m}(\vec{r})|g_{m'}\rangle\langle g_m|, \tag{25}$$

where the coupling matrix $V_{m',m}$ is given by

$$V_{m',m}(\vec{r})=-\sum_{m''}\frac{[\vec{E}^{(-)}(\vec{r})\cdot\vec{D}^{(+)}_{m',m''}][\vec{D}^{(-)}_{m'',m}\cdot\vec{E}^{(+)}(\vec{r})]}{\Delta_{m''}}. \tag{26}$$

Here superscripts $(+)$ and $(-)$ refer to the positive and negative frequency components of the electric field and dipole operators (the positive frequency part is the part of the operators which removes an excitation, e.g., $\vec{D}^{(+)}_{m',m}=\langle g_{m'}|\vec{D}|e_m\rangle$) (Loudon, 2004). (Note that $H'_{\rm int}$ is not the same as $H_{\rm int}=-\vec{E}\cdot\vec{D}$, since $H'_{\rm int}$ contains a contribution from $H_{\rm A}$ as discussed in Appendix A.)

2. Interaction with many atoms

Now consider the situation where we have many atoms. We are mainly interested in describing the interaction of a weak quantum field with an ensemble driven by a strong classical field. In this section we describe only the interaction between the atoms and the forward propagating quantum fields and ignore the spontaneous emission due the coupling to all other electromagnetic modes. We include the decoherence caused by spontaneous emission in Sec. II.C. To simplify the theory we derive only equations of motion for the initially fully polarized ensemble $\langle J_x(\vec{r},t)\rangle \approx n(\vec{r})/2$ [we ignore the difference between the density distribution $n(\vec{r})$ and its average value $\bar{n}(\vec{r})$]. The atomic operators defined in Eq. (21) are, however, well-behaved annihilation operators even for an ensemble which is not fully polarized provided that the fluctuations of the mean spin are small.

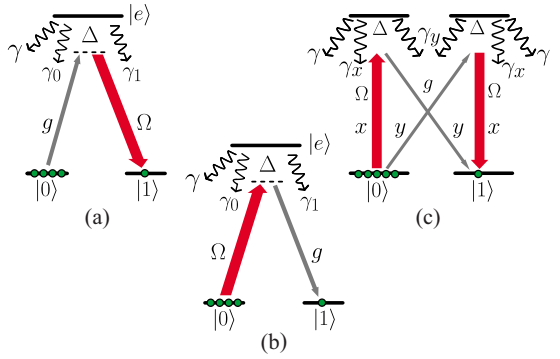

FIG. 2. (Color online) Λ configuration with dominant population of level $|0\rangle$: (a) Beam-splitter interaction with the quantum field of the single photon Rabi frequency g on the $|0\rangle\rightarrow|e\rangle$ and the strong light with the Rabi frequency Ω on the $|e\rangle\rightarrow|1\rangle$ transition. The two fields are in two-photon resonance with a detuning Δ from the excited state $|e\rangle$. Decay due to spontaneous emission goes back to one of the ground states at the rates $\gamma_{0(1)}$ or to other levels (not shown) summing up to a total rate γ. (b) Parametric-gain interaction. (c) Faraday interaction: Atoms are polarized to $|0\rangle$, the strong field is linearly polarized along x and drives the up transitions with the Rabi frequency Ω, and the quantum field in y polarization couples to the cross transitions with the single photon Rabi frequency g. The fields are in two photon resonance with a detuning Δ from the excited states. Decay due to spontaneous emission goes back to one of the ground states at the rates $\gamma_{x(y)}$ or to other levels (not shown) at the rate γ.

This will, for instance, be the case if an ensemble containing many atoms is prepared with imperfect optical pumping.

The interaction Hamiltonian can be obtained by summing the single-atom Hamiltonian (25) over all atoms. This sum may be replaced by an integral by introducing the continuous atomic annihilation operator defined in Eq. (21):

$$H=\int d^3\vec{r}\{[\sqrt{n(\vec{r})}a_A(\vec{r})V_{01}(\vec{r})+\text{H.c.}]+n(\vec{r})V_{00} + a_A^\dagger(\vec{r})a_A(\vec{r})(V_{11}-V_{00})\}, \tag{27}$$

where we have used the replacement (24) for the spin operator $j_x(\vec{r})$. In Appendix B we use this general Hamiltonian to derive Hamiltonians for the three different model systems in Figs. 1(b) and 1(b)–1(d).

For some situations the three-dimensional (3D) Hamiltonians derived in Appendix B can be reduced to one dimension. We perform this reduction for the beam-splitter interaction Hamiltonian in Eq. (B1), corresponding to the level configuration as shown in Fig. 2(a), where both classical and quantum field is traveling in the z direction. Now assume that the density is independent of the transverse coordinate $n(\vec{r})=n(z)$, and that the classical laser field is also constant transverse to the propagation direction. Since the mode functions $u_m(\vec{r}_\perp;z)$ form a complete set in the plane, we can expand the atomic operator $a_A(\vec{r})$ in the same set

$$a_A(\vec{r}) = \sum_m u_m(\vec{r}_\perp; z) a_{A,m}(z), \tag{28}$$

where

$$a_{A,m}(z) = \int d^2\vec{r}_\perp u_m^*(\vec{r}_\perp; z) a_A(\vec{r}). \tag{29}$$

These new operators will then have the appropriate commutation relation $[a_{A,m}(z), a^\dagger_{A,m'}(z')] = \delta(z-z')\delta_{m,m'}$. We insert this expansion into the Hamiltonian (B1), and then use the orthogonality relation (9) integrate over the transverse coordinate to obtain the one-dimensional (1D) Hamiltonian

$$H_{\rm BS} = \int dz \left[\frac{-|\Omega(z,t)|^2}{4\Delta} \sum_m a^\dagger_{A,m}(z) a_{A,m}(z) - \frac{|g(z)|^2}{\Delta} \sum_m a^\dagger_{L,m}(z) a_{L,m}(z) - \left(\frac{g^*(z)\Omega(z,t)}{2\Delta} \sum_m a^\dagger_{L,m}(z) a_{A,m}(z) + \text{H.c.} \right) \right], \tag{30}$$

where the the coupling constant $g(z)$ and slowly varying resonant Rabi frequency $\Omega(z,t)$ are given by

$$g(z) = \sqrt{2\pi\omega n(z)/c} D_0,$$

$$\Omega(z,t) = 2\vec{D}^{(-)}_{e,1} \cdot \langle \vec{E}^{(+)} \rangle \exp[-i(k_0 z - \omega_0 t)], \tag{31}$$

and the dipole element for the $|0\rangle$-$|e\rangle$ transition with the polarization of the quantum field $\vec{e}_{\rm q}$ is given by $D_0 = \vec{D}^{(-)}_{e,0} \cdot \vec{e}_{\rm q}$. The Hamiltonian above consists of three terms: the first line is the ac-Stark shift of the atomic ground state, the second is the index of refraction of the gas, and the last line, which is the most important for our discussion here, describes the exchange of excitations between atoms and light.

Note that each of the transverse modes of the light field in Eq. (30) talks to a single transverse mode of the atoms, which then couples back to the same transverse light mode. Since the dynamics is actually the same for all involved transverse modes, the atomic ensembles may in fact be used as a memory for for multiple transverse modes (Camacho *et al.*, 2007; Shuker *et al.*, 2008; Vasilyev *et al.*, 2008; Vudyasetu *et al.*, 2008). A similar description of the reduction from three to one dimension is also presented in André (2005).

We have used here the same central frequency ω_0 for both the quantum and classical fields, which is true for degenerate $|0\rangle$ and $|1\rangle$ states. If they are not degenerate, the energy difference between the two states can be accounted for by changing the frequency ω_0' of the classical field. In this case, however, an additional phase factor $\exp[i(k_0'-k_0)z]$ associated with the difference of the k vectors appears. We discuss the effect of this phase factor in Secs. II.G and VII.

For the parametric-gain Hamiltonian (B2) [cf. Fig. 2(b)], the reduction from three to one dimension can be achieved using the same procedure as above. The only difference is that instead of Eq. (29) we should now define the discrete atomic operator by

$$a_{A,m}(z) = \int d^2\vec{r}_\perp u_m(\vec{r}_\perp; z) a_A(\vec{r}). \tag{32}$$

Although the omission of the complex conjugate in this expression compared to Eq. (29) may seem of minor importance, it actually does play a role for several experiments as discussed in Sec. IV.C. Omitting the sum over multiple modes, we arrive at the Hamiltonian

$$H_G = \int dz \left[\frac{|\Omega(z,t)|^2}{4\Delta} a^\dagger_A(z) a_A(z) - \left(\frac{g^*(z)\Omega(z,t)}{2\Delta} a^\dagger_L(z) a^\dagger_A(z) + \text{H.c.} \right) \right]. \tag{33}$$

Finally we derive the one dimensional Hamiltonian for the QND (Faraday) interaction as shown in Fig. 2(c), where the x-polarized classical field couples the vertical transitions and a quantum field in y polarization couples diagonal transitions. From the figure we see that the Faraday interaction is essentially a combination of the beam-splitter and the parametric-gain interaction taken with the same coupling strength. In fact, as discussed in Appendix B the three-dimensional Hamiltonian for the Faraday interaction is simply $H_F = (H_{\rm BS} - H_G)/\sqrt{2}$. To reduce the problem to one dimension we introduce atomic operators similar to Eqs. (29) and (32), but now there is an ambiguity as to which of the two forms one should use. To avoid this ambiguity we assume that the mode functions $u_m(\vec{r}_\perp; z)$ are real [for Hermite-Gaussian modes (Milonni and Eberly, 1988), this condition can only be satisfied if the Fresnel number is much greater than unity $F = w_0^2/\lambda L \gg 1$, where w_0 is the beam waist, L is the length of the medium, and λ is the wavelength of light (Müller *et al.*, 2005; Sørensen and Sørensen, 2008)], and that $g^*(\vec{r})\Omega(\vec{r},t)$ has a constant phase, which we take to be zero. With these assumptions the Hamiltonian can be reduced to the simple form

$$H_F = -\int dz \frac{g^*(z)\Omega(z,t)}{\sqrt{2}\Delta} p_L(z) p_A(z). \tag{34}$$

We have omitted here the index of refraction of the gas for the reasons discussed in Appendix B.

We emphasize that the above 3D to 1D reduction provides a highly simplified treatment of the propagation of light through an atomic gas. In particular a more general treatment should include the spontaneous emission, the density-density correlation of the atoms, and the optically induced dipole-dipole interaction of the atoms. For the Faraday interaction a detailed study of the reduction from three to one dimension is presented by Sørensen and Sørensen (2008). In essence this study confirms the treatment presented here provided that the gas is ideal and that the mode functions $u_m(\vec{r}_\perp; z)$ are solutions to the propagation equation including the index of refraction. Little work has been done so far on the optically induced dipole interactions.

3. Equations of motion

The addition of the Hamiltonian for light H_L to the atomic part of the Hamiltonian H_A and the interaction $H_{\rm int}$ discussed above allows describing the propagation of light through the ensemble. As shown in Appendix C the equation of motion is derived by introducing a rescaled time $\tau=t-z/c$ and becomes a differential equation in space (z) instead of time t.

For the beam-splitter interaction, we find the equations of motion by calculating the commutator with $H_{\rm BS}$

$$\frac{\partial}{\partial z}a_L(z,t)=i\frac{|g(z)|^2}{\Delta}a_L(z,t)+i\frac{g^*(z)\Omega(t)}{2\Delta}a_A(z,t),$$
$$\frac{\partial}{\partial t}a_A(z,t)=i\frac{|\Omega(t)|^2}{4\Delta}a_A(z,t)+i\frac{g(z)\Omega^*(t)}{2\Delta}a_L(z,t). \tag{35}$$

The above equations can be solved analytically (Kozhekin *et al.*, 2000; Kupriyanov *et al.*, 2005; Gorshkov *et al.*, 2007b; Mishina *et al.*, 2007; Nunn *et al.*, 2007). We will defer a discussion of the solutions until Sec. II.C where the spontaneous emission is included.

Similarly we can find the equations of motion for the parametric gain:

$$\frac{\partial}{\partial z}a_L(z,t)=i\frac{g^*(z)\Omega(z,t)}{2\Delta}a_A^\dagger(z,t),$$
$$\frac{\partial}{\partial t}a_A(z,t)=-i\frac{|\Omega(z,t)|^2}{4\Delta}a_A(z,t)+i\frac{g^*(z)\Omega(z,t)}{2\Delta}a_L^\dagger(z,t). \tag{36}$$

Again these equations have an analytical solution (Carman *et al.*, 1970; Raymer and Mostowski, 1981).

For the Faraday interaction the equations of motion are much simpler when expressed in terms of x and p and read

$$\frac{\partial}{\partial z}x_L(z,t)=-\frac{g^*(z)\Omega(t)}{\sqrt{2}\Delta}p_A(z,t),$$
$$\frac{\partial}{\partial z}p_L(z,t)=0,$$
$$\frac{\partial}{\partial t}x_A(z,t)=-\frac{g^*(z)\Omega(t)}{\sqrt{2}\Delta}p_L(z,t),$$
$$\frac{\partial}{\partial t}p_A(z,t)=0. \tag{37}$$

Because the two momentum operators are conserved quantities these equations describe a QND interaction, where one can, make a measurement of the position operator x_L after the interaction and thereby obtain a QND measurement of the atomic momentum operator p_A, as will be further explained in Sec. IV.A.

The presence of the conserved quantities p_A and p_L makes it straightforward to solve the equations of motion. The only z dependence in the above expressions comes from the z dependence of the density $n(z)$. We can then define the symmetric operators by

$$X_A=\frac{\int dz\sqrt{n(z)}x_A(z)}{\sqrt{\int dzn(z)}},$$
$$P_A=\frac{\int dz\sqrt{n(z)}p_A(z)}{\sqrt{\int dzn(z)}}. \tag{38}$$

If the transverse mode function includes all atoms in the ensemble, these operators are equivalent to the symmetric operators defined in Eq. (16). Similar integrated operators for the light field are

$$X_L=\frac{\int dt\Omega(t)x_L(t)}{\sqrt{\int dt\Omega^2(t)}},$$
$$P_L=\frac{\int dt\Omega(t)p_L(t)}{\sqrt{\int dt\Omega^2(t)}}, \tag{39}$$

where we assume that Ω is real. Expressed in terms of these variable the equations of motions have the simple solutions

$$X_{L,\rm out}=X_{L,\rm in}+\kappa P_{A,\rm in},$$
$$P_{L,\rm out}=P_{L,\rm in},$$
$$X_{A,\rm out}=X_{A,\rm in}+\kappa P_{L,\rm in},$$
$$P_{A,\rm out}=P_{A,\rm in}. \tag{40}$$

The subscripts in and out mean input and output variables, e.g., $X_{L,\rm in}=X_L(z=0)$ and $X_{L,\rm out}=X_L(z=L)$ for light and $X_{A,\rm in}=X_A(t=0)$ and $X_{A,\rm out}=X_A(t=T)$ for atoms. The coupling constant κ is given by

$$\kappa^2=\int dt\frac{|\Omega(t)|^2}{2\Delta^2}\int dz|g(z)|^2$$
$$=\frac{\pi\omega D_-^2}{c}\int dt\frac{|\Omega(t)|^2}{\Delta^2}\int dzn(z). \tag{41}$$

In the last line we have inserted the expression for the coupling constant $g(z)$ Eq. (31) and have denoted the dipole matrix element by D_- to indicate that it is the coupling constant for σ-polarized light.

The coupling constant κ (and the generalization of it) plays an important role for characterizing the strength of the interaction regardless of the level scheme being used. Note that κ only depends on the total integrated

density. This property can be shown to also apply to the Λ schemes by a simple rescaling of the z coordinate (Gorshkov *et al.*, 2007b). We therefore for simplicity only consider a constant density below.

C. Theory including spontaneous emission

In Sec. II.B the spontaneous emission was omitted. In this section we give the theory including the spontaneous emission and discuss solutions to the equations.

Instead of repeating the calculations in Sec. II.B now with a nonzero decay, we note that if the spontaneous emission from each atom is independent, it can be accounted for by making the substitution

$$\Delta_m \to \Delta_m \pm i\gamma_m/2 \tag{42}$$

all calculations. The choice of the sign is discussed in Appendix D and the results are stated below. It is also important to note that the quantity $\langle j_x(\vec{r})\rangle$ used to define the operator $a_A(\vec{r},t)$ in Eq. (21) is not necessarily a constant. To ensure that the operator $a_A(\vec{r},t)$ has the right normalization we should always normalize by the time-dependent expectation value $\langle j_x(\vec{r},t)\rangle$. The time derivative of $\langle j_x(\vec{r},t)\rangle$ will introduce extra terms as discussed in Appendix D.

1. Beam-splitter interaction

As discussed in Appendix D for the beam-splitter interaction we should use the minus sign in the substitution (42), and the time derivative of $\langle j_x(\vec{r})\rangle$ can be neglected because the strong classical field talks to an almost empty level. For a constant atomic density the equations of motion then become

$$\begin{aligned}\frac{\partial}{\partial z}a_L(z,t) &= \frac{i|g|^2}{\Delta - i\frac{\gamma}{2}}a_L(z,t) + \frac{ig^*\Omega(t)}{2\Delta - i\gamma}a_A(z,t),\\ \frac{\partial}{\partial t}a_A(z,t) &= \frac{i|\Omega(t)|^2}{4\left(\Delta - i\frac{\gamma}{2}\right)}a_A(z,t) + \frac{ig\Omega^*(t)}{2\Delta - i\gamma}a_L(z,t),\end{aligned} \tag{43}$$

where γ is the total decay rate of the excited state and we have omitted the noise operators given in Eq. (D6). The admixed noise is vacuum in both equations of motion, and since the equations only couple annihilation operators to annihilation operators we can ignore the noise for the calculation of any normally ordered products. In the above equations the imaginary part of the first terms on the right-hand side of each line refers to the phase shift caused by the index of refraction of the medium and the ac-Stark shift of the atoms, and the real part of these terms represent damping by spontaneous emission. The last term on each line represents the coupling of light and atoms which is our main interest here.

Solving these equation for a resonant field $\Delta=0$ with no classical field $\Omega=0$, we find that the intensity is reduced by a factor of $\exp(-d)$, with the optical depth d given by

$$d = L4|g|^2/\gamma = (3\lambda^2\gamma_0/2\pi\gamma)nL = n\sigma_0 L, \tag{44}$$

where we have used the expression for the coupling constant g Eq. (31) and have introduced the spontaneous decay rate $\gamma_0=4\omega^3|D_0|^2/3c^3$ from the excited state $|e\rangle$ into the ground state $|0\rangle$ (Milonni and Eberly, 1988) and the absorption cross section for an atom $\sigma_0 = 3\lambda^2\gamma_0/2\pi\gamma$ (Jackson, 1975).

It is sufficient in our case to solve the operator equations of motion (43) as "classical equations" with the operators replaced by complex functions (Raymer and Mostowski, 1981; Gorshkov *et al.*, 2007a). The reason is that the equations are linear in the operators. The solutions to the operator equations will therefore be of the form

$$\hat{a}_{L,\mathrm{out}}(t) = \int_0^L dz m(\Omega(t');t,L-z)\hat{a}_{A,\mathrm{in}}(z) + \cdots, \tag{45}$$

where the operators are identified with hats for clarity, and the argument $\Omega(t')$ indicates that the solution depends on the driving field at all times. The remaining terms denoted by dots in Eq. (45) are similar linear combinations of the input light and noise operators. If we for instance solve the equations of motion with a complex function $a_{A,\mathrm{in}}(z)$ as the initial condition, we get the same solution only without the hats due to the linearity of the equations

$$a_{L,\mathrm{out}}(t) = \int_0^L dz m(\Omega(t),t,L-z)a_{A,\mathrm{in}}(z). \tag{46}$$

We can thus obtain most of the solution (45) by simply inserting hats in the solution. Because we have ignored some input operators, however, the resulting operators will not necessarily have the right commutation relation. If there is no incident light all of these other modes will be in vacuum, and one can obtain the right commutation relation by adding a suitable amount of vacuum noise (Gorshkov *et al.*, 2007a). Another way to see why the complex number equations are sufficient to obtain full information about the dynamics is to note that if all input modes are in classical coherent states, we can take expectation values of the equations of motion (43) and obtain the same equations of motion for the mean values. These classical equations of motion are thus identical to the quantum equations of motion (Raymer and Mostowski, 1981). The equations of motion correspond to a general beam-splitter relation, so that with coherent states as input states the output quantum states will also be a set of coherent states with amplitudes given by the mean values. Since any initial state can be expanded on the set of coherent states, knowledge about the evolution of the coherent states obtained by solving the equations of motion for the mean values gives complete information about the evolution for any quantum state.

The equations of motion can in fact be solved analytically (Gorshkov *et al.*, 2007b). If we consider the situation where the only nonvanishing initial value is a_A, we find the solution for the output light in Eq. (46) with

$$m(\Omega(t');t,z)=\sqrt{\frac{\gamma d}{L}}\frac{(-i)\Omega(z,t)}{4\left(\Delta-i\frac{\gamma}{2}\right)}\times\exp\left(i\left[\frac{2\Delta+i\gamma}{2\gamma}\frac{h(0,t)}{d}+\frac{d\gamma z}{4L(\Delta-i\gamma/2)}\right]\right)\times I_0\left(-ie^{i\phi}\sqrt{h(0,t)\frac{z}{L}}\right),\tag{47}$$

where $I_0(x)$ denotes the zeroth-order Bessel function of the first kind. Here we have assumed that the coupling constant is real, which can always be done by absorbing any phase into the definition of Ω, and we have replaced the coupling constant by the optical depth through Eq. (44). The function $h(t,t')$ is defined by

$$h(t,t')=\int_t^{t'}dt''\frac{d\gamma|\Omega(t'')|^2}{4\Delta^2+\gamma^2},\tag{48}$$

and this is also the function characterizing the strength of the Faraday interaction. Finally the phase ϕ is defined by

$$\tan(\phi)=\gamma/2\Delta.\tag{49}$$

Similarly we find for the output atomic variables

$$a_{A,\mathrm{out}}(z)=\int_0^T dtm(\Omega^*(T-t);T-t,z)a_{L,\mathrm{in}}(t).\tag{50}$$

The fact that the kernel $m(\Omega^*(T-t);T-t,z)$ is similar to the kernel in Eq. (46) is a direct consequence of time reversal symmetry (Gorshkov *et al.*, 2007b).

While the above solutions for the equations of motion are exact, they are sufficiently complicated and it is hard to gain any physical intuition from them. More insight can be gained by applying to the equations the Laplace transform in space using

$$a_A(u,t)=\frac{1}{\sqrt{L}}\int_0^\infty dze^{-uz/L}a_A(z,t),\tag{51}$$

where we have chosen the normalization so that u is a dimensionless number of order unity. We can then derive the equations of motion for the Laplace transformed variables, which only couple operators with the same parameter u. (Note, however that because the atomic operators only have support on $z\in[0,L]$ and not $[0,\infty[$ different Laplace components are not orthogonal and care should be taken when applying these formulas (Gorshkov *et al.*, 2007b)). Since the Laplace transformed equation for the light field does not involve derivatives, we can then eliminate the light field and obtain a single equation for the atomic operator

$$\frac{\partial}{\partial t}a_A(u,t)=\frac{i|\Omega(t)|^2}{4[\Delta-i(\gamma/2)(1+d/2u)]}a_A(u,t)+\frac{ig\sqrt{L}\Omega^*(t)}{2u[\Delta-i(\gamma/2)(1+d/2u)]}a_{L,\mathrm{in}}(t).\tag{52}$$

This equation now has a simple interpretation. Suppose that the incident light field is in vacuum so that we can ignore the last line in Eq. (52). The initial atomic state can then decay through two different mechanisms: either through spontaneous emission or through coherent interaction with the forward light mode. Consider now the fraction in the first line of Eq. (52). The imaginary part of the first term, proportional to the detuning Δ will give rise to an unimportant phase, while the real part describes decay of the atomic excitation at an effective rate (proportional to) $\gamma(1+d/2u)$. Here the decay rate γ is due to spontaneous emission whereas the second term $\gamma d/2u$ is due to the coherent interaction with the forward light mode. The optical depth d has been introduced in Eq. (52) through its relation with the coupling constant g in Eq. (44), and thus characterizes the strength of the coherent interaction with the forward light mode. For a sufficiently high optical depth $d\gg1$ and sufficiently smooth atomic excitations $u\sim1$ the coherent interaction will dominate the spontaneous emission $\gamma d/u\gg\gamma$ and we can obtain an efficient interface between atoms and light.

2. Parametric gain-interaction

In case of the parametric-gain interaction we need to use the plus sign in one of the substitutions as well as include some terms associated with the time derivative of $\langle j_x(\vec{r},t)\rangle$ as discussed in Appendix D. We then find

$$\frac{\partial}{\partial z}a_L(z,t)=i\frac{g^*(z)\Omega(z,t)}{2\Delta-i\gamma}a_A^\dagger(z,t),$$
$$\frac{\partial}{\partial t}a_A(z,t)=-i\frac{|\Omega(z,t)|^2\Delta}{4\Delta^2+\gamma^2}a_A(z,t)+i\frac{g^*(z)\Omega(z,t)}{2\Delta-i\gamma}a_L^\dagger(z,t),\tag{53}$$

where the z dependence of the Rabi frequency is given by the $\exp[i\int dz'|g(z')|^2/(\Delta-i\gamma/2)]$ dependence associated with the change in the propagation of the classical field caused by the index of refraction and scattering of the medium. To arrive at these equations, we have assumed that the decay from the excited state goes into some states $|a_m\rangle$ different from $|0\rangle$ and $|1\rangle$, cf. Fig. 2(b). This model for the decay is not always best for real systems used for parametric-type interaction, for example, in DLCZ (Duan-Lukin-Cirac-Zoller) -type applications (Duan *et al.*, 2001) a much stronger decay to auxiliary states would decrease the effective optical depth, and a large optical depth is crucial for the interface. The model used here is, however, the simplest possible model, and we therefore restrict ourself to this situation. The interpretation of the above equation is similar to the interpretation of the equation of motion for the beam-splitter interaction (43), only in these equations there is no coupling of the light to itself because the light talks to an almost empty transition. The reason why there is no decoherence term in the atomic equation is that spontaneous emission drives atoms from state $|0\rangle$ into some other state $|a\rangle$, where they are lost from the system. Collective states like the one in Eq. (18) are, however, immune to removing one of the atoms in state

$|0\rangle$ and this source of decoherence has therefore no effect within the approximations we are using here; see Mewes and Fleischhauer (2005) for detailed discussion of the robustness of collective atomic states.

These equations of motion can also be solved analytically (Carman *et al.*, 1970; Raymer and Mostowski, 1981). The solution is similar to the solution for the beam-splitter interaction and we shall not go further into it here. Again it can be shown that it is possible to obtain a large coherent coupling with a large optical depth, by Laplace transforming the equations. By doing so one finds a strong gain term for the Laplace component with argument u, which is $\sim d/u$ times the single atom scattering rate. For a large optical depth d we are thus dominated by the coherent interaction, regardless of the assumption about the final state after the decay, which we made above. Unlike the beam-splitter interaction, where one can work at any detuning, this strong coherent interaction only works in the far off-resonant regime, because the classical beam would be completely depleted if one works on resonance in a medium with large optical depth.

3. Faraday interaction

The Faraday interaction is a combination of the beam-splitter interaction and the parametric gain with equal weights, and the easiest way to obtain the equations of motion is therefore to combine the results obtained previously. As discussed in Appendix D the resulting equations of motion are then (assuming Ω and g to be real)

$$\begin{aligned}
\frac{\partial}{\partial z}x_L(z,t) &= -\frac{2\sqrt{2}\Delta g(z)\Omega(t)}{4\Delta^2+\gamma^2}p_A(z) - \frac{\gamma g^2}{4\Delta^2+\gamma^2}x_L(z),\\
\frac{\partial}{\partial z}p_L(z,t) &= \frac{\sqrt{2}\gamma g(z)\Omega(t)}{4\Delta^2+\gamma^2}p_A(z) - \frac{\gamma g^2}{4\Delta^2+\gamma^2}p_L(z),\\
\frac{\partial}{\partial t}x_A(z,t) &= -\frac{2\sqrt{2}\Delta g(z)\Omega(t)}{4\Delta^2+\gamma^2}p_L(z) - \frac{\gamma\Omega^2}{2(4\Delta^2+\gamma^2)}x_A(z),\\
\frac{\partial}{\partial t}p_A(z,t) &= \frac{\sqrt{2}\gamma g(z)\Omega(t)}{4\Delta^2+\gamma^2}p_L(z) - \frac{\gamma\Omega^2}{2(4\Delta^2+\gamma^2)}p_A(z),
\end{aligned} \tag{54}$$

where we have omitted the noise operators, which are given in Eq. (D9). Again these equation are derived under the assumption that the decay goes to some auxiliary state $|a_m\rangle$. For a treatment with decay back to the interface levels, see, for instance, Duan, Cirac, *et al.* (2000), Madsen and Mølmer (2004), and Hammerer (2006).

Now consider the solution of Eq. (54) in the limit of a small damping. The Faraday interaction is only used with far off-resonant light $\Delta \gg \sqrt{d}\gamma$ since the classical field would be completely absorbed if we were working close to resonance. We therefore ignore the first term in the evolution of the momentum operators p_L and p_A, which is much smaller than the similar term in the evolution of x_L and x_A. Furthermore, a time-dependent driving $\Omega(t)$ can be accounted for by a simple rescaling (see Appendix E), so we only consider a constant driving field Ω. Because the quantities p_L and p_A appearing in the coupling to the operators x_A and x_L are conserved quantities apart from the small decays, the dynamics effectively only involve the integrated operators

$$\begin{aligned}
X_L &= \frac{1}{\sqrt{T}}\int_0^T dt x_L(t),\\
P_L &= \frac{1}{\sqrt{T}}\int_0^T dt p_L(t),\\
X_A &= \frac{1}{\sqrt{L}}\int_0^L dz x_A(z),\\
P_A &= \frac{1}{\sqrt{L}}\int_0^L dz p_A(z),
\end{aligned} \tag{55}$$

where the normalization is chosen as for single mode operators $[X,P]=i$. In the limit of small scattering the resulting dynamics are then given by

$$\begin{aligned}
X_{L,\mathrm{out}} &\approx e^{-\eta_L/2}X_{L,\mathrm{in}} + \kappa P_{A,\mathrm{in}},\\
P_{L,\mathrm{out}} &\approx e^{-\eta_L/2}P_{L,\mathrm{in}},\\
X_{A,\mathrm{out}} &\approx e^{-\eta_A/2}X_{A,\mathrm{in}} + \kappa P_{L,\mathrm{in}},\\
P_{A,\mathrm{out}} &\approx e^{-\eta_A/2}P_{A,\mathrm{in}}.
\end{aligned} \tag{56}$$

Apart from the decay, this solution is the same as the results derived in Eq. (40) with a minor modification of the coupling constant (41), which is now given by

$$\kappa^2 = h(0,t)4\Delta^2/(4\Delta^2+\gamma^2), \tag{57}$$

where the function $h(0,t)$ is the same as the function introduced for the beam-splitter interaction in Eq. (48). In the limit of large detuning Δ the coupling constant here is the same as the one derived in Eq. (41).

In the solutions above, the light and atomic operators are damped by factors of $\exp(-\eta_L/2)$ and $\exp(-\eta_A/2)$, respectively. The damping factor for the light is given by

$$\eta_L = \frac{\gamma|g|^2L}{4(\Delta^2+\gamma^2/4)} = \frac{d}{2}\frac{\gamma^2}{4\Delta^2+\gamma^2}. \tag{58}$$

Note that the optical depth used here is for linear polarization. The definition of d therefore differs by a factor of 2 from Eq. (44) because we have taken g to be the coupling constant for circular polarized light and not for linear polarization. From the expression above it is clear that we can ignore the decay of the light field if we use a sufficiently large detuning $\Delta \gg \sqrt{d}\gamma$. A large detuning also reduces the coupling constant but this can be compensated by using stronger laser fields.

The atomic decoherence can be related to the coupling constant through

$$d\eta_A = \frac{\gamma d \int dt|\Omega|^2}{4\Delta^2+\gamma^2} = \kappa^2. \tag{59}$$

This relation between d, η_A, and κ is valid regardless of which assumption one makes about the final state after a decay. But different decay channels will have different effects in the equations of motion, and Eq. (54) is only directly applicable for the particular model considered here. Nevertheless, with a fixed interaction strength κ^2 we can always obtain negligible decoherence with a sufficiently large optical depth d. Conversely, for a given optical depth d there is always an optimal damping factor η_L balancing the losses against the gains in some figure of merit (such as, e.g., state transfer efficiency, light-matter entanglement, etc.) which depends on the coupling strength κ, see, e.g., Hammerer *et al.* (2004).

4. Scaling with atom and photon number

Further insight into the connection between the coupling constant, atomic decoherence, and dissipation of light can be obtained by expressing these parameters through the number of atoms N_A and photons N_P of the classical field. Assume that the classical beam has a square profile with a cross section of area A. Using the definitions of the electric field (12) and Rabi frequency (31) we find

$$\int dt|\Omega|^2 = \gamma_c(3\lambda^2/2\pi A)N_P, \tag{60}$$

where γ_c (γ_q) is the decay rate between the two states coupled by the classical (quantum) field with an emitted photon of the same polarization as the classical (quantum) field. The function $h(0,T)$ characterizing the strength of the interaction in the far off-resonant limit can be then expressed as

$$h(0,T) = \left(\frac{3\lambda^2}{2\pi A}\right)^2 \frac{\gamma_c\gamma_q}{4\Delta^2+\gamma^2} N_A N_P = \frac{\sigma_c\sigma_q}{A^2}\frac{\gamma^2}{4\Delta^2+\gamma^2} N_A N_P, \tag{61}$$

where in the last line we have introduced the resonant cross sections for the scattering of the quantum and classical fields ($\sigma_m = 3\lambda^2\gamma_m/2\pi\gamma$). The atomic and light decoherence can then be related by

$$N_A\eta_A = N_P\eta_L, \tag{62}$$

which simply reflects the fact that the number of scattered photons is the same as the number of atoms which have scattered a photon. If the number of input classical photons is much larger than the number of atoms $N_P \gg N_A$ the decay of light is much smaller than the atomic decoherence and can be neglected.

The function $h(0,t)=\kappa^2$ characterizes the solution of all three model systems considered here. Further insight into the reason for this can be gained by rewriting the equations in terms of rescaled dimensionless variables (Appendix E).

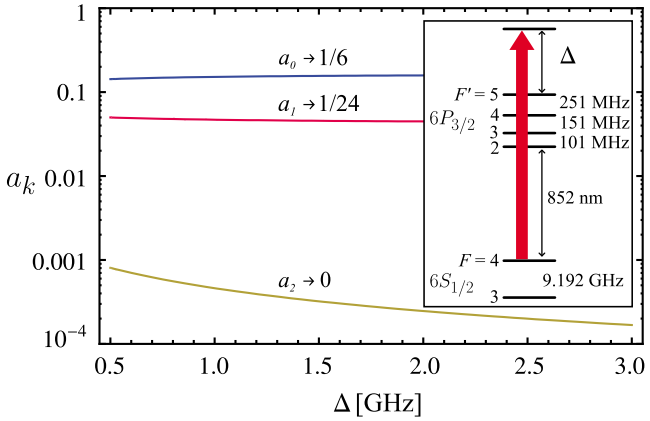

FIG. 3. (Color online) Coefficients a_0, a_1, a_2 for, respectively, scalar, vector, and tensor polarizability vs detuning Δ of probe light driving the $6S_{1/2} \to 6P_{3/2}$ transition in ^{133}Cs. The inset shows the relevant levels and energy scales.

D. Realistic multilevel atoms

In the previous section we derived the main equations describing three types of light-matter interactions, the beam splitter, the parametric gain, and the Faraday-QND type, Eqs. (30), (33), and (34), respectively, for simple few-level model atoms. In this section we give examples of how these interactions are commonly realized with real atoms.

1. Faraday interaction

Applying the Faraday interaction (34) to a full hyperfine level with many nearly degenerate Zeeman states would at first sight seem to violate the simple two-level approximation that we have used in the theoretical derivation. For alkali atoms, however, the full theory actually reduces to what we have derived previously if the detuning is much larger than the hyperfine splitting in the excited state. Consider the $S_{1/2} \to P_{3/2}$ transition in alkali atoms as shown in Fig. 3. If atoms are optically pumped into one of their hyperfine ground-state levels F, an off-resonant probe will couple in general to three dipole allowed transitions $F \to F' = F-1, F, F+1$. Each of these transitions will contribute to the effective Hamiltonian in Eq. (25) describing the interaction of a single atom with off-resonant light. It will be convenient to rewrite this Hamiltonian as

$$H_{\rm int} = \vec{E}^{(-)}(\vec{r})\vec{\vec{\alpha}}\vec{E}^{(+)}(\vec{r}),$$

where we introduced the atomic polarizability tensor operator (Happer and Mathur, 1967; Happer, 1972; Deutsch and Jessen, 1998)

$$\vec{\vec{\alpha}} = \sum_{m,m'} \sum_{F'} \sum_{m''=-F'}^{F'} \frac{\vec{D}^{(+)}_{m',m''} \wedge \vec{D}^{(-)}_{m'',m}}{\Delta_{F'}} |g_{m'}\rangle\langle g_m|$$

and $\vec{D}^{(+)}_{m',m''} \wedge \vec{D}^{(-)}_{m'',m}$ denotes the dyadic vector product. The polarizability operator is a rank-2 spherical tensor (Edmonds, 1964; Zare, 1988) and can therefore be decomposed into irreducible tensor components,

$$\vec{\vec{\alpha}} = (4D_0^2/\Delta)[a_0(\Delta)\vec{\vec{T}}^{(0)} + a_1(\Delta)\vec{\vec{T}}^{(1)} + a_2(\Delta)\vec{\vec{T}}^{(2)}],$$

where the tensor operators $\vec{\vec{T}}^{(k)}$ transform under rotations as a scalar, vector, and matrix for $k=0,1,2$, respectively. In this expression $\Delta=\Delta_{F'=F+1}$ is the laser detuning from the uppermost level and $2D_0=\langle J'\|\vec{D}\|J\rangle$ is the reduced dipole matrix element for the $S_{1/2}\rightarrow P_{3/2}$ transition. It relates to the spontaneous decay rate introduced in Sec. II.C as $\gamma_0=4\omega^3|D_0|^2/3c^3$.

The real coefficients $a_k(\Delta)$ follow from elementary calculations (Julsgaard, 2003; Kupriyanov *et al.*, 2005; Geremia *et al.*, 2006; Hammerer, 2006) and are given in Appendix F. The essential feature of these coefficients, which is proven in the Appendix F, is that for a laser detuning, which is large compared to the hyperfine splitting of excited states, $|\Delta| \gg |\Delta_{F+1}-\Delta_{F'}|$, the rank-2 tensor component vanishes, $a_2(\Delta)\rightarrow 0$. For the case of ^{133}Cs the coefficients $a_k(\Delta)$ are shown in Fig. 3.

In the asymptotic limit the interaction Hamiltonian is thus given by

$$H = \frac{D_0^2}{\Delta}\left\{ a_0 \vec{E}^{(-)}(\vec{r}) \cdot \vec{E}^{(+)}(\vec{r}) + \frac{i}{2} a_1 \vec{E}^{(-)}(\vec{r}) \cdot [\vec{j} \times \vec{E}^{(+)}(\vec{r})] \right\}.$$

For an atomic ensemble, the first term will give rise to an index of refraction, while the second term accounts for the Faraday effect. For light propagating along z and the classical light polarized along x the Faraday Hamiltonian (34) can be easily derived.

When the detuning is larger than the hyperfine splitting, the interaction is thus essentially the same as for a spin 1/2 ground state, where a_2 vanishes exactly for all detunings. This can be understood by looking at how the energy levels of an alkali atom appear. The full Hamiltonian can be written $H=H_0+H_{\rm FS}+H_{\rm HFS}+H_{\rm int}$, where the four Hamiltonians represents the Coulomb, fine structure, hyperfine structure, and interaction with light. Normally one just considers the first three terms as an atomic Hamiltonian and does perturbation theory in the interaction Hamiltonian. When the detuning is larger than the hyperfine structure it is, however, more appropriate to do the adiabatic elimination before treating the hyperfine interaction. Without the hyperfine interaction the optical fields only talk to the electron spin, where there cannot be a rank-2 tensor, since the spin cannot be changed by two, and a_2 therefore only appears as a perturbation in $H_{\rm HFS}/\Delta$.

The Faraday interaction of light with a true spin 1/2 ground-state atom, which therefore has only scalar and vector polarizability, can be achieved with the ytterbium isotope ^{171}Yb, as explored by Takeuchi *et al.* (2006, 2007).

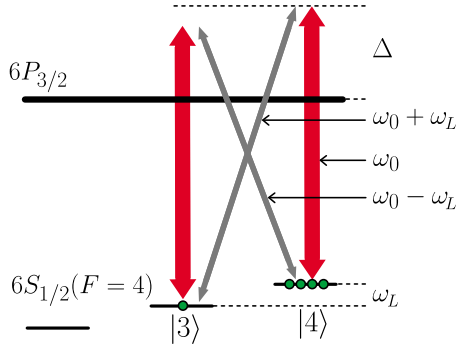

FIG. 4. (Color online) A magnetic field along the axis of polarization causes Zeeman splitting ω_L of ground-state levels. Photons will be scattered from the classical light, driving the π transitions, to the quantum field, coupling to the cross σ transitions, at sideband frequencies $\omega_0\pm\omega_L$ from the carrier frequency ω_0.

2. Λ Systems

Although for the beam-splitter and the parametric-gain interaction, which require a Λ configuration, magnetic sublevels are sometimes used (Novikova *et al.*, 2007), the most common implementation makes use of $S_{1/2}(F=I\pm 1/2)$ hyperfine levels as ground states $|0\rangle$ and $|1\rangle$ and one of the P states as an excited state $|e\rangle$ (Chou *et al.*, 2004, 2005, 2007; Matsukevich and Kuzmich, 2004; Chaneliere *et al.*, 2005, 2007; Chen, Zhao, *et al.*, 2007; Chen *et al.*, 2008; Choi *et al.*, 2008). This approach gives excellent results in zero magnetic field even if atoms are not optically pumped initially to one Zeeman substate. It has also been suggested by Kupriyanov *et al.* (2005), Mishina *et al.* (2007) , and de Echaniz *et al.* (2008) to make use of the second-rank tensor polarizability to engineer effective Λ schemes for the beam-splitter and parametric-gain interactions using two degenerate Zeeman states and polarized light.

E. Ensemble in magnetic field

Our theory for light matter interaction so far assumed degenerate ground-state levels. For pure three-level Λ schemes nondegenerate ground states do not make any difference, as the level splitting can be compensated for by choosing appropriate frequencies for light. In this section we deal mainly with the Faraday interaction for atoms in an external magnetic field along the axis of atomic polarization (Fig. 4). The Zeeman splitting caused by this field can be advantageous in several respects. On the one hand, combined with the homodyne detection typically used in connection with the Faraday interaction, this results in low-noise ac signals, as detailed in Sec. II.F. On the other hand, it can also simplify and enhance protocols aiming for an efficient creation of

entanglement of two ensembles (Sec. IV) or between an ensemble and light (Sec. VI).

The free Hamiltonian for an ensemble of atoms in a uniform magnetic field [Eq. (24)] oriented along the x axis is

$$H_0 = \frac{\omega_L}{2}\int dz[x_A^2(z) + p_A^2(z)], \tag{63}$$

where ω_L is the Larmor frequency. This Hamiltonian generates Larmor precession of the transverse spin density components $x_A(z)$ and $p_A(z)$ about the x axis. The full Hamiltonian describing Faraday interaction in a magnetic field is $H=H_0+H_F$, where H_F is given in Eq. (34). In an interaction picture with respect to H_0 this Hamiltonian is

$$H_F^I = -\int dz \frac{g^*(z)\Omega(z,t)}{\sqrt{2}\Delta} p_L(z) \times [\cos(\omega_L t)p_A(z) + \sin(\omega_L t)x_A(z)]. \tag{64}$$

Operators x_A and p_A refer now to spin components in a frame rotating at ω_L about the x axis. For simplicity we use in the following the same symbols for canonical operators in both frames, as it will be clear from the context, to which one we are referring. In the rotating frame the canonical operators for transverse spin components are related to the spin components in the laboratory frame via

$$j_y(z)/\sqrt{n(z)} = \cos(\omega_L t)x_A - \sin(\omega_L t)p_A,$$

$$j_z(z)/\sqrt{n(z)} = \cos(\omega_L t)p_A + \sin(\omega_L t)x_A,$$

with the number density of atoms $n(z)$.

The Maxwell-Bloch equations in the rotating frame are accordingly

$$\begin{aligned}
\frac{\partial}{\partial z}x_L(z,t) &= -\frac{g^*(z)\Omega(t)}{\sqrt{2}\Delta}[\cos(\omega_L t)p_A(z) \\
&\quad + \sin(\omega_L t)x_A(z)], \\
\frac{\partial}{\partial z}p_L(z,t) &= 0, \\
\frac{\partial}{\partial t}x_A(z,t) &= -\frac{g^*(z)\Omega(t)}{\sqrt{2}\Delta}\cos(\omega_L t)p_L(z,t), \\
\frac{\partial}{\partial t}p_A(z,t) &= \frac{g^*(z)\Omega(t)}{\sqrt{2}\Delta}\sin(\omega_L t)p_L(z,t).
\end{aligned} \tag{65}$$

Now the atomic momentum operator, i.e., the spin projection along the axis of light propagation, is not conserved anymore and the overall interaction is not of QND character. Integration of these equations becomes somewhat more involved than before. We resort to this problem in Secs. IV and VI.

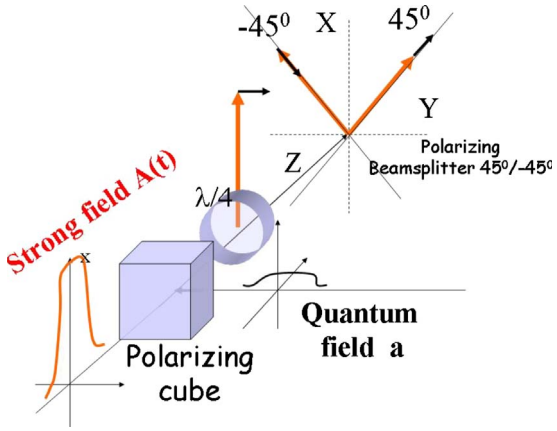

FIG. 5. (Color online) Polarimetric measurement of light.

F. Quantum measurement and feedback

In this section we deal with measurements which can be done on light and then fed back onto atoms. We focus on homodyne detection of light, which is of importance for experiments using Faraday interaction and EIT but also describe photon counting, which is used in combination with parametric-gain and beam-splitter interactions.

1. Homodyne detection of light

The discussion of the quantum interface in the language of canonical variables for light is most fruitful because these variables can be measured with almost perfect efficiency by the balanced homodyne technique. We concentrate here on the polarization homodyne version, which is relevant for several protocols described here. In particular, in the context of the Faraday interaction the polarimetric measurement of light is an important tool. Balanced homodyning employs overlapping the quantum field of interest with a strong coherent field, a local oscillator, on a 50/50 beam splitter and measurement of the difference of the power in the two outputs. In its polarization version as shown in Fig. 5, the local oscillator field and the quantum field are overlapped on a polarizing cube so that they have orthogonal polarizations and the role of the beam splitter is played by a polarizing beam splitter which splits the light into 45° and −45° modes. The measurement of the differential power of these two modes corresponds to the measurement of the S_y Stokes operator, whereas with an extra λ/4 plate in front of the beam slitter the S_z Stokes operator is measured

$$\begin{aligned}
S_x(t) &= (a_{L,x}^\dagger a_{L,x} - a_{L,y}^\dagger a_{L,y})/2, \\
S_y(t) &= (a_{L,+45^\circ}^\dagger a_{L,+45^\circ} - a_{L,-45^\circ}^\dagger a_{L,-45^\circ})/2 \\
&= (a_{L,x}^\dagger a_{L,y} + a_{L,y}^\dagger a_{L,x})/2, \\
S_z(t) &= (a_{L,\sigma^+}^\dagger a_{L,\sigma^+} - a_{L,\sigma^-}^\dagger a_{L,\sigma^-})/2 \\
&= -i(a_{L,x}^\dagger a_{L,y} - a_{L,y}^\dagger a_{L,x})/2.
\end{aligned}$$

The third Stokes operator S_x is equal to the total photon number of the strong field for the case of the strong coherent field $|\alpha\rangle$ in linear x polarization, such that $\langle S_x(t)\rangle = |\alpha|^2/2$. In this case the measurement of the two other Stokes operators amounts to a homodyne detection of y-polarized light with the coherent field in x serving as the local oscillator,

$$\frac{S_y(t)}{\sqrt{\langle S_x\rangle}} \simeq \frac{1}{\sqrt{2}}[a_{L,y}(t) + a_{L,y}^\dagger(t)] = x_L(t),$$

$$\frac{S_z(t)}{\sqrt{\langle S_x\rangle}} \simeq -\frac{i}{\sqrt{2}}[a_{L,y}(t) - a_{L,y}^\dagger(t)] = p_L(t).$$

The homodyne detection can also provide suppression of the technical (classical) noise if the frequency of the local oscillator and the quantum field differ by ω_L lying in the radio-frequency domain, see Fig. 4. In this case the relevant canonical variables are encoded in sideband modulation modes of y-polarized light, which are read in the $\cos(\omega_L t)$ and $\sin(\omega_L t)$ components of the photodetector output,

$$\begin{aligned} X_{L_c} &= \sqrt{\frac{2}{T}}\int dt\, \cos(\omega_L t) x_L(t), \\ P_{L_c} &= \sqrt{\frac{2}{T}}\int dt\, \cos(\omega_L t) p_L(t), \\ X_{L_s} &= \sqrt{\frac{2}{T}}\int dt\, \sin(\omega_L t) x_L(t), \\ P_{L_s} &= \sqrt{\frac{2}{T}}\int dt\, \sin(\omega_L t) p_L(t). \end{aligned} \tag{66}$$

These components of the photocurrent can be measured by lock-in amplifiers. The bandwidth of this measurement can be adjusted to $BW \approx \tau^{-1}$, where τ is the optical pulse duration. In this way fluctuations at all frequencies outside this bandwidth are effectively irrelevant. In the case where atomic ground-state levels are nondegenerate, e.g., are split by the Larmor frequency ω_L as discussed in Sec. II.E and shown in Fig. 4, the atoms couple to the sidebands of light and the entire measurement and interaction can be encoded at sideband frequencies $\pm\omega_L$, as in several experiments described later.

2. Feedback

Another important tool in many quantum information protocols is the feedback of results of measurement of light onto atoms. The theory of quantum feedback is a wide field on its own, especially in the case of continuous measurement and feedback (Thomsen *et al.*, 2002a). Here we deal with a relatively simple measurement and feedback scheme, where light observables of the type (66) are measured by integrating a photocurrent over the whole pulse duration and the measurement result, a single number, is fed onto the atoms. The operations which need to be done on the collective spins are small rotations about the y or z axis, i.e., small tilts of the collective spin. In the language of canonical operators X_A, P_A this amounts to displacements in the phase plane (Arecchi *et al.*, 1972).

In this case—feedback of integrated measurement results via displacement operations—a simple rule can be applied for describing the overall effect on a state of the atoms. Assume that the state of the system is described by certain input-output relations of the type (40). If a quadrature of light, say X_L, is measured and the corresponding measurement result ξ is used to displace the atomic state, i.e., to tilt the collective atomic spin, in such a way that the mean of, say P_A, is transformed as $\langle P_A\rangle \to \langle P_A\rangle + g\xi$, then the statistics of P_A after the feedback operation can be calculated from

$$P_{A,\text{final}} = P_A + gX_L, \tag{67}$$

that is, one simply needs to add the measured observable multiplied by the gain to the operator which is subject to the feedback. This rule for describing the feedback holds strictly as an operator identity, irrespectively of the state of the system being Gaussian or non-Gaussian.

The proof is most easy in the Schrödinger picture. Assume the state of some bipartite system is $\hat{\rho}_{AL}$, where the indices refer, to atoms and light respectively. A measurement of X_L gives a result ξ with probability $p_\xi = \langle\xi|\mathrm{tr}_A\{\rho_{AL}\}|\xi\rangle$, where $X_L|\xi\rangle = \xi|\xi\rangle$, and the state of the system A collapses to

$$\rho_A^{(1)} = p_\xi^{-1}\langle\xi|\rho_{AL}|\xi\rangle.$$

The feedback affecting the desired displacement is described by a unitary transformation of the state of the system A,

$$\rho_A^{(2)} = e^{ig\xi X_A}\rho_A^{(1)}e^{-ig\xi X_A},$$

which gives in the ensemble average over all possible measurement results the final state

$$\begin{aligned} \rho_A^{(3)} &= \int d\xi p_\xi \rho_A^{(2)} = \int d\xi e^{ig\xi X_A}\langle\xi|\rho_{AL}|\xi\rangle e^{-ig\xi X_A} \\ &= \int d\xi \langle\xi| e^{igX_L X_A}\rho_{AL}e^{-igX_L X_A}|\xi\rangle \\ &= \mathrm{tr}_L\{e^{igX_L X_A}\rho_{AL}e^{-igX_L X_A}\}. \end{aligned}$$

From this equation all the moments of P_A can be calculated as

$$\langle P_A^n\rangle = \mathrm{tr}_A\{P_A^n\rho_A^{(3)}\} = \mathrm{tr}_{AL}\{(P_A + gX_L)^n\rho_{AL}\},$$

where the cyclic property of the trace was used in the second equality. This justifies the rule given above.

Note that for Gaussian states, for which it is enough to keep track only of the first and the second moments in order to have the full knowledge of the state, the simple linear transformation of operators as above is exactly equivalent to a full description in the Schrödinger picture, e.g., on the basis of the Wigner function. The measurement of and the feedback on more than one mode

can be described by an immediate generalization of Eq. (67) as shown by Hammerer, Polzik, and Cirac (2005) and Sherson, Krauter, *et al.* (2006), provided the measurement involves commuting observables only.

3. Photon counting

In some cases measurements in the Fock state basis, i.e., photon counting, are convenient for characterization of the interface performance. As discussed in Sec. V, storage and retrieval of some nonclassical states can be characterized by the measurement of the second-order correlation function $g^2(1,2)$, which is a normalized probability of photon counts at two points in space-time (Loudon, 2004). Atoms typically used for the interface are rubidium and caesium and the corresponding spectral lines are around 780 and 850 nm, respectively. In this spectral domain commercial avalanche photodiodes typically have quantum efficiency around 40–50 % and the dark count rate of a few hundred per second. Such parameters are sufficient to determine nonclassical correlations via $g^2(1,2)$, which are insensitive to losses if dark counts are neglected.

G. Other strategies

In the discussion so far we have focused on what we consider to be the main protocols in this field. There are, however, numerous variations of all of these protocols, some of which we discuss here.

1. Noncopropagating beams

In the derivation we have only considered the situation where the quantum and classical light fields are copropagating. For many applications of the beam-splitter and parametric-gain interaction this assumption is, however, not necessary (Braje *et al.*, 2004; Balić *et al.*, 2005; Chaneliere *et al.*, 2005). For instance, an incoming photon which is absorbed in an atomic ensemble using a copropagating classical field generates an excitation of the form of Eq. (18). The reason why one can later retrieve this quantum state is constructive interference. During readout all atoms will radiate in phase in the direction of the classical laser and this is the effect, which allows for efficient interfaces between atoms and light in the limit of a large number of atoms (high d). If the photon which is absorbed has a different direction than the classical drive field, the generated atomic excitation will still have the form of Eq. (18). The only difference is that the state will have a phase factor $\exp(i\Delta\vec{k}\cdot\vec{r}_i)$ on the component, where the ith atom is in state $|1\rangle$, with $\Delta\vec{k}$ the difference between the k vectors for the two fields. In order to have constructive interference in the readout process the difference in the k vectors of the outgoing photon and the classical field in the readout process should cancel the phase factor imprinted on the atoms in the first step of the protocol (see also Sec. V.D for a discussion of the effect of difference in the k vectors).

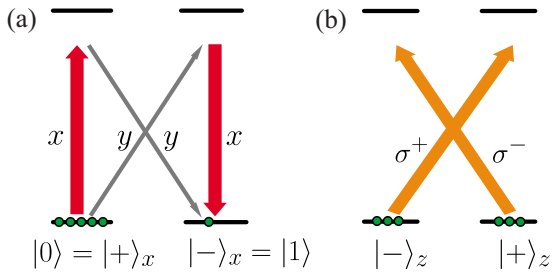

FIG. 6. (Color online) Level scheme for Faraday interaction. (a) For the quantization axis along x: Atoms are polarized to $|+\rangle_x$, laser light is linear polarized along x and drives the up transitions, while the quantum field in y polarization couples to the cross transitions. (b) The same interaction with the axis of quantization taken along z: Circular light components of equal intensity cause ac-Stark shifts of equally populated states $|\pm\rangle_z$.

Expressed in different terms, the initial atomic state $|000\ldots.0\rangle$ has a homogeneous phase corresponding to a zero momentum state. The initial process involving the absorption of a photon from one beam and the emission of a photon into a different beam imprints the difference momentum $\Delta\vec{k}$ onto the atomic spin wave. Constructive interference is achieved for processes returning the atoms to the initial zero-momentum spin wave $|000\ldots.0\rangle$ and the differential momentum in the readout process must therefore carry away the momentum in the spin wave. To achieve momentum conservation (or equivalently phase matching) the total momentum of all absorbed photons should thus match the total momentum of all emitted photons.

A disadvantage of using noncopropagating beams is that the storage into nonsymmetric modes limits the storage to the time it takes atoms to move a distance $\sim 1/|\Delta\vec{k}|$. In particular for room-temperature gasses (see Sec. III.A) this, as well as the differential Doppler shift, makes it undesirable to use geometries, where the beams are not nearly copropagating. Even for cold atomic ensembles this effect limits the storage time, as observed experimentally by Zhao *et al.* (2009). On the other hand, it is often a major experimental advantage not to have the classical and quantum beams copropagating since this makes it much easier to count photons in the quantum beam.

2. Interaction based on phase shift

It is instructive to have a look at the Faraday interaction from another perspective. Consider first Fig. 6(a) where, as before, the quantization axis is taken along x, the direction of polarization of both atoms and light. Selection rules for dipole transitions dictate that strong classical x-polarized light with amplitude $a_x \simeq \alpha$ drives the $|\pm\rangle_x \rightarrow |\pm\rangle_x$ transitions, while the $|\pm\rangle_x \rightarrow |\mp\rangle_x$ cross transitions are coupled to the weak quantum field a_y in y polarization. In this picture it is evident that the Faraday interaction is the sum of the beam-splitter and parametric-gain interactions, cf. Fig. 2. The same level configuration can also be looked at by taking the axis of

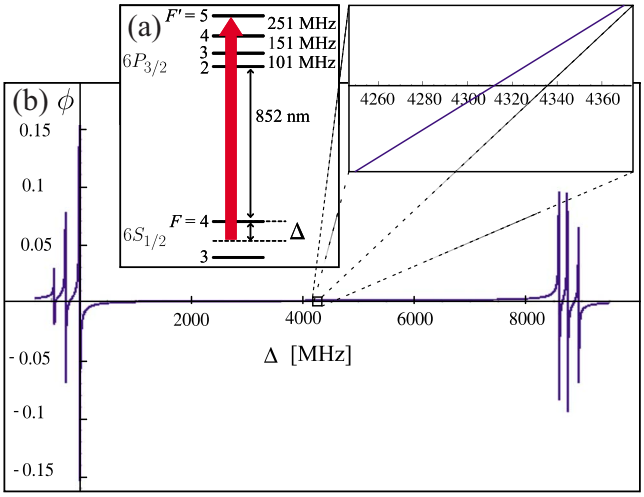

FIG. 7. (Color online) QND interaction for measurement of pseudospin composed of hyperfine ground states of Cs. (a) Level scheme for ^{133}Cs with probe light tuned in between hyperfine levels $F=3,4$ of the $6^2S_{1/2}$ ground state. (b) Differential phase shift Φ due to the $F=3\rightarrow F'=2,3,4$ and the $F=4\rightarrow F'=3,4,5$. At magic frequencies the phase shift vanishes.

quantization along the z direction, as shown in Fig. 6(b), where $|\pm\rangle_z=(|+\rangle_x\pm|-\rangle_x)/\sqrt{2}$. Light propagating along this direction naturally couples with its circular components $a_{\sigma^\pm}=(a_x\pm ia_y)/\sqrt{2}\simeq(\alpha\pm ia_y)/\sqrt{2}$ to the cross transitions $|\pm\rangle_z\rightarrow|\mp\rangle_z$ only. The off-resonant coupling will thus give rise to ac-Stark shifts on atomic levels $|\pm\rangle_z$ depending on light intensities of $\sigma^\pm$-polarization components. Light polarization is thus rotated according to the difference in level populations $|\pm\rangle_z$.

From this observation it is clear that all that is required for a Faraday interaction is a mechanism of nondestructive measurement of level populations via phase shifts of light. Making use of the vector polarizability for probing the collective hyperfine spin-angular momentum as described above is therefore one way to achieve a Faraday or QND interaction. In addition, several proposals and experiments pursue the idea to probe coherences of the pseudospin consisting of the two $S_{1/2}(F=I\pm1/2)$ hyperfine levels (Oblak *et al.*, 2005; Chaudhury *et al.*, 2006; Petrov *et al.*, 2007; Windpassinger *et al.*, 2008). As shown in Fig. 7 at a certain detuning the phase shift of the probe light due to $F=I\pm1/2\rightarrow F'$ transitions exactly cancels for equal populations of $F=I\pm1/2$ levels. Any imbalance of populations will yield an interferometrically detectable phase shift.

3. Other Hamiltonians and level structures

There are several possibilities involving more complicated atomic level structures than the ones shown in Fig. 2. A particular example is the so-called double Λ systems, with two excited states. An interesting feature of this system is its potential application for four wave mixing; see Fleischhauer *et al.* (2005) for a review.

In the derivation of the theory we adiabatically eliminated the excited state to arrive at the effective ground-state Hamiltonian. As discussed in Sec. II.D this adiabatic elimination in general leads to a Hamiltonian involving spherical tensors of rank zero, one, and two with strength characterized by the three coefficients a_0, a_1, and a_2. The three protocols that we have considered correspond to suitable initial states and particular combinations of these spherical tensors. By adjusting the detuning as well as laser polarizations and atomic initial state there is, however, much freedom in varying the relative strength and effect of the different tensors, which allow for a richer dynamics. Kupriyanov *et al.* (2005) and Mishina *et al.* (2007) considered how the higher-order tensor operators modify the equations of motion and in particular how the Faraday interaction is influenced by the rank two tensor. For instance, Mishina *et al.* (2007) showed that a particular choice of detuning removes the ac-Stark for a detuned beam-splitter interaction and thus removes the need to adjust the frequency of the classical driving field in order to keep the field in two photon resonance with the ac-Stark shifted transition.

To arrive at the Faraday interaction we combined the beam-splitter and parametric-gain interaction with the same strength, but Mishina *et al.* (2006) showed that an arbitrary combination of the parametric-gain and beam-splitter interaction can be obtained by choosing suitable initial conditions, detunings, and combinations of the elements of the spherical tensor.

An example of a protocol where the light-atom interface involves excited states without adiabatic elimination is shown in Fig. 1(a) (Kuzmich *et al.*, 1997; Hald *et al.*, 1999). Another protocol of this type is considered in Sec. V.E, where we discuss spin echo techniques. A disadvantage of such protocols is, however, that the storage time is limited by the coherence time of the optically excited state, which is often shorter than the coherence time of ground states.

4. Optical cavities

The key parameter in characterizing the applicability of an atomic ensemble for a light matter quantum interface is its optical depth, which for a free space ensemble is limited by the size and atomic interaction. An alternative strategy is to use multiple passes of the light through the atomic ensemble by enclosing the ensemble in an optical cavity (Josse *et al.*, 2004; Black *et al.*, 2005; Dantan *et al.*, 2005; Thompson *et al.*, 2006; Simon, de Riedmatte, *et al.*, 2007; Simon, Tanji, *et al.*, 2007). In this case the parameter characterizing the usefulness of the system is the cooperativity parameter $C=N_Ag_c^2/\kappa_c\gamma$, where g_c is the coupling constant for a single atom to the cavity mode and κ_c is the cavity decay rate. The cooperativity can also be expressed as $C\sim\mathcal{F}d$, where $\mathcal{F}$ is the finesse of the cavity which roughly equals the number of passes that the photon makes through the cavity (Gorshkov *et al.*, 2007a). The gain achieved by using a cavity thus equals the number of round trips.

5. Non-Gaussian operations

In this review we consider the quantized light fields which are much weaker than classical control and driving light, and the quantum fluctuations of the atomic ensemble which are much smaller than the mean spin. In this limit we only include the lowest-order terms in the atomic and light field operators a_A and a_L. Because there are no first-order terms the effective Hamiltonian will be quadratic in the harmonic oscillator operators. The operations which may be performed thus fall into the class of Gaussian operations and the solution of the equations will in general be a Bogoliubov transformation of the incident mode operators (Braunstein and van Loock, 2005). For any input state with a Gaussian Wigner function the output Wigner function will also be Gaussian. The main advantage of using atomic ensembles is that the dynamics resulting from these Gaussian operation are collectively enhanced so that a perfect operation is achieved in the limit of large optical depth. While the resulting dynamics allow for a variety of quantum information protocols to be performed, such as quantum teleportation and quantum memory (Secs. V and VI), the fact that higher-order terms are not collectively enhanced limits the applications for quantum information processing. In particular it is known that Gaussian operations alone do not allow for distillation of entanglement from Gaussian states (Eisert *et al.*, 2002; Fiurasek, 2002; Giedke and Cirac, 2002) and that algorithms for efficient classical simulation of any evolution involving only Gaussian operation and Gaussian initial states exist (Lloyd and Braunstein, 1999; Bartlett *et al.*, 2002). These limitations may, however, be avoided by combining the Gaussian operation with photon counting (Genes and Berman, 2006; Neergaard-Nielsen *et al.*, 2006; Ourjoumtsev *et al.*, 2006). Duan *et al.* (2001) proposed such photon counting techniques as a means for quantum communication over long distances using the probabilistic entanglement protocols discussed in Sec IV.C. Such techniques could in principle also allow for even more advanced quantum information protocols to be implemented.

The fundamental obstacle for *directly* achieving non-Gaussian operations is that they rely on an interaction between individual excitations. Such interactions between the excitations can for instance be achieved if two photons interact with the same atom. But since this is essentially a single-atom effect it is not enhanced by a large optical depth. An approach which allows for an enhancement of this nonlinear effect by optically imprinting a Bragg mirror which localizes excitation similar to an optical cavity is explored by André and Lukin (2002) and Bajcsy *et al.* (2003). An alternative approach to non-Gaussian operations is to engineer a strong interaction between excitations stored in different atoms. Interesting proposals in this direction are to use the collisional interactions of atoms in optical lattices (Muschik *et al.*, 2008) or the so-called Rydberg blockade, where the excitation of a single atom to a Rydberg level blocks the excitation of other atoms, and therefore creates a uniform long-distance interaction (Lukin *et al.*, 2001). Alternatively one can exploit the fact that atomic ensembles are particularly well suited for "catching" traveling photons and then afterwards transfer the excitation to some other system for processing the information. A proposal along these lines is presented by Rabl *et al.* (2006) based on a transfer of excitations from an ensemble of dipolar molecules to a solid state system. A review of techniques for achieving other types of operations, e.g., Kerr interactions, is given by Fleischhauer *et al.* (2005).

H. Summary of the theory

We have presented a detailed theory for the quantum interfaces between light and atomic ensembles. In particular we have presented a unified theory for the three model systems shown in Figs. 2(a)–2(c), the beam-splitter, the parametric gain, and the QND (Faraday) interaction. The three systems have distinct features, but are also interconnected, e.g., the Faraday interaction is just a combination of the beam-splitter and parametric-gain interaction with equal weights. Most importantly all three systems achieve ideal operation in the limit of high optical depth d. This feature can be understood as constructive interference or collective enhancement of the coupling: the coupling between the state where all atoms are in the ground state and the collective state (18) scales as $\sqrt{N_A}$, whereas spontaneous emission is a single-atom effect, which is independent of the atom number. We emphasize, however, that the theory is derived without the optical broadening present in many experimental realization. One therefore cannot directly replace the optical depth d appearing in the equations of this section with the actual measured optical depth in the presence of inhomogeneous broadening. Neverthless, the optical depth in one version or the other remains the key parameter for characterizing the usefulness of an atomic ensemble (see Sec. VII for a discussion of inhomogeneous broadening).

For all three types of interaction, in the far off-resonant limit $\Delta \gg d\gamma$, the strength of the coupling is parametrized by exactly the same function $h(0,T) \approx \kappa^2$, cf. Eqs. (46)–(48), (56), and (57), which is most easily seen by rewriting the equations in the dimensionless form as in Appendix E. In this limit the decay and phase shift of the light can be ignored and the coupling constant can be related to η_A, the spontaneous emission probability per atom, through $\kappa^2 = \eta_A d$, which we explicitly derived for the Faraday interaction, but which also applies to the other systems. From this expression one thus directly sees that the spontaneous emission can be eliminated for high optical depth. In a special case of the beam-splitter interaction, the resonant EIT setting, these arguments are not directly applicable, but the ratio between the desired evolution and spontaneous emission, i.e., the constructive interference discussed above, is completely independent of detuning (Gorshkov, André, Fleischhauer, *et al.*, 2007; Gorshkov *et al.*, 2007b).

It is instructive to discuss the bandwidth of the quantum interface, i.e., how fast an operation such as a storage or a read process can be performed. In the theory we have adiabatically eliminated the excited state, which means that the shortest time τ on which an operation can be performed is limited by the low saturation parameter condition $s \ll 1$ and the condition on the value of the coupling constant κ necessary for a particular process. Bearing in mind that $\eta_A = \gamma\tau s$, $\tau = (BW)^{-1}$, we can draw some general conclusions on the Fourier limited bandwidth of the process. For protocols where $\kappa^2 \sim 1$ the low saturation condition yields the limitation on the bandwidth of the light pulse, $BW \ll \gamma d$ (again the arguments given here only directly apply in the far off-resonant limit, but the conclusion is also valid for EIT). Going beyond the low saturation regime $s \sim 1$ allows us to increase the bandwidth somewhat (Gorshkov *et al.*, 2008), but it remains limited by $BW \lesssim \gamma d$. For a typical alkali atomic ensemble the bandwidth of the order of 10 MHz can be achieved. This scaling of the bandwidth provides an upper limit, e.g., for an atomic EPR entanglement protocol discussed later where the conditions $\kappa^2 \gg 1, \eta \approx 1/\sqrt{d}$ has to be met, $BW \ll \gamma\sqrt{d}$. Note, however, that the term bandwidth is also often used in connection with the number of different modes which can, e.g., be stored in an atomic ensemble. This is a different question, which we return to in Sec. V.E.

III. ATOMIC MEDIA FOR QUANTUM INTERFACE

A few common requirements can be formulated for all ensemble-based interfaces described previously. A long-lived (ground) state of atoms is commonly used. This could, e.g., be Zeeman levels or hyperfine levels. The ensemble should be initialized to a polarized state (coherent spin state), that is, one of the ground substates should be populated by optical pumping or other means. Most importantly, the sample should have a large resonant optical depth d. Current, experimental realizations of the ensemble-based interfaces utilize alkali atom gases at room temperature, alkali atoms cooled and trapped at temperatures of a few tens or hundreds of microkelvin, or impurity centers in solid state. Below we describe these and other media used for quantum interfaces.

A. Room-temperature gases

A gas sample of alkali atoms is one of the simplest atomic ensembles to have in the laboratory. Surprisingly enough such an object can also work very well as a quantum memory, if proper care of decoherence is taken. The thermal motion and Doppler broadening associated with it are not necessarily a problem. For the Faraday interaction, the Doppler broadening plays a small role if the detuning is much greater than the Doppler width (200–300 MHz for cesium or rubidium). For other protocols such as the beam-splitter interaction the Doppler broadening has a detrimental but still tolerable effect as discussed in Sec. VII.

In addition to the Doppler broadening, the atomic motion also leads to changes in the atomic positions. A quick glance at the solution to the beam-splitter interactions (47) and (50) reveals that the atomic operators with different longitudinal coordinates experience different dynamics. The atomic motion in the process of interaction leads to washing out of these spatial modes which is a much more pronounced problem for the beam-splitter interaction, as compared to the Faraday interaction.

In order to reduce the deleterious effect of atomic motion a buffer gas is usually used in the experiments which utilize the beam-splitter interaction in gas cells at room temperature (Eisaman *et al.*, 2005; Novikova *et al.*, 2007). Adding a few torr of a noble gas allows one to sufficiently localize the diffusive motion of alkali atoms. An extra benefit of this approach is that it prevents alkali atoms from depolarizing collisions with the walls of the cell which otherwise could lead to a rapid decoherence. The lifetime of the atomic memory in cells with a buffer gas can reach milliseconds (Novikova *et al.*, 2007). Note that for some protocols collisions of atoms in the excited state with the buffer gas lead to an energy redistribution of scattered photons, which may lead to large errors in the absence of careful spectral filtering (Manz *et al.*, 2007). Despite the difficulties, alkali atom cells with a buffer gas has been successfully used for experiments on quantum memory using EIT (Eisaman *et al.*, 2005).

The effect of atomic motion for the Faraday interaction can be almost completely eliminated. As follows from the propagations equations (40) the Faraday interaction couples light to a symmetric atomic mode defined in Eq. (16). In this case atoms with different coordinates z along the direction of light propagation couple to light in the same way. Hence the atomic motion along z does not affect the interaction. The transverse motion of atoms along x and y axes will affect the performance if the spatial profile of the light beam is inhomogeneous, which is almost always the case. This effect can be reduced in two extreme cases: either for times short compared to the motion time or in case when the duration of the light pulse is so long that atoms have a chance to cross the beam many times during the interaction and the effect of motion averages out. The latter was the case of the experiments by Julsgaard *et al.* (2001, 2004) and Sherson, Fiurasek, *et al.* (2006), where pulses of about 1 msec duration have been used.

The possibility to eliminate the effect of atomic motion on the efficiency of the interface based on the Faraday interaction has allowed one to conduct high-fidelity experiments with room-temperature cesium atoms (Julsgaard *et al.*, 2001, 2004; Sherson, Fiurasek, *et al.*, 2006). Atoms were contained in cells with a paraffin coating of the internal walls (Fig. 8). Such coating has been used in precision magnetometers for the past three decades (Alexandrov, 2003; Groeger *et al.*, 2006), and ground-state coherence times of up to a second have been demonstrated. In paraffin coated cells atoms can withstand tens

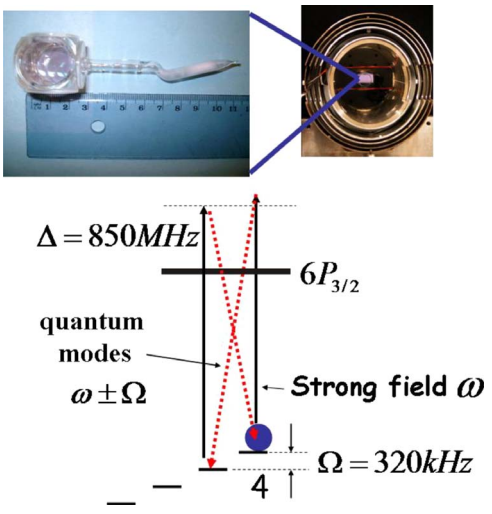

FIG. 8. (Color online) Paraffin coated cesium cell.

of thousands collisions with the cell walls before significant spin depolarization occurs. Since it is the number of collisions with walls that matters, the larger is the cell, the longer is the quantum memory lifetime. As discussed in Secs. IV–VI, quantum memory time of the order of several milliseconds has been achieved in cells with dimensions $25\times25\times25$ mm^3.

Room-temperature ensembles of cesium atoms of a few cubic cm size contain about $10^{11}-10^{12}$ atoms. For off-resonant Faraday-type interfaces the Doppler broadening does not affect the ensemble effective resonant optical depth (see Sec. VII), which is the same as for atoms at rest reaching the values of the order 50 or even higher. The experimental challenge lies with the fact that the quantum spin noise of such an ensemble is $\sqrt{N_A}^{-1}\approx10^{-6}$. In order to reach the level of the spin quantum noise, all types of technical spin fluctuations, such as driven by stray magnetic fields or fluctuations of the lasers used for optical pumping, have to be reduced below this level. The solution to this problem used in Julsgaard *et al.* (2001, 2004) and Sherson, Fiurasek, *et al.* (2006) has been to apply a bias magnetic field along the direction of the collective atomic spin. A field of the order of 1 G provides the Zeeman splitting of the ground state ω_L of a few hundred kHz. As discussed in Sec. II.E this means that the collective transverse components of the spin which correspond to the atomic canonical variables rotate at the Zeeman frequency. At the same time, as described in Sec. II.F, canonical variables of light which couple to the rotating atomic spin can be measured via homodyne detection also at the Zeeman frequency. Thus all relevant variables for light and atoms are now encoded at a frequency of a few hundred kHz. At these frequencies technical noise can be reduced below the 10^{-6} level, so that both spin and light fluctuations are dominated by quantum noise. In practice the photocurrent detected in the homodyning process is measured with lock-in amplifiers which allow access to the light variables (66) encoded at the frequency ω_L. In the experiments by Julsgaard *et al.* (2001, 2004) and Sherson, Fiurasek, *et al.* (2006), the bandwidth of the memory has been reduced to around 1 kHz as discussed in Sec. II.H.

B. Cold and trapped atoms

Cold and trapped ensembles of alkali atoms have been among the first atomic objects to be used for quantum interfaces with light. The first experiment mapping quantum properties of light onto atoms was performed with cesium atoms in a MOT, a magneto-optical trap (Hald *et al.*, 1999). A MOT provides a relatively simple way to achieve a cold atom sample suitable for the quantum interface however, it also has its limitations. A typical resonant optical depth in a MOT lies in the range between 2 and 10 which is not very high. Another consideration concerns the transverse cross section of the light beam which couples to the atoms. In most of the experiments on interfaces which use a MOT, light is focused down to a few tens of microns, which is much less than a typical MOT crossection of a millimeter (Chou *et al.*, 2004; Chaneliere *et al.*, 2005; Dantan *et al.*, 2005; Simon *et al.*, 2007; Chen *et al.*, 2008). Such geometry limits the atomic memory lifetime to the transient time it takes the atoms to leave the probe volume. For a typical MOT temperature of 100 μK this time is around hundreds of microseconds, as demonstrated by Zhao *et al.* (2009). If, on the other hand, the beam cross section is such that the light couples to the entire MOT the transient effects become irrelevant. However, in this case the number of photons in the strong driving field N_P grows proportionally to the cross section A, as evident from Eq. (61). When a photon number of the strong field is too high it becomes more difficult to implement protocols based on separating and photon counting of the quantum mode. Protocols based on homodyne detection also place limits on the maximal number of photons in the driving field. In most cases the driving field is also used as the local oscillator for homodyne detection. This implies that in order for the detection to be shot noise limited the classical fluctuations of the strong field should be suppressed to better than $N_P^{-1/2}$. In practice this places the limit $N_P\leqslant10^{10}$. For higher values of N_P modulation techniques similar to those used with thermal ensembles allow one to get down to shot noise limited detection.

Another difficulty of working with a MOT is due to the presence of gradient magnetic fields and the associated difficulty of optical pumping and magnetic state decoherence. This problem can be overcome by switching off the MOT fields, which in turn limits the lifetime of the interface, and using a clock transition as done by Zhao *et al.* (2009) where the memory lifetime up to 1 msec was achieved. An advantage of using a small subensemble of a large MOT is that a single MOT can then serve as a source of two or more atomic ensembles (Matsukevich and Kuzmich, 2004; Chen, Chen, *et al.*, 2007; Choi *et al.*, 2008).

Using a far-detuned dipole trap allows one to overcome a number of problems associated with the MOT. A dipole trap forms an atomic ensemble with a typical

transverse size of around 10–50 μm, which is a good size for the interface. The resonant optical depth can reach 20 or more. Dipole trapped atomic ensembles demonstrate coherence times exceeding 10 msec (Windpassinger *et al.*, 2008) and storage times for single excitations exceeding 100 μs (Chuu *et al.*, 2008) or even a few msec (Zhao *et al.*, 2009). Dipole trapping can also be insensitive to the magnetic quantum number and, in some cases, to the hyperfine quantum number. A detailed investigation of dipole trapped atoms as the medium for the spin squeezing and the interface is given by Oblak *et al.* (2005) and Windpassinger *et al.* (2008).

A Bose-Einstein condensate (BEC) is an attractive medium for the quantum interface due to its very high resonant optical depth. Indeed, BEC has been the medium where classical coherent storage of light, the so-called stopped light has first been first demonstrated (Liu *et al.*, 2001). It is important to note that it is not only the on-axis optical depth that defines the strength of the interface coupling. For example, a "one-dimensional" sample will not couple efficiently to a focused Gaussian beam because the diffraction of the beam means that it will not be overlapping with the ensemble if the Fresnel number is less than unity (Müller *et al.*, 2005).

One problem with a BEC-based quantum interface is the low rate at which experiments can be performed. A typical BEC requires tens of seconds to be created. Then the sample can be used for interface experiments a few times, after which a new sample should be created. BEC on a chip (Hansel *et al.*, 2001; Schneider *et al.*, 2003) offers an attractive alternative where much faster loading times can be combined with efficient optical coupling.

C. Solid state

An optically dense collection of atomlike impurities in a solid state host is an excellent candidate for the quantum interface. Both Λ schemes as well as the photon echo-based memory (see Sec. V.E) have been investigated. The absence of motion in solid state means that complex spatial structures can be generated by light and stored. Recently substantial progress has been achieved with crystals or glasses doped with rare-earth elements, such as erbium (Er), thulium (Tm), praseodymium (Pr), neodymium (Nd), and europium (Eu). The rare-earth ions doped into glass and crystal materials (REIC) display up to a second coherence times of the ground state at liquid helium temperatures. The ions experience strong inhomogeneous broadening up to 100 GHz due to local lattice fields. The technique of spectral hole burning (Nilsson *et al.*, 2004) followed by spectrally selective antihole populating allows to create a subensemble of ions with nearly natural optical transition bandwidth. A substantial optical depth can be created, although its value is usually limited by the ion-ion interaction at high density of doping. Note, however, that one cannot directly compare the measured optical depth in the presence of inhomogeneous broadening with the optical depth introduced in the theoretical derivation in Sec. II; see Sec. VII. EIT- and Raman-based memory (Longdell *et al.*, 2005) have been explored in REIC materials as well as a photon echo approach based on controlled reversible inhomogeneous broadening (CRIB) (Moiseev and Kröll, 2001; Kraus *et al.*, 2006; Staudt *et al.*, 2007; de Riedmatten *et al.*, 2008; Hétet *et al.*, 2008).

The optical Raman coupling to the nuclear spin coherence has been investigated for the past decades in REIC, mostly in praseodymium- or europium-doped crystals. These materials seem particularly suitable for the EIT- and Raman-based quantum memory protocols since they exhibit a hyperfine structure where a Λ system can be found, together with long optical coherence lifetimes, and also long hyperfine coherence lifetimes [15 msec for Eu:YSO and 550 μsec, that can be extended up to 30 sec by dynamic decoherence control techniques, for Pr:YSO (Fraval *et al.*, 2005)]. The absorption wavelength of these materials is in the domain of dye lasers (606 nm for Pr and 580 nm for Eu). In order to take advantage of their long optical coherence lifetimes, the dye laser sources must be stabilized down to less than 1 kHz. The absorption wavelength of Tm lies in the convenient range of diode lasers (793 nm). It also exhibits long optical coherence lifetimes, similar to that of Pr. It has recently been shown that it is possible to build a Λ system in thulium by applying a magnetic field in a very specific orientation (Louchet *et al.*, 2008). In rare-earth ion-doped crystals, the transitions are not polarization selective, so the only way to address them separately is to use a source whose bandwidth is smaller than the ground-state sublevel splitting. In Pr and Eu the splittings are fixed (10 and 17 MHz for Pr:YSO, 75 and 102 MHz for Eu:YSO), whereas in Tm they can be adjusted with magnetic field (36 MHz/T in Tm;YAG). The hyperfine coherence lifetime of up to 300 μsec has been measured in Tm:YAG.

Er-doped materials are studied with photon echo techniques (Staudt *et al.*, 2007). The prime interest in this ion is due to the optical wavelength in the telecom band 1.5 μm. The optical coherence lifetime of this material is very short (a few μsec at most), but can be dramatically increased by applying an intense magnetic field. The most promising results up to date have been achieved in Pr-doped crystals (Longdell *et al.*, 2005; Hétet, Longdell *et al.*, 2008).

Materials containing a high concentration of quantum dots may be interesting candidates for the ensemble-based interface. Experiments with spin polarized dots show sufficient ground state coherence times and possibility of optical pumping and quantum nondemolition coupling (Atature *et al.*, 2007). However, up to now the work with ensembles of dots has not reached quantum limits probably due to an insufficient optical depth. A different solid state medium which can be used for a quantum interface is nitrogen vacancies in diamond, where EIT has been observed by Hemmer *et al.* (2001).

D. Other possible media

Optical lattices have attracted much attention lately due to the exciting possibilities for generation of entanglement by controlled atom-atom interaction (Mandel *et al.*, 2003). The lattices can also display high optical depth since structures of up to $100\times100\times100$ atoms spaced by half a micron can be created. In the recent experiment by (Zhao *et al.*, 2009) long memory lifetimes exceeding 6 msec were achieved in a one-dimensional optical lattice. A quantum interface with such a lattice would offer an exciting possibility to transfer entanglement from atoms to light and to combine the quantum information processing capabilities of lattices with the quantum networking provided by the quantum interface. Theoretical studies of quantum interfacing of light with lattices have recently appeared (Eckert *et al.*, 2008; Muschik *et al.*, 2008) and the first EIT-based storage of classical light with the coherence time of 240 msec has been demonstrated (Schnorrberger *et al.*, 2009).

Another system where a collection of atoms can be efficiently interfaced with light is a large ion crystal in an ion trap. Very clean and large ion crystals have been created and first attempts towards achieving quantum coupling to light have been undertaken (Herskind *et al.*, 2008).

IV. ENTANGLEMENT OF ATOMIC ENSEMBLES

In this section we describe generation of entangled states of two distant macroscopic objects. The first method, which is based on QND interaction, measurement, and feedback, generates an EPR (two-mode squeezed) state of atomic spins. The second method, which relies on parametric-gain and beam-splitter interactions and single photon counting, creates Bell states in two collective spins.

van Enk *et al.* (2007) gave a useful classification of the various types of entanglement, which are generated in experiments. They distinguish *a priori* entanglement, which can be deterministically generated, *a posteriori* entanglement, which is generated probabilistically and destroyed when measured, and finally heralded entanglement, which is as well probabilistically generated, but success can be testified by measuring an auxiliary system, such that the entangled state is still available for use. Using postselection of successful cases, all types of entanglement are in principle equally useful. When combining a large number of entangled states, e.g., via entanglement swapping in a quantum network, the overall success probability will be dramatically different for a posteriori entanglement as compared to heralded or *a priori* entanglement. This observation lies at the heart of the original quantum repeater protocol (Duan *et al.*, 2001), which is based on entanglement of atomic ensembles heralded by detection of single photons, as will be described in Sec. IV.C. Our main focus in Sec. IV.B will be on the *a priori* entanglement achieved via a QND-Bell measurement and feedback on two ensembles. To introduce this method, we first explain how a single atomic ensemble can be prepared in a spin squeezed state by means of a QND interaction, homodyne detection of light, and feedback on atoms. Note that in Sec. 5.4 we describe the memory experiment (Choi *et al.*, 2008), which involves a heralded entanglement as an intermediate step.

A. Spin squeezing in a single ensemble

Spin-squeezed states of atomic ensembles were introduced by Kitagawa and Ueda (1993) in analogy to squeezed states of the radiation field and suggested by Wineland *et al.* (1992, 1994) to be of use for enhancing the sensitivity in atomic spectroscopy, Ramsey interferometry, and atomic clocks. Accordingly, Kitagawa and Ueda (1993) defined the state of a collective spin J to be squeezed if the variance of one spin component $J_\perp$ transverse to its mean polarization is smaller than the transverse variance corresponding to an atomic coherent (Bloch) state (Arecchi *et al.*, 1972), which is a product state of fully polarized atoms. With this definition, a state is squeezed if $\xi_S=\Delta J_\perp/\sqrt{J/2}<1$ and necessarily consists of correlated atoms. Wineland *et al.* (1992, 1994), on the other hand, showed that the figure of merit for the suppression of quantum fluctuations, which ultimately limit the sensitivity of atomic Ramsey interferometry, is $\xi_R=(2J)^{1/2}\Delta J_\perp/|\langle\vec{J}\rangle|<1$ and provides an alternative, stronger definition of spin squeezing.

We follow here yet another definition and refer to a spin state as squeezed if $\xi=\Delta J_\perp/(|\langle\vec{J}\rangle|/2)^{1/2}<1$, which is stronger than the definition due to Kitagawa and Ueda but weaker than the one due to Wineland *et al.*, because $\xi_R\geqslant\xi\geqslant\xi_S$ as can be easily seen. The conditions are the same for nearly fully polarized states $\langle\vec{J}\rangle\approx J$. If we take the mean polarization along x, and assume that the transverse component with minimal variance is along z, the definition of spin squeezing adopted here is

$$\Delta P_A^2<\tfrac{1}{2}, \tag{68}$$

where we use the Gaussian approximation (16). We use this definition because it immediately translates into the entanglement criterion for a bipartite state of two ensembles in Sec. IV.B.

Various ways to create squeezed states in ensembles of two-level systems were proposed. They involve direct interaction of spins (Sørensen and Mølmer, 1999; Pu and Meystre, 2000; Sørensen *et al.*, 2001; Andre *et al.*, 2002), mapping of squeezed light onto atoms (Kuzmich *et al.*, 1997; Hald *et al.*, 1999; Dantan, Cviklinski, Giacobino, *et al.*, 2006; Appel *et al.*, 2008; Honda *et al.*, 2008), multiple passes of light through atoms (Hammerer *et al.*, 2004; Takeuchi *et al.*, 2005), or a projective, Faraday interaction based QND measurement (Braginsky and Khalili, 1996), as used by Kuzmich *et al.* (1998, 2000). The main idea in the last method is that light correlated with a collective atomic spin via a Faraday interaction can be used as a meter system, reading out one of the spin components. Homodyne measurement of light, as discussed in Sec. II.F, then provides information about this spin

component, projecting the collective spin into a state with reduced fluctuations in this component.

Mean values and variances of transverse spin components conditioned on a homodyne measurement of light can be easily evaluated by means of the following classical formulas for the mean value and variance of a Gaussian random variable ξ conditioned on the measurement of another (possibly correlated) Gaussian random variable ζ with an outcome z,

$$\langle\xi\rangle|_{\zeta=z} = \langle\xi\rangle - \langle\xi\zeta\rangle z/\langle\zeta^2\rangle, \quad \Delta\xi^2|_{\zeta=z} = \Delta\xi^2 - \langle\xi\zeta\rangle^2/\langle\zeta^2\rangle.$$

If we assume that both light and atoms are initially prepared in their vacuum states, i.e., atoms are completely polarized along x, then the states of atoms and light after the Faraday interaction still have Gaussian statistics, as given by Eq. (40), and the above formulas apply. Suppose that X_L is measured on the state after the interaction with an outcome x_L. According to the formulas above, the conditional variances of atomic spin components are then given by

$$\Delta X_A^2|_{X_L=x_L} = \frac{1+\kappa^2}{2}, \quad \Delta P_A^2|_{X_L=x_L} = \frac{1}{1+\kappa^2}\frac{1}{2}, \tag{69}$$

and exhibit spin squeezing.

Conditioned on the measurement outcome x_L, P_A is squeezed with the mean value given by

$$\langle P_A\rangle|_{X_L=x_L} = \kappa x_L/(1+\kappa^2).$$

If we ignore the measurement outcome the evolution is given by Eq. (40) and there is no squeezing since P_A is conserved. If a feedback operation is applied to the atoms, e.g., by applying a pulse of magnetic field, the atomic spin can be tilted such that P_A is displaced by $-\kappa x_L/(1+\kappa^2)$, and the mean value is zero $\langle P_A\rangle=0$. The variances (69) for the (anti)squeezed variances then hold also in the ensemble average.

In Sec. II.F we introduced another method for describing the linear feedback and it is instructive to apply it here. The result x_L is fed back on atoms by displacing P_A by an amount gx_L, where g is a suitable gain factor. Using Eq. (67) and (40), the P_A component after feedback is in the ensemble average given by

$$P_{A,\text{final}} = P_{A,\text{out}} + gX_{L,\text{out}} = (1+g\kappa)P_{A,\text{in}} + gX_{L,\text{in}}. \tag{70}$$

Minimizing the variance of $P_{A,\text{final}}$ with respect to the gain g, yields an optimal feedback gain $g=-\kappa/(1+\kappa^2)$ and the reduced variance of Eq. (69), in agreement with the discussion above. An experiment along these lines has been reported by Kuzmich *et al.* (2000). Spin squeezing of 1.8 dB in the collective spin of a cold ensemble of ytterbium atoms was reported by Takano *et al.* (2009). Recently spin squeezing on atomic clock transitions has been demonstrated for cesium by Appel *et al.* (2009), with $\xi=-4.5$ dB and $\xi_R=-3.4$ dB, and for rubidium in Schleier-Smith *et al.* (2010), with $\xi_R=-3.2$ dB.

The discussion so far ignores the impairing effects of spontaneous emission and light absorption. In order to take it into account we have to resort to using Eq. (56). For the relevant case of small atomic decay, $\eta_A \ll 1$, and dominant light losses due to reflection at glass cells and detector inefficiency parametrized by ϵ ($1 \gg \epsilon \gg \eta_L$) these equations read

$$X_{A,\text{out}} = \sqrt{1-\eta_A}(X_{A,\text{in}} + \kappa P_{A,\text{in}}) + \sqrt{\eta_A} f_{X_A},$$

$$P_{A,\text{out}} = \sqrt{1-\eta_A} P_{A,\text{in}} + \sqrt{\eta_A} f_{P_A},$$

$$X_{L,\text{out}} = \sqrt{1-\epsilon}(X_{L,\text{in}} + \kappa P_{A,\text{in}}) + \sqrt{\epsilon} f_{X_L},$$

$$P_{L,\text{out}} = \sqrt{1-\epsilon} P_{L,\text{in}} + \sqrt{\epsilon} f_{P_L},$$

where we explicitly included Langevin noise operators for atoms $f_{X_A(P_A)}$ and light $f_{X_L(P_L)}$. For both systems one can to a good approximation assume vacuum properties $\langle f_\alpha f_\beta\rangle = \delta_{\alpha,\beta}/2$. Using these expressions and minimizing the variance with respect to the gain g yields a minimal variance

$$\Delta P_{A,\text{final}}^2 = \frac{1+\eta_A(1-\epsilon)\kappa^2}{1+(1-\epsilon)\kappa^2}\frac{1}{2} \geqslant \frac{\eta_A}{2}. \tag{71}$$

The bound on the achievable squeezing is not so surprising, given that the state of atoms suffered essentially a decay by a fraction η_A. Due to the relation $\kappa^2 = d\eta_A$, cf. Eq. (59), there is always an optimal choice for the decay η_A given a certain optical depth d (Hammerer *et al.*, 2004). For the decoherence model adopted here the limit to spin squeezing by QND measurement and feedback is $\Delta P_{A,\text{final}}^2 \geqslant (1+\sqrt{1+d})^{-1} \sim d^{-1/2}$, for large optical density. For a detailed discussion on the limits of spin squeezing by means of Faraday interaction and QND measurement see Bouchoule and Mølmer (2002). The limits strongly depend on the particulars of the QND scheme. For example, for the so-called two-color probing (Windpassinger *et al.*, 2008) the $1/d$ scaling of the squeezing limit is achievable.

Our description here covers only feedback where the *integrated* photocurrent of the homodyne detection is taken as the measurement result and used to correct the atomic state after the probe pulse has passed. It is of course possible to perform a continuous feedback of the photocurrent while the probe pulse is still on. An exhaustive theory for this procedure giving a description in terms of the stochastic Schrödinger equation can be found in Thomsen *et al.* (2002a, 2002b).

It is interesting to note that, beyond atomic interferometry, spin-squeezed states received renewed interest in the theory of many particle entanglement. Sørensen *et al.* (2001) showed that spectroscopic squeezing $\xi_R<1$ is a sufficient condition for bipartite entanglement within each pair of spins in the atomic ensemble, see also Wang and Sanders (2003). More general spin-squeezing inequalities were fruitfully studied in the context of experimental verification of multipartite entanglement (Sørensen and Mølmer, 2001; Korbicz *et al.*, 2005a, 2005b; Tóth *et al.*, 2007).

B. Deterministic entanglement

The procedure discussed in the previously can be applied to deterministically create entanglement between two spatially separated atomic ensembles, as proposed by Duan, Cirac, *et al.* (2000). A precursor to this proposal involving entangled light resource has been put forward by Kuzmich and Polzik (2000). Each of the ensembles is described by a collective spin $\vec{J}_i$ $(i=1,2)$, or, taking polarizations along x for both systems and adopting the Gaussian approximation, by a pair of canonical operators $[x_{A_i},p_{A_j}]=i\delta_{i,j}$. Consider a probe pulse undergoing Faraday interaction with both ensembles, first with ensemble 1 and then, after propagating some distance, with ensemble 2. By linearity, the state of light is desribed by

$$X_{L,\mathrm{out}} = X_{L,\mathrm{in}} + \kappa(P_{A_1,\mathrm{in}} + P_{A_2,\mathrm{in}}),$$

$$P_{L,\mathrm{out}} = P_{L,\mathrm{in}},$$

cf. Eq. (40). Note that for both ensembles $P_{A_i,\mathrm{out}}=P_{A_i,\mathrm{in}}$ is a conserved quantity in the Faraday interaction. Just as for the single ensemble, a measurement of $X_{L,out}$ will then give a reduced variance of the *nonlocal* observable $P_{A_1}+P_{A_2}$,

$$\Delta(P_{A_1} + P_{A_2})^2 = 1/(1+\kappa^2) < 1,$$

where the bound corresponds to uncorrelated ensembles in coherent states. Using feedback this nonlocal squeezing can be achieved unconditionally. In a second step, the spins of both ensembles are rotated by an angle of $\pi/2$ about the x axis in such a way that

$$P_{A_1} \to X_{A_1}, \quad X_{A_1} \to -P_{A_1},$$

$$P_{A_2} \to -X_{A_2}, \quad X_{A_2} \to P_{A_2}.$$

A second light pulse interacting with both ensembles as before will then read out the observable $X_{A_1,\mathrm{in}}-X_{A_2,\mathrm{in}}$, i.e.,

$$X_{L,\mathrm{out}} = X_{L,\mathrm{in}} + \kappa(X_{A_1,\mathrm{in}} - X_{A_2,\mathrm{in}}),$$

such that a measurement and feedback procedure will produce a squeezed variance of $X_{A_1}-X_{A_2}$, as before. Note that simultaneous squeezing of these two observables is possible only, because we are dealing with here commuting observables, $[P_{A_1}+P_{A_2},X_{A_1}-X_{A_2}]=0$. The counterwise rotation of the two spins about x is therefore crucial. Overall, this will produce a state which fulfills the inequality

$$\Delta(P_{A_1} + P_{A_2})^2 + \Delta(X_{A_1} - X_{A_2})^2 < 2. \tag{72}$$

Losses and decoherence will affect this result similarly as the single ensemble spin squeezing in Eq. (71). The significance of this inequality is that it constitutes a necessary and sufficient entanglement condition for symmetric (with respect to $1 \leftrightarrow 2$) Gaussian states of two systems (Duan, Giedke, *et al.*, 2000; Simon, 2000).

In the limit of large squeezing, where the variances of both nonlocal observables vanish, the corresponding state approaches the (unphysical) ideally correlated state with Wigner function $W \sim \delta(X_{A_1}-X_{A_2})\delta(P_{A_1}+P_{A_2})$, which was considered by Einstein, Podolsky, and Rosen (EPR) in their famous gedanken experiment (Einstein *et al.*, 1935), speculating about the incompleteness of quantum mechanics; see Keyl *et al.* (2003) for comments on whether and how this limit can be understood in a more rigorous mathematical sense. Because of this connection, the quantity on the left-hand side of Eq. (72) is sometimes termed EPR-Variance and denoted by Δ_{EPR}. Its importance is supported by the fact that for symmetric Gaussian states the quantity provides an entanglement measure and uniquely determines the entanglement of formation of the state (Wootters, 1998; Giedke *et al.*, 2003; Wolf *et al.*, 2004) via $E_{\mathrm{oF}} = \cosh^2(r)\log_2(\cosh^2 r) - \sinh^2(r)\log_2(\sinh^2 r)$. As follows from the discussion of losses and decoherences, we have to assume a lower limit on the EPR variance $\Delta_{\mathrm{EPR}} \gtrsim 2d^{-1/2}$and thus an upper bound on the bipartite entanglement between the two ensembles of, $E_{\mathrm{oF}} \lesssim 1.15$ ebits ($E_{\mathrm{oF}} \lesssim 2.77$ ebits) for an optical density of $d=10$ ($d=100$). A useful and comprehensive review of the theory of entanglement in systems of continuous variables was given by Adesso and Illuminati (2007), for a concise introduction to the basic facts on the same topic see Eisert and Plenio (2003).

1. Protocol with counter-rotating spins

As explained in Sec. II.E, for ensembles at room temperature containing a very large number of atoms a constant magnetic field helps to reduce technical noise, because scattered light can be detected at sideband Zeeman frequencies. In the following we show that application of an external magnetic field provides in fact an elegant and efficient way to achieve entanglement of two atomic ensembles with a single probe pulse, as demonstrated by Julsgaard *et al.* (2001).

In order to show this, we have to resort to the Maxwell-Bloch equations (65). It is straightforward to generalize these equations to the case of two atomic ensembles and to include Larmor precession of the two spins. We assume that the two collective spins precess in opposite directions, which can be achieved by either using oppositely oriented fields or by using parallel fields with atoms prepared in opposite Zeeman substates. Replacing $\omega_L \to -\omega_L$ for the second ensemble when using Eqs. (65), the equations of motion for light quadratures are

$$\frac{\partial}{\partial z}x_L(z,t) = -\frac{g^*(z)\Omega(t)}{\sqrt{2}\Delta}\{\cos(\omega_L t)[p_{A_1}(z,t) + p_{A_1}(z,t)] + \sin(\omega_L t)[x_{A_1}(z,t) - x_{A_2}(z,t)]\}, \tag{73}$$

$$\frac{\partial}{\partial z}p_L(z,t)=0.$$

Obviously light reads out sums of momenta and differences of positions, which are commuting observables for oppositely rotating spins. It will be instructive to study directly the evolution of these global observables. One finds

$$\begin{aligned}
&\frac{\partial}{\partial t}[x_{A_1}(z,t)+x_{A_2}(z,t)]=-\frac{g^*(z)\Omega(t)}{\sqrt{2}\Delta}\cos(\omega_L t)p_L(z,t),\\
&\frac{\partial}{\partial t}[p_{A_1}(z,t)+p_{A_2}(z,t)]=0,\\
&\frac{\partial}{\partial t}[x_{A_1}(z,t)-x_{A_2}(z,t)]=0,\\
&\frac{\partial}{\partial t}[p_{A_1}(z,t)-p_{A_2}(z,t)]=-\frac{g^*(z)\Omega(t)}{\sqrt{2}\Delta}\sin(\omega_L t)p_L(z,t).
\end{aligned} \tag{74}$$

The solutions fall into two groups,

$$\begin{aligned}
&X_{L_c,\mathrm{out}}=X_{L_c,\mathrm{in}}+\kappa P_{A_+,\mathrm{in}},\quad X_{L_s,\mathrm{out}}=X_{L_s,\mathrm{in}}-\kappa X_{A_-,\mathrm{in}},\\
&P_{L_c,\mathrm{out}}=P_{L_c,\mathrm{in}},\quad P_{L_s,\mathrm{out}}=P_{L_s,\mathrm{in}},\\
&X_{A_+,\mathrm{out}}=X_{A_+,\mathrm{in}}+\kappa P_{L_c,\mathrm{in}},\quad X_{A_-,\mathrm{out}}=X_{A_-,\mathrm{in}},\\
&P_{A_+,\mathrm{out}}=P_{A_+,\mathrm{in}},\quad P_{A_-,\mathrm{out}}=P_{A_-,\mathrm{in}}+\kappa P_{L_s,\mathrm{in}},
\end{aligned} \tag{75}$$

which involve nonlocal atomic variables

$$\begin{aligned}
X_{A_\pm}&=\frac{1}{\sqrt{2L}}\int dz[x_{A_1}(z)\pm x_{A_2}(z)],\\
P_{A_\pm}&=\frac{1}{\sqrt{2L}}\int dz[p_{A_1}(z)\pm p_{A_2}(z)],
\end{aligned}$$

and cosine and sine modulation modes, X_{L_c},P_{L_c} and X_{L_s},P_{L_s}, which were introduced in Eq. (66) in Sec. II.F. From the discussion of squeezing in a single ensemble it is evident that a measurement of the sine and cosine component of the X_L quadrature will produce a two mode squeezed state with reduced EPR variance (72).

2. Implementation

Experimental demonstration of deterministic entanglement of two atomic ensembles has first been reported by Julsgaard *et al.* (2001), with further developments reported by Polzik *et al.* (2003) and Sherson, Julsgaard, and Polzik (2006). The experiments have been performed with cesium vapor at temperatures in the range 15–50 °C. Atoms are contained in glass cells coated from inside with a transparent layer of paraffin (Alexandrov, 2003), as discussed in Sec. III.A. The temperature stabilized cells are placed inside cylindrical magnetic shields, see Fig. 9. Windows made in the shields allow for optical axis in two directions—one along the axis of the shield used for optical pumping and another in the radial direction used for the probe light. A solenoid produces a homogeneous axial magnetic field inside each shield. Typical cells have the near-cubic shape with the size of 25–30 mm. The magnetic field inhomogeneity is of the order of 10^{-3}. This rather modest homogeneity is sufficient since the duration of the light-atom interaction of 1 msec is sufficiently long so that the atomic motion leads to the effective time averaging of the spatially dependent Zeeman shifts. As a result the magnetic field inhomogeneity has only a quadratic effect on decoherence.

The experimental sequence begins with a few msec pulse of optical pumping along the direction of the axial magnetic field, see Fig. 9. The level scheme and frequencies of light pulses are shown in Figs. 3 and 4. The two cells are pumped with the same lasers with opposite circular polarization of optical pumping in the first and second cell. 99% or more of the atoms in $F=4$ state are pumped into the $m_F=4$ magnetic substate in one cell and into $m_F=-4$ in the other cell, as verified by the magneto-optical resonance method (Julsgaard *et al.*, 2004; Sherson, Julsgaard, and Polzik, 2006). The total angular momentum J_x of $F=4$ state is calibrated by measuring the Faraday rotation angle of a weak linearly polarized light pulse propagating in the direction of the optical pumping. After optical pumping a probe pulse linearly polarized in x-y plane is fired and its polarization rotation, i.e., the value of the operator S_y, is measured by two detectors via a balanced polarization measurement, see Fig. 5. The detected photocurrent pulse is sent into the lock-in amplifier which detects the $\cos(\omega_L t)$ and $\sin(\omega_L t)$ components X_{L_c} and X_{L_s} introduced in Sec. II.F.

The critical condition for the implementation of the deterministic interface based on homodyne mesaurements is quantum noise limited measurement of light and atoms. This is made possible by employing light and atomic detection at high frequency, typically around $\omega_L=320$ kHz. Homodyne detectors utilize silicon photodiodes with quantum efficiency more than 98–99 % and low noise photoamplifiers with the response peaked around ω_L. The photodetectors have dark noise equal to shot noise of light for the light power as low as 100 μW. This means that with a few mW probe pulse, the detection can be almost perfectly shot noise limited. Light losses have been dominated by reflection off the inner surfaces of the cell windows (the outside surfaces are antireflection coated), amounting to 15% and propagation losses from cells to detectors of about 8%.

The duration of the interaction is chosen to fulfill the condition of optimal entanglement which, analogous to the case of spin squeezing, is $\kappa_{\mathrm{opt}}^2=\sqrt{d}$ obtained with $\eta_A=1/\sqrt{d}$ [cf. Eq. (59)]. In the experiment the detuning has been chosen within the range 800–1000 MHz to be larger than the Doppler width and the hyperfine splitting of the excited state. Together with the optimal value of the optical power set by the detectors around a few mW, the above conditions lead to the minimal pulse duration of the order of a msec and the corresponding

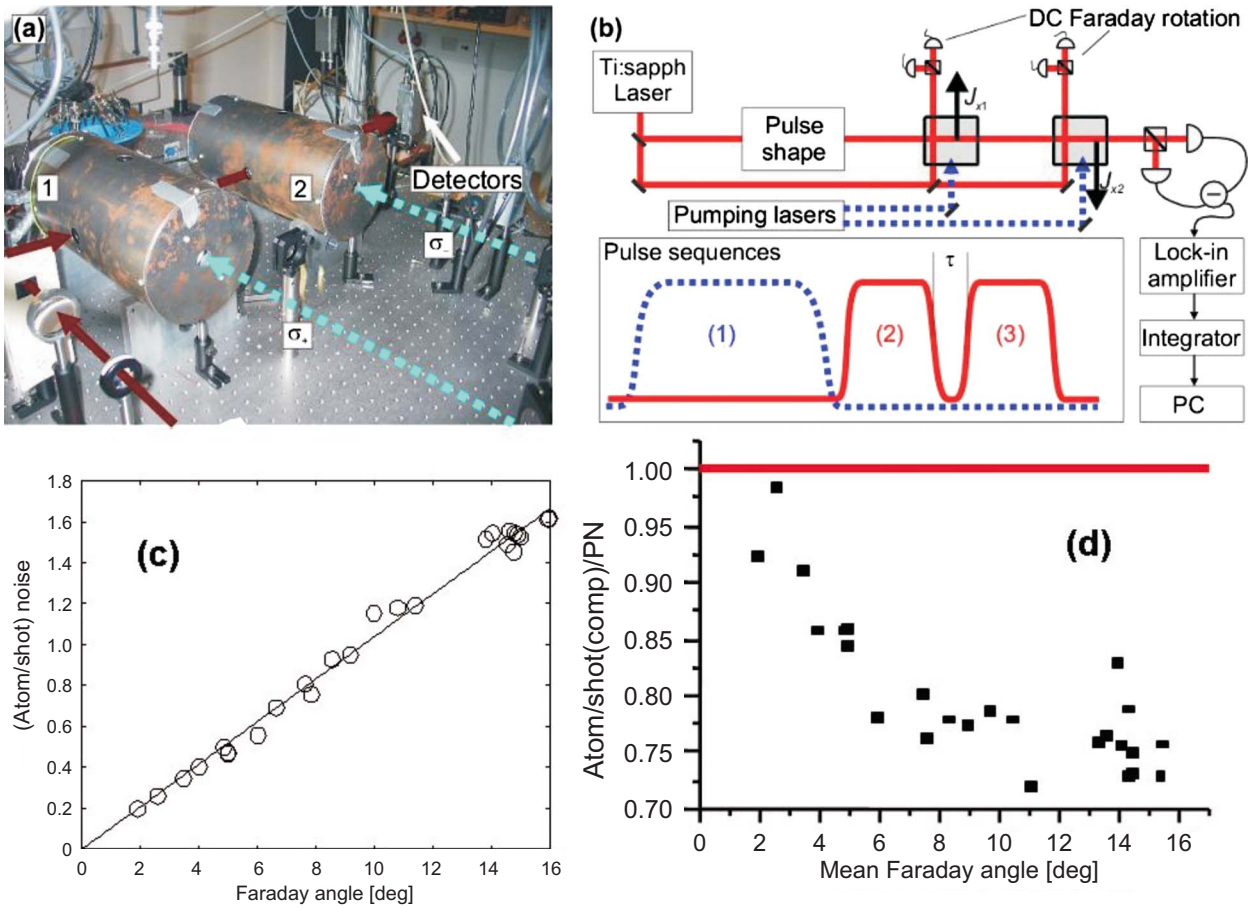

FIG. 9. (Color online) Deterministic entanglement of two atomic ensembles via QND measurement. (a) Experimental setup. Dashed lines, optical pumping; solid arrow, entangling light direction. (b) Pulse sequence and the layout of the experiment. (1) optical pumping pulse, (2) entangling pulse, (3) verifying pulse. (c) Projection noise of atoms. (d) EPR variance of the entangled state normalized to the projection noise level, i.e., to the variance for a separable coherent state of two ensembles.

bandwidth in the kHz range. This value can be in principle increased by reducing the transverse size of the sample and/or using different detectors.

The first experimental run in the presence of atoms aims at the establishment of the projection noise level of the atomic ensembles. As seen from Eq. (75) the sum variables X_{A_-}, P_{A_+} can be measured in a QND way using a single probe pulse. In the experiment the sequence of the optical pumping followed by the QND measurement is repeated several thousand times and the variance of the measured photocurrent pulses is calculated. The variance is then plotted as a function of the macroscopic spin of the sample, see Fig. 9(c). The linear dependence along with the almost perfect spin polarization proves that the spin noise is at the projection noise level. The projection noise level has been also independently calculated from the macroscopic collective angular momentum of the sample measured via Faraday rotation of the auxiliary probe pulse (Sherson, Julsgaard, and Polzik, 2006). The calculated value agreed with the measured projection noise to within 10% which is well within the uncertainty of this calculation. The projection noise level defines the right hand side in Eq. (72). When normalized to the shot noise of the probe the projection noise value is equal to the total κ^2 of the two samples according to Eq. (75).

After the projection noise level is established the experiment proceeds with generation and verification of the entangled state. In the original paper (Julsgaard *et al.*, 2001) no feedback was applied to atoms and hence a conditional entangled state was demonstrated, that is a nonlocal state with reduced variance but with a nondeterministic mean value. For possible applications, e.g., teleportation this entanglement is as good as the unconditional one because the knowledge gained with the measurement on the first entangling pulse can be applied to achieve teleportation. The creation of a deterministically and unconditional entangled state has been achieved subsequently (Polzik *et al.*, 2003). The experimental sequence which realizes such entanglement (Sherson, Julsgaard, and Polzik, 2006) involves a feedback applied to the atoms in between the two probes [Fig. 9(b)]. The feedback pulse of 320 kHz magnetic field with the cosine and sine components proportional to $X_{L_c,\mathrm{out}}$ and $X_{L_c,\mathrm{out}}$, respectively, is applied to the rf magnetic coils surrounding the cells. An appropriate electronic gain must be chosen so that the feedback pulse rotates the atomic collective spins such as to generate

the minimal EPR variance that is the minimal variance of the angle between the spins. The choice of the gain $g=-\kappa/(1+\kappa^2)$ minimizes the EPR variance in the absence of decoherence. In the experiment the optimal gain has been chosen operationally by minimizing the EPR variance [see Sherson, Julsgaard, and Polzik (2006) for details]. The results for the EPR entangled state of two atomic ensembles are shown in Fig. 9. The variance of the entangled state obtained after applying the feedback pulse is measured by the verifying pulse. Figure 9 shows this variance normalized to the projection noise variance as a function of the number of atoms. A higher number of atoms leads to a higher value of κ and hence to a higher degree of entanglement. The mimimal EPR variance observed in these experiments was $\Delta_{\mathrm{EPR}}=1.3$. This variance corresponds to an entanglement of formation of $E_{\mathrm{oF}}=0.28$ ebits.

C. Probabilistic entanglement

One of the main motivations for studies of atom light quantum interfaces is an application for quantum repeaters, which would enable long distance quantum communication (Briegel *et al.*, 1998). A protocol (also known as the DLCZ protocol) for such a repeater based on atomic ensembles and linear optics was first presented by Duan *et al.* (2001). Several improvements of the protocol have been suggested (Chen, Zhao, *et al.*, 2007; Jiang *et al.*, 2007; Sangouard *et al.*, 2007, 2008; Simon *et al.*, 2007; Zhao *et al.*, 2007). We leave the detailed discussion of the DLCZ protocol and quantum repeaters for a dedicated review. In this section we provide a basic discussion of the probabilistic entanglement generation.

The entanglement generation in the DLCZ protocol uses the parametric-gain interaction Eq. (E3) between the light and atoms as shown in Fig. 10(a). In principle this interaction could be used in the strong coupling regime ($\kappa\sim 1$ in the notation below) to generate continuous variable entanglement along the lines of the entanglement generation protocol used for quantum teleportation in Sec. VI. Instead the DLCZ protocol works in the weak coupling limit ($\kappa\ll 1$) and generates probabilistic entanglement. The first term in Eq. (E3) for a_A is the ac-Stark shift of the ground state, which can be removed by a simple rescaling, and the phase ϕ vanishes for a large detuning. In the limit of weak coupling the dynamics involves only collective operators analogous to the ones defined in Eq. (55) and is equivalent to the evolution with the ideal two mode parametric-gain evolution operator $\exp[i\kappa(a_L^\dagger a_A^\dagger+\mathrm{H.c.})/2]$. For $\kappa\ll 1$ the joint state of the collective atomic and light harmonic oscillator degrees of freedom is then

$$|00\rangle_{AL}+\frac{\kappa}{2}|11\rangle_{AL}+O(\kappa^2), \tag{76}$$

where $|mn\rangle_{AL}$ describes the state with m (n) excitations in the atomic (light) harmonic oscillator. This result can be understood rather intuitively from the level scheme in Fig. 10(a), which shows that the interaction generates simultaneous excitations of the atoms and the light as described by Eq. (76).

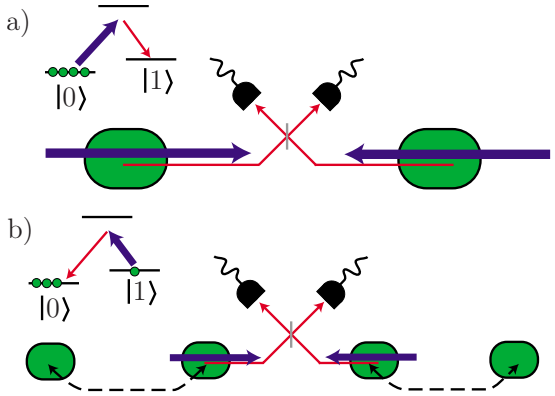

FIG. 10. (Color online) DLCZ protocol. (a) Entanglement between light and atoms is generated by a parametric gain interaction in two distant ensembles. Detection of a photon by one of the two photodetectors after the optical beam splitter probabilistically generates entanglement between the two ensembles. (b) The atomic excitation in one-half of an entangled pair of atomic ensembles (dashed line) is read out onto light with the light-atom beam-splitter interaction and mixed on an optical beam splitter with its counterpart from another entangled pair of ensembles. Photodetection swaps the entanglement so that now the outmost ensembles become entangled.

The state in Eq. (76) is in itself an entangled state, but in the DLCZ protocol it is used to probabilistically generate an entangled stated of two atomic ensembles. The outgoing light modes from two different ensembles are combined on a beam splitter as shown in Fig. 10. Conditioned on a click in one of the two photodetectors the ensembles are prepared in the state $(|01\rangle\pm|10\rangle)/\sqrt{2}$, because one cannot know from which ensemble the photon was emitted (the sign in the superposition depends on which detector detected the photon). If two pairs of ensembles are independently entangled in this fashion, as shown in Fig. 10(b), the entanglement can be extended to a larger distance. Towards this end the atomic states from the two closest atomic ensembles, each belonging to a different entangled pair, must be read out onto light modes which are mixed on another beam splitter. Detection of a photon after the beam splitter extends the entanglement to twice the distance by entanglement swapping. This read out process can for instance be done using the beam-splitter interaction as discussed in Sec. V.D. Note, however, that the atomic mode functions (29) and (32) suitable for the parametric-gain and beam-splitter interactions are different, leading to a mode mismatch if the excitations are read out in the same direction as the entanglement generation. This problem can be avoided by reading out in the backward direction (André, 2005) [this analysis assumes that the atoms retain their positions throughout the experiment; see also Duan *et al.* (2002) for a discussion of the limit, where the motion of the atoms leads to an averaging over the atomic position].

Following the initial DLCZ protocol several experiments have been performed, which demonstrate a number of important ingredients of the repeater, of which here we only mention a few. The first experiments (Kuzmich *et al.*, 2003; van der Wal *et al.*, 2003; Chou *et al.*, 2004; Matsukevich and Kuzmich, 2004) demonstrated quantum correlations in pairs of photons generated via the creation of pairs of atomic excitations and photons in Raman scattering, followed by a beam-splitter interaction converting the atomic excitations into another photon after a programmable delay. Chaneliere *et al.* (2005) and Eisaman *et al.* (2005) reported the storage and controlled release of single photons, which are deterministically created from a first atomic ensemble, in a second one via electromagnetically induced transparency. Chou *et al.* (2005), Felinto *et al.* (2006), Chaneliere *et al.* (2007), and Yuan *et al.* (2007) demonstrated the quantum interference of photons emitted from two independent atomic ensembles in Raman scattering, with Chou *et al.* (2005) proving entanglement of the two atomic ensembles. Chou *et al.* (2007) implemented an elementary link for a DLCZ-type quantum repeater as shown in Fig. 10. Other steps towards the DLCZ quantum repeater were performed by Chen *et al.* (2008), where the teleportation of photonic to atomic qubits held in an atomic ensemble has been demonstrated, and by Choi *et al.* (2008) where storage and release of photonic entanglement from two atomic ensembles has been reported.

V. QUANTUM MEMORY FOR LIGHT

Atomic quantum memory for light is an important ingredient for a number of quantum information routines. It is implicit in many quantum communication protocols, in particular in those which require local operations on more than just a single optical pulse, so that storage is necessary. It is required for linear optics quantum computing and for scalable cluster state quantum computing with photons. Quantum memory is a necessary ingredient of a quantum repeater. Different applications demand quantum memories fulfilling different requirements. Some applications, such as those which include local operations and classical communication, benefit from a high-fidelity deterministic write-in operation into the memory. By deterministic we mean a protocol which works with probability 1, so that the fidelity is calculated for every try. Others can tolerate lower probability of write in and read out, provided the success is heralded. Nonetheless, the latter protocols, such as a quantum repeater, would also benefit from deterministic write in which would lead to a higher efficiency, higher rate, and eventually to longer distances.

In this section we review several main approaches to the quantum memory for light. We first discuss a figure of merit and a classical benchmark for determining the quality of a quantum memory. We present the protocol based on a QND interaction and feedback, which demonstrates a quantum memory channel with the fidelity higher than the classical benchmark. We then discuss the memory based on the Λ scheme, concentrating on the recent achievement of the EIT-based memory experiments. We conclude with a discussion of memories based on various types of the photon echo.

A. Figure of merit

From a fundamental perspective a quantum memory can be analyzed as a quantum channel, acting in time. A perfect quantum memory is nothing but the identity map taking arbitrary states as input and returning them unchanged, some time later. A realistic memory will be imperfect and the question arises what figure of merit to use in order to evaluate its performance. One sensible measure characterizing the performance of a memory is the fidelity, i.e. the average state overlap (Nielsen and Chuang, 2000), which can be achieved between an input state drawn from a predefined set of states according to a predefined probability distribution and the state which is finally read out of the memory. The fidelity is of fundamental relevance if it exceeds the best classical fidelity, in which case the channel is thus outperforming the best classical channel. The classical fidelity relies on the simple strategy of measuring the given quantum state, storing the resulting classical data and on demand reconstructing the quantum state as good as possible.

For example, in a special case where both input and output states are Gaussian states with amplitudes $\langle X_{\mathrm{in(out)}}\rangle$, $\langle P_{\mathrm{in(out)}}\rangle$ and variances $\Delta X^2_{\mathrm{in(out)}}$, $\Delta P^2_{\mathrm{in(out)}}$ the fidelity is given by

$$F=[(\Delta X^2_{\mathrm{in}}+\Delta X^2_{\mathrm{out}})(\Delta P^2_{\mathrm{in}}+\Delta P^2_{\mathrm{out}})]^{-1/2}\times\exp\left[-\frac{(\langle X_{\mathrm{in}}\rangle-\langle X_{\mathrm{out}}\rangle)^2}{2(\Delta X^2_{\mathrm{in}}+\Delta X^2_{\mathrm{out}})}-\frac{(\langle P_{\mathrm{in}}\rangle-\langle P_{\mathrm{out}}\rangle)^2}{2(\Delta P^2_{\mathrm{in}}+\Delta P^2_{\mathrm{out}})}\right]. \tag{77}$$

In experiments the average of this fidelity can be taken with respect to a Gaussian distribution of coherent states centered at vacuum with a mean occupation number $\bar{n}$. If the average fidelity for a flat (infinitely broad) distribution of coherent input states equals unity, the memory is ideal and would also store any non-Gaussian state perfectly. This follows from the fact that coherent states provide an (overcomplete) basis for the Hilbert space.

It is worth emphasizing that the performance of a quantum memory can be, in principle, tested with coherent states only. Knowing the performance of the memory (a quantum channel) for all coherent states, which is performing a quantum tomography of the memory process with coherent states, one can predict the fidelity of the memory channel for an arbitrary class belonging to a single mode. In this sense the often used division between continuous variable memory and discrete variable memory is not quite justifiable. It is more appropriate to speak about the protocols which are based on continuous variable measurements (homodyning) and discrete variable measurements (photon counting).

The question then remains what exactly a measured average fidelity smaller than unity guarantees. The benchmark maximum fidelity of a classical channel F_{class} is known for a limited number of quantum states including qubit states and coherent states with a Gaussian distribution in phase space of width $\bar{n}$. For the latter case Braunstein *et al.* (2000) conjectured and Hammerer, Wolf *et al.* (2005) proved that

$$F_{\text{class}} = \frac{1+\bar{n}}{1+2\bar{n}} \to \frac{1}{2}, \quad \bar{n} \to \infty. \tag{78}$$

In the former case, for a class of arbitrary qubit states the maximum classical fidelity is $F_{\text{class}}=2/3$ (Massar and Popescu, 1995). Recently a classical benchmark fidelity for a third class of states, namely, the displaced squeezed states, has been found (Adesso and Chiribella, 2008; Owari *et al.*, 2008). For a class of pure squeezed states with the variance s in vacuum units, arbitrary orientation, and arbitrary displacements, the classical benchmark approaches zero for large s as $F_{\text{class}}=\sqrt{s}/(1+s)$. Quantum memory which exceeds these classical benchmark fidelities thus shows performance which is classically impossible. For similar fidelity benchmarks for finite-dimensional systems see Keyl and Werner (1999).

The fidelity is not necessarily the one and only figure of merit for a quantum memory protocol. A relatively high fidelity may still be compatible with errors which are hard to correct. On the other hand, a lower fidelity protocol with particular kinds of errors may be more appropriate for a specific application. For instance, Brask and Sørensen (2008) showed that different types of errors can have a different effect on the repeater protocol of Duan *et al.* (2001), and Surmacz *et al.* (2006) argued that in certain applications it might be more important to preserve entanglement, when one partner of an entangled pair is stored, than to conserve the quantum state itself.

For an important class of protocols discussed in Secs. V.D and V.E, the performance is theoretically described by a simple beam-splitter relation between the input and output operators $\hat{a}_{\text{out}}=\sqrt{\eta}\hat{a}_{\text{in}}+\sqrt{1-\eta}\hat{v}$, where η is the efficiency, e.g., for mapping the input light intensity to the output light intensity, and $\hat{v}$ is a vacuum operator. The memory performance is then completely characterized by the single parameter η, and quantities such as the fidelity for a given distribution of states may later be derived from it. The performance is therefore often discussed in terms of the single parameter η and we use this characterization in Secs. V.D and V.E. In an assessment of a given experiment one should, however, verify that the simple beam-splitter relation is indeed applicable for this experiment.

It is possible to define other figures of merit and also to consider different benchmarks than the one given by a classical measure and prepare strategy, in order to quantify the quality of storage—in quantum memories—but also of transmission of quantum states—as in quantum teleportation; cf. Sec. VI. For experiments with single photons, it is common to consider the conditional fidelity, which characterizes the fidelity conditioned on the detection of a photon after the interface. Since this conditioning suppresses the effect of losses, the conditional fidelity is often much higher than the unconditional fidelity discussed above. When a conditional fidelity is used, another parameter often called efficiency is introduced which describes the probability of success of the protocol. In the context of teleportation of coherent states, the question of the "right" figure of merit was subject to considerable debate; see Ralph and Lam (1998), Braunstein *et al.* (2001), Grosshans and Grangier (2001), and Bowen *et al.* (2003), and references therein. In particular, Grosshans and Grangier (2001) emphasized the importance of a benchmark $F_{1\to 2}$ given by the maximal fidelity achievable in a 1 to 2 cloning machine. For $F>F_{1\to 2}$ the memory output is guaranteed to be the best possible copy of the input state. For coherent input $F_{1\to 2}\simeq 0.68$, as shown by Cerf *et al.* (2005), and is thus more demanding than the classical fidelity benchmark F_{class}, which can also be interpreted as the maximal fidelity of a 1 to ∞ cloning machine (Hammerer, Wolf, *et al.*, 2005). Figures of merit different from fidelity were used in Ralph and Lam (1998), Bowen *et al.* (2003a, 2003b), and Hétet *et al.* (2008), to characterize both quantum storage and teleportation. There is, however, a consensus that the most sensible figure of merit ultimately depends on the specific application of the quantum memory or teleportation link within a quantum network for, e.g., quantum cryptography or optical quantum computation.

B. QND and feedback protocol

The first demonstration of a quantum memory (Julsgaard *et al.*, 2004) beating a classical benchmark (Hammerer, Wolf, *et al.*, 2005) was based on the QND-Faraday interaction of a pulse of light, carrying the quantum state to be stored, with two collective spins counter-rotating in an external magnetic field. The basic input-output equations describing the interaction are given by Eq. (75). Each of these constitutes a realization of the simpler input-output relations (40) for a pulse interacting with a single atomic ensemble without the magnetic field. For simplicity, we base the theoretical discussion of the main idea on this single ensemble setup, and return to the actual implementation based on the setup involving two atomic ensembles in the experimental part.

The input light is described by canonical operators $X_{L,\text{in}}$ and $P_{L,\text{in}}$ while the collective spin is prepared in the fully polarized state $\langle X_{A,\text{in}}\rangle=\langle P_{A,\text{in}}\rangle=0$ and $\Delta X^2_{A,\text{in}}=\Delta P^2_{A,\text{in}}=1/2$. With a choice of $\kappa=1$ in Eq. (40) the entangled state of atoms and light after the interaction is described by

$$X_{L,\text{out}} = X_{L,\text{in}} + P_{A,\text{in}}, \quad P_{L,\text{out}} = P_{L,\text{in}},$$

$$X_{A,\mathrm{out}} = X_{A,\mathrm{in}} + P_{L,\mathrm{in}}, \quad P_{A,\mathrm{out}} = P_{A,\mathrm{in}}.$$

Following the interaction the light quadrature $X_{L,\mathrm{out}}$ is measured and the corresponding measurement result ξ is fed back displacing the atomic state such that $P_{A,\mathrm{out}} \rightarrow P_{A,\mathrm{out}} - \xi$. As shown in Sec. II.F, the final transformation of the collective atomic spin in the ensemble average is given by

$$\begin{aligned} X_{A,\mathrm{out}} &= X_{A,\mathrm{in}} + P_{L,\mathrm{in}}, \\ P_{A,\mathrm{out}} &= P_{A,\mathrm{in}} - X_{L,\mathrm{out}} = -X_{L,\mathrm{in}}. \end{aligned} \tag{79}$$

This concludes the mapping of the quantum state of light onto atoms: the mean values are transmitted faithfully (apart from an unimportant phase change) as $\langle X_{A,\mathrm{out}}\rangle = \langle P_{L,\mathrm{in}}\rangle$ and $\langle P_{A,\mathrm{out}}\rangle = -\langle X_{L,\mathrm{in}}\rangle$. The operator $X_{L,\mathrm{in}}$ is mapped perfectly onto the atomic collective spin, while the operator $P_{L,\mathrm{in}}$ is mapped with the addition of one unit of vacuum operator which comes from the initial coherent state of the atomic ensemble. This latter imperfection can be remedied if the initial atomic spin state is squeezed before the memory operation, such that $\Delta X^2_{A,\mathrm{in}} \rightarrow 0$. If such squeezing operation is performed by, for example, an additional QND measurement, the fidelity of the quantum memory operation can, in principle, approach 100%.

In the experiment the quantum memory performance has been tested with a set of coherent states of light taken from a Gaussian distribution of coherent states centered at vacuum with a mean photon number $\bar{n}$. Given the measured gains and the measured variances, $\Delta X_{A,\mathrm{out}}$ and $\Delta P_{A,\mathrm{out}}$ of the state of the memory, the fidelity can be calculated as

$$\begin{aligned} F = &[\bar{n}(1-\kappa)^2 + 1/2 + \Delta X^2_{A,\mathrm{out}}]^{-1/2} \\ &\times [\bar{n}(1-g)^2 + 1/2 + \Delta P^2_{A,\mathrm{out}}]^{-1/2}. \end{aligned}$$

As discussed above, if the protocol starts with the atomic ensemble in a coherent state $\Delta X^2_{A,\mathrm{out}} = 1$, $\Delta P^2_{A,\mathrm{out}} = 1/2$, and hence $F = \sqrt{2/3} \approx 82\%$ with the choice of $\kappa = g = 1$ which is optimal for the class of arbitrary coherent states. For an unknown qubit state $(\alpha|0\rangle + \beta|1\rangle)/\sqrt{2}$ the same protocol yields the fidelity of 80% for optimal values of g and κ.

The experimental setup and the sequence of operation for writing into the quantum memory are similar to the sequence described in the section on deterministic entanglement. The quantum light mode which corresponds to the ω_L sidebands in the polarization orthogonal to the strong field now carries the quantum state of light to be mapped. The state is generated by an electro-optical modulator (EOM) as shown in Fig. 11. The quantum sidebands together with the strong pulse propagate through the atomic cells and are analyzed with the polarization homodyning technique (Fig. 5). The strong pulse thus serves a dual purpose, first as a strong driving pulse for the interaction with atoms, and second as a local oscillator for the homodyne measurement.

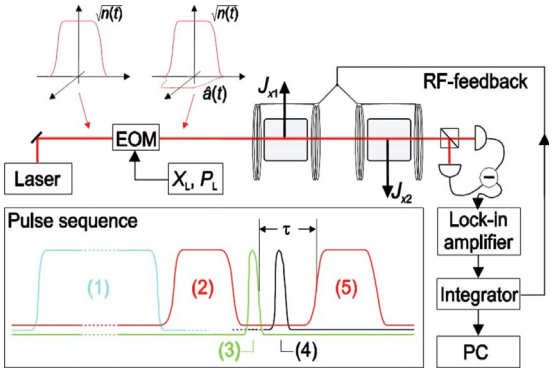

FIG. 11. (Color online) QND+feedback memory experimental setup and pulse sequence. The state of light is encoded by the EOM in the sidebands of the strong pulse $\sqrt{n(t)}$. Two cells serve as the quantum memory unit. The feedback pulse proportional to the photodetector signal is applied to the rf magnetic coils. Inset: (1) optical pumping, (2) input pulse, (3) feedback rf pulse, (4) rf pulse rotating atomic P into X used for half of verification pulses, (5) verifying pulse. From Julsgaard, Sherson, Fiurek, *et al.*, 2004.

In the experiment two cells in a magnetic field play the role of one quantum memory unit. As discussed above this approach allows one to achieve quantum limited noise for ensembles of trillions of atoms because quantum information is encoded and processed at $\omega_L = 320$ kHz sidebands where classical noise can be strongly suppressed. For two cells with magnetic field according to Eq. (75) the light variable $X_{L_c} = \sqrt{2/T}\int dt \cos(\omega_L t) x_L(t)$ should be measured and the result fed back to the atomic variable $P_{A_+,\mathrm{out}}$. The method for measuring X_{L_c} by the homodyne measurement of the Stokes parameter S_z of the light and the subsequent processing of the photocurrent by the lock-in amplifier shown in Fig. 11 is discussed in Sec. II.F, Eq. (66). Note that at the same time the variable $X_{L_s} = \sqrt{2/T}\int dt \sin(\omega_L t) x_L(t)$ can be measured and fed back into the $X_{A_-,\mathrm{out}}$ variable of atoms. The memory could hence be used as a two-mode memory, although this direction has not been pursued.

After the projection noise level of atoms is established, as described in the section on entanglement, the optimal feedback gain must be determined. The gain is chosen to optimize the fidelity for the class of states to be stored in the memory. An example corresponding to the class of coherent states distributed around vacuum with $\bar{n} = 8$ is shown in Fig. 12. The optimal values for this class of states are $\kappa = 0.8, g = 0.8$. After the memory sequence (cf. Fig. 11) is over the atomic variable $P_{A_+,\mathrm{out}}$ is measured with a strong QND verifying pulse. The quantum sideband modes of this pulse are initially in the vacuum state. After propagating through the memory the quantum sideband modes contain the atomic memory variable $P_{A_+,\mathrm{out}}$ according to Eq. (75). Figure 12 shows that the mean values of this variable for various light input states are proportional to the mean values of the input light canonical variables. As also shown in the figure the same is true for the other canonical variable of

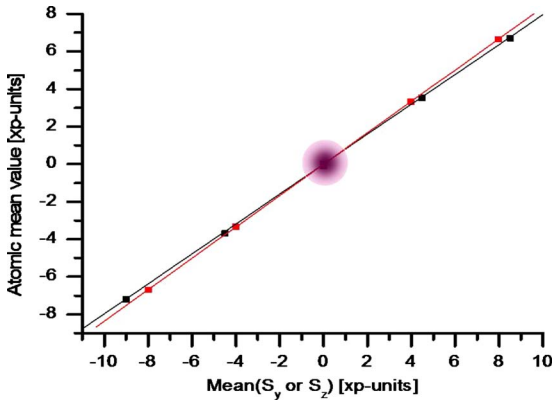

FIG. 12. (Color online) Atomic coherent memory results. The mean values for both quadratures of the input light, atomic memory, and the output light are identical to within a chosen factor (here 0.8). From Julsgaard, Sherson, Fiurasek, *et al.*, 2004.

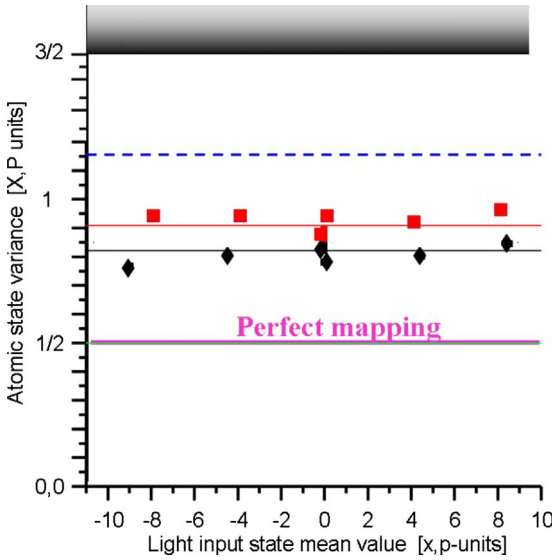

FIG. 13. (Color online) Variance of the atomic memory state for input coherent states with $n \leqslant 8$. The variance of 1/2 corresponds to the memory variance equal to the input light variance, that is, to a perfect memory. Above the 3/2 level is the classical memory performance for arbitrary coherent states. The dashed line is the best classical performance for the states within the $n \leqslant 8$ class. Diamonds and squares are experimental results from Julsgaard, Sherson, Fiurasek, *et al.* (2004).

light P_{L_c} stored in the memory variable $X_{A_+,\text{out}}$. $X_{A_+,\text{out}}$ has been measured in another experimental sequence, where an rf pulse rotating the collective atomic spins by $\pi/2$ and thus converting $P_{A_+,\text{out}}$ into $X_{A_+,\text{out}}$ has been applied before the verifying pulse (Fig. 11). The memory is thus shown to work very well as a classical memory for light since the mean amplitude and phase of the input light pulse and the retrieved light pulse are equal to within a chosen factor. Note that as a classical coherent memory this Faraday+feedback memory can have unity retrieval efficiency because the gain is adjustable, whereas for the Raman, EIT, and photon echo-based memories discussed below the efficiency is less than unity in the presence of losses.

The decisive demonstration of the quantum character of the memory follows from the analysis of the variances of the stored quantum state. Figure 13 shows the experimental variances of the state of the atomic memory for input light states with the mean photon number between zero and eight. From these values the experimental fidelity of 64% has been calculated, which is higher than the benchmark classical fidelity 52% for this class of states.

C. Multipass approaches

The Faraday+feedback quantum memory and the protocols for entanglement and spin squeezing in Sec. IV rely on a pulse of light [or two pulses in the case of Duan, Cirac, *et al.* (2000)] interacting with the medium once. It is of course possible to have a pulse of light interacting several times with one (or more) atomic ensembles, as suggested in several theoretical studies. This section provides an overview over proposals relying on multiple passes of light through atoms.

Common to all these proposals is that they take advantage of the possibility to perform phase shifts on light and to rotate atomic spins in between the passes. A relative phase shift ϕ between the classical field and the quantum field, in x and y polarization, respectively, will give rise to a rotation of field quadratures,

$$X_L \to \cos\phi X_L + \sin\phi P_L,$$
$$P_L \to \cos\phi P_L - \sin\phi X_L. \tag{80}$$

Rotation of atomic spins about the axis of polarization, via, e.g., fast rf pulses, allows for an analogous rotation of X_A and P_A. Alternatively light can be sent through atoms from a different direction. As light is sensitive to the projection of the collective atomic spin along the axis of propagation, this is equivalent to a rotation of the atoms. Especially for room-temperature atoms in a cell, optical access from two orthogonal directions can be afforded trivially, while light impinging from different sides still talks to the same symmetric mode of atoms due to thermal averaging.

The first proposal along this line is due to Kuzmich and Polzik (2003) and presents a protocol for atomic state read out, i.e., mapping of the atomic spin state onto the polarization of light. As shown in Fig. 14, in a first pass a pulse of light propagating along x interacts with atoms in a QND fashion, generating a state described by (40). A phase shift of $\phi=\pi/2$ then changes $X'_{L,\text{in}}=P_{L,\text{out}}$ and $P'_{L,\text{in}}=-X_{L,\text{out}}$, where primed variables refer to the second pass of light. The pulse is redirected to the ensemble along the negative y direction, such that the input output relations become, taking $\kappa=1$,

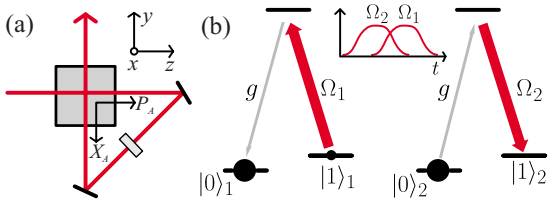

FIG. 14. (Color online) Protocols for state swapping. (a) Setup for two-pass protocol for read-out of atomic states as suggested by Kuzmich and Polzik (2003) and, with an additional magnetic field applied along x, for full state exchange or creation of entanglement between light and atoms as suggested by Muschik *et al.* (2006). (b) State swap between two ensembles coupled to a common cavity mode based on adiabatic passage as demonstrated by (Simon, Tanji, Ghosh, *et al.*, 2007). The classical pulses Ω_i are applied in a counterintuitive sequence.

$$\begin{aligned} X_{L,\text{out}} &= X_{L,\text{in}} - X_{A,\text{in}} \\ &= P_{L,\text{in}} - (X_{A,\text{in}} + P_{L,\text{in}}) \\ &= -X_{A,\text{in}}, \\ P_{L,\text{out}} &= P_{L,\text{in}} = -X_{L,\text{in}} - P_{A,\text{in}}. \end{aligned} \tag{81}$$

Aside from an unimportant phase change, the state of atoms is mapped on light. The spurious effect of light noise $X_{L,\text{in}}$ in the second line can be removed by using squeezed light. The overall input-output relations are similar to the ones for quantum memory for light in Eq. (79), but require neither measurement nor feedback.

The previous protocol naturally raises the question whether in principle a perfect state transfer, or state swapping, could be achieved in several passes and specific rotations on atoms and light without using squeezed light. Kraus *et al.* (2003) addressed this question in full generality and gave necessary and sufficient conditions for what types of quadratic Hamiltonians can be achieved in two modes, given a specific interaction—such as the Faraday interaction $\sim P_L P_A$—when combined with "local" operations of the type (80). They found that the Faraday, or QND, interaction is most capable for simulating, in this sense, other interactions, while the beam-splitter and parametric-gain interactions have no potential to emulate any other interaction. Furthermore, optimal strategies for generation of squeezing and entanglement were devised in the same paper. Fiurasek (2003) extended these results asking what types of unitary transformations (instead of Hamiltonian interactions) can be achieved and showed in particular that a perfect state swap can be performed with three passages of light, and not for less; see also Takano *et al.* (2008). Hammerer *et al.* (2004) applied these general results to the specific situation of a light-matter quantum interface, showing that atomic decay and light losses can be tolerated. See also Kurucz and Fleischhauer (2008) for a discussion of memory conditions and a comparison of these multipass approaches to Raman and EIT-based memories.

These protocols all assume a QND interaction in light and matter, which is practical for large cells with room-temperature atoms only when two cells and counter-rotating spins are used, as discussed in Sec. IV.B. This makes multiple passes with different directions of propagation a difficult issue. Another complication is due to the fact that room-temperature ensembles require msec pulses, implying an unreasonable long delay line in the loop of Fig. 14 in order to prevent the pulse meeting itself in the atomic medium. These problems were overcome by Fiurasek *et al.* (2006), Muschik *et al.* (2006), and Sherson, Fiurasek, *et al.* (2006), who showed that protocols for quantum memory and entanglement generation involving multiple passes of one or more pulses can be matched to Larmor precessing ensembles and that light traversing atoms simultaneously from different directions can in fact be advantageous. In particular, Muschik *et al.* (2006) considered a single-cell Larmor precessing in a magnetic field oriented along x in a setup as shown in Fig. 14, assuming a loop length much smaller than the pulse length, such that the pulse "meets" itself in the medium. For atoms rotating in the sense of the light propagating along the loop, solution of the corresponding Maxwell-Bloch equations, taking care of propagation effects, yields input-output relations for atomic variables,

$$X_{A,\text{out}} = e^{-\kappa^2/2} X_{A,\text{in}} + \sqrt{1-e^{-\kappa^2}}\, X^+_{L,\text{in}},$$

$$P_{A,\text{out}} = e^{-\kappa^2/2} P_{A,\text{in}} + \sqrt{1-e^{-\kappa^2}}\, P^+_{L,\text{in}},$$

where $X^+_{L,\text{in}}$, $P^+_{L,\text{in}}$ refer to a light mode centered at the upper side band frequency $\omega_0+\omega_L$ (ω_0 is the carrier frequency of the classical driving pulse and ω_L is the Larmor frequency) with a weakly exponentially decaying mode function. κ is again given by Eq. (41). An analogous input-output relation holds for light, such that this scheme realizes an exponentially efficient state exchange of atoms and light.

The Faraday interaction was achieved as a sum of the beam-splitter and parametric-gain interactions, cf. Fig. 2. What we effectively achieve by having multiple passes is that we add two Faraday interactions with different relative phases between the beam-splitter and parametric gain interactions in Fig. 2(c). A suitable choice of geometry and phase shifts leads to cancelation of the parametric-gain interactions after the two passes, and we are left with the beam-splitter interaction making an ideal memory transformation. With other configurations it is the beam-splitter interaction which cancels and the parametric gain interaction takes effect, generating an entangled state of light and atoms, whose EPR variance (cf. Sec. IV.B), scales asymptotically as $\Delta_{\text{EPR}} \sim \exp(-\kappa^2)$ (Muschik *et al.*, 2006).

D. Raman and EIT approach

The beam-splitter interaction is a quite natural choice for a quantum memory since the interaction maps excitations from light to atoms and back. The beam-splitter interaction was proposed for a quantum memory by Kozhekin *et al.* (2000) who considered the far-detuned

Raman limit $\Delta \gg d\gamma$. The same Raman limit was also considered by Nunn *et al.* (2007). Most of the attention to the beam-splitter interaction, however, came with the realization that on resonance with the atomic transition, electromagnetically induced transparency (EIT) can be used for quantum memory for light. The principles of EIT and its applications for coherent memory for light have been reviewed (Lukin, 2003; Fleischhauer *et al.*, 2005); hence we concentrate here mostly on the recent advances on quantum memory. The EIT is achieved when a strong control optical pulse renders the Λ system transparent for the signal pulse, see Fig. 1(b). This transparency is accompanied by a strong reduction in the group velocity of the signal pulse. The result is that the signal pulse entering the atomic ensemble is spatially compressed. If the compression is sufficient to make the signal pulse fit inside the sample, the control field can be turned off at this point and the signal pulse is "frozen" into the atomic ground state coherence—the dark state polariton wave. The process can be inverted by turning on the control field after some delay, which leads to the generation of a signal pulse which "remembers" the classical and quantum properties of the input signal pulse.

To see what happens in this situation now consider the $\Delta \to 0$ limit of the solution in Eqs. (46), (47), and (50). If we assume a sufficiently large incident classical driving field so that $h(0,t)z/L \gg 1$, we may use the asymptotic form of the Bessel function and write the integral kernel (47) as

$$m(\Omega;t,z) \approx \sqrt{v_g}\sqrt{\frac{d}{L}}\frac{1}{2\sqrt{2}\pi\sqrt[4]{v_g t z}}e^{-d(\sqrt{v_g t}-\sqrt{z})^2/L}, \qquad (82)$$

where we have for simplicity assumed that the classical driving field is time independent and have introduced the group velocity

$$v_g = \Omega^2 L/\gamma d. \qquad (83)$$

For a large optical depth this kernel is centered around $z=v_g t$. If the spin wave mode is slowly varying on a length scale $L/\sqrt{d}$, or if the incoming field is slowly varying on a time scale $L/\sqrt{d}v_g$, i.e., the input field is inside the EIT-transparency window (Fleischhauer *et al.*, 2005), the expression above can be approximated by a delta function $m=\sqrt{v_g}\delta(z-v_g t)$. The solutions of Eqs. (46) and (50) then become

$$\begin{aligned} a_{A,\mathrm{out}}(z) &= \frac{1}{\sqrt{v_g}}a_{L,\mathrm{in}}(T-z/v_g), \\ a_{L,\mathrm{out}}(t) &= \sqrt{v_g}a_{A,\mathrm{in}}(L-v_g t). \end{aligned} \qquad (84)$$

The first line describes the writing of the input field into the atomic memory, whereas the second one describes the read out of the atomic memory back into light. To accomplish the writing (storage) process the control field must be turned off when the entire input pulse is inside the medium, which requires $T_{\mathrm{signal}} < L/v_g$. This prompts the reduction of v_g to zero and hence "stopping" of light. The process of the read out or the retrieval is accomplished according to the second line by turning the control field on again which leads to the mapping of the atomic memory operator back onto the light operator.

Recently several experimental implementations of the EIT atomic memory (Kuzmich *et al.*, 2003; Chaneliere *et al.*, 2005; Eisaman *et al.*, 2005; Choi *et al.*, 2008) have demonstrated that such quantum features of light as violation of a Cauchy-Schwarz inequality and entanglement can be preserved by the memory. The EIT-based memory for quantum fluctuations has also been demonstrated using squeezed vacuum light in Appel *et al.* (2008) and Honda *et al.* (2008). As mentioned by Honda *et al.* (2008) a fidelity calculation along the lines of the discussion in Sec. V.A would be misleading for the case studied in these two papers since only one particular state has been used and, in addition, the overlap of this weakly squeezed state with vacuum is not far from unity. An overall efficiency of storage and retrieval of around 10–15 % has been achieved, and weakly squeezed light (around –0.2 dB) has been retrieved from the memory.

The experiments (Kuzmich *et al.*, 2003; Chaneliere *et al.*, 2005; Eisaman *et al.*, 2005; Choi *et al.*, 2008) have had a relatively low overall efficiency of the storage-retrieval process; however it did not preclude observation of the storage of nonclassical light. The reason is that the violation of the Cauchy-Schwarz inequality is based on the measurement of the normally ordered second-order correlation function $g^2(1,2) \equiv \langle :\hat{n}_1\hat{n}_2: \rangle / \langle \hat{n}_1 \rangle \langle \hat{n}_2 \rangle$ where $\hat{n}_{1,2}$ denote photon number operators measured at space-time points 1,2. $g^2(1,2)$, which describes the normalized probability of detecting a photon at point 2 conditioned on the detection at point 1, is insensitive to losses because they affect the numerator and the denominator in the same proportion. For an ideal single-photon state $g^2(1,2)=0$, whereas any $g^2(1,2)<1$ is a signature of the nonclassical character of the field which for the case of a stationary photon flux is referred to as photon antibunching.

The source of the nonclassical field used by Chaneliere *et al.* (2005), Eisaman *et al.* (2005), Matsukevich *et al.* (2006), Yuan *et al.* (2007), and Choi *et al.* (2008) has been an atomic ensemble prepared in an approximate atomic single excitation state by a weak parametric-gain interaction (see Sec. IV.C), which was then retrieved onto light by a beam-splitter process. Nonclassical states prepared in this way have been reported by Kuzmich *et al.* (2003), van der Wal *et al.* (2003), Chou *et al.* (2004), Matsukevich and Kuzmich (2004), Balić *et al.* (2005), Chaneliere *et al.* (2005), Eisaman *et al.* (2005), and Du *et al.* (2008). The sequence is similar to that described in Sec. IV.C except that only one atomic ensemble is involved at this stage. The layout of the experimental setup of Eisaman *et al.* (2005) is shown in Fig. 15. The weak parametric-gain interaction driven by the "write" classical field so that $\kappa \ll 1$ creates a single atomic excitation in the "source" ensemble conditioned on the detection of a photon in a particular spatial "Stokes" mode. The requirement of low gain $\kappa \ll 1$ is necessary so that multiphoton pulses are suppressed, which is a typi-

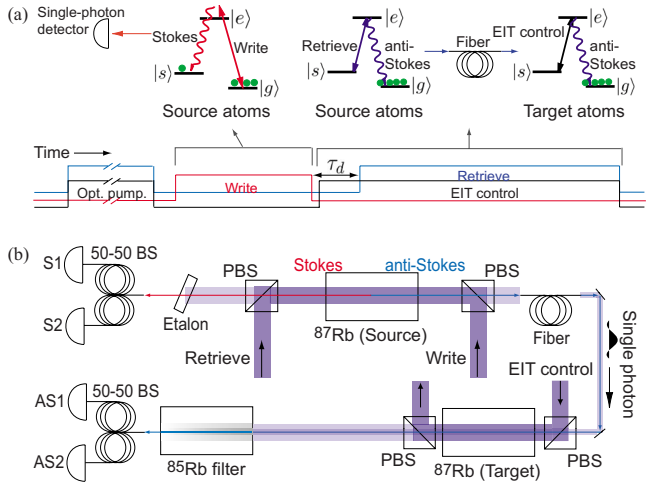

FIG. 15. (Color online) EIT-based memory setup. (a) Level scheme and sequence of control pulses. Left, parametric interaction for a probabilistic generation of an excitation in the source ensemble; center and right, EIT-based beam-splitter interactions for storage and retrieval. (b) Setup showing the source ensemble of the nonclassical photon flux and the memory ensemble (target atoms). A count in detector S1 or S2 is a condition for starting the process. Detectors AS1 and AS2 analyze the statistics of the input and output memory photons. From Eisaman *et al.*, 2005.

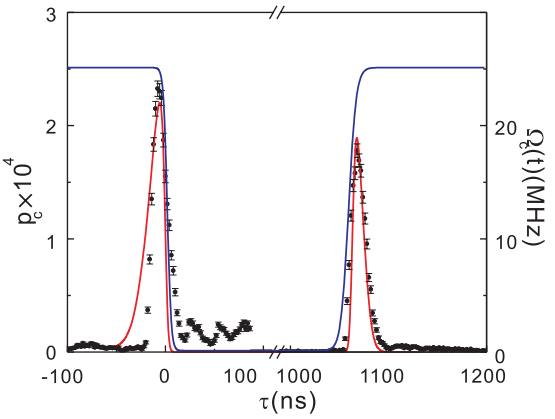

FIG. 16. (Color online) EIT-based memory. Probability of detecting a photon downstream the memory ensemble (left axis). The points around $\tau=0$, the moment when the input pulse is launched are due to the imperfect memory leading to the leakage of photons through it. The strong field (right axis) is turned off around $\tau=0$ and turned on again at $\tau=1$ μsec leading to the retrieved pulses with the overall storage retrieval probability of 17%. From Choi *et al.*, 2008.

cal situation for the parametric-type interaction. The "retrieve" strong pulse converts the atomic excitation into an "anti-Stokes" light pulse. The nonclassical character of this field is manifested by the correlation function conditional on the detection of one Stokes photon $g^2(AS\|n_S=1)<1$. This condition means that if a Stokes photon has been detected and if there is a photon in the anti-Stokes pulse, then the probability of having a second photon in the anti-Stokes pulse is less than that for a random process. In the ideal case this probability is zero and the anti-Stokes pulse contains either no photons or just a single one.

The nonclassical light pulses produced by the source ensemble are then directed towards the memory ensemble. There they are stored and retrieved using the EIT pulse sequence as shown in Fig. 16 from Choi *et al.* (2008). The figure shows the probability of detecting a photon after the storage medium. The strong "storage" driving EIT field has a constant amplitude until the quantum input pulse appears at $\tau=0$. Then the driving field is turned off leading to the storage of the light in the medium. For ideal storage there should be no counts corresponding to the input pulse. The counts around $\tau=0$ hence correspond to the "leakage" of light through the memory ensemble. After a delay time of 1 μsec the strong "read" control field is applied and the atomic excitation is read out generating a light pulse as prescribed by Eq. (50). An overall storage-retrieval probability of 17% has been shown by Choi *et al.* (2008). This experiment and the one by Chaneliere *et al.* (2005) used, Cs and Rb atoms cooled and trapped in a magneto-optical trap (MOT), respectively, whereas Eisaman *et al.* (2005) used Rb atoms in a neon buffer gas cell at room temperature. In the two former experiments a small subensemble of atoms contained within the volume of the focused optical beam inside the sample served as the memory. The storage time in these experiment was restricted by the motion of atoms and/or by magnetic field inhomogeneity to about 1 μsec. The two lower levels of the Λ system were the two ground-state $S_{1/2}$ hyperfine levels and the upper level was the $P_{3/2}$ level.

The experiment by Choi *et al.* (2008) has taken the EIT approach one step further by demonstrating it for an entangled state, more precisely for a superposition state of a photon being in one of two possible pathways (Fig. 17). In this experiment a conditional nonclassical state with $g^2(AS\|n_S=1)<1$, an approximate single photon state, was split on a beam splitter in two parts. Conditioned on the registration of the Stokes photon in the source ensemble (not shown in Fig. 17) the input consisted of a single photon with 15% probability. The rest was mostly vacuum with a small addition of a two-photon component with the probability of 9% of that for a Poisson source with the same average photon number. The input state with these properties has the concurrence of 0.10 corresponding to an entanglement of for-

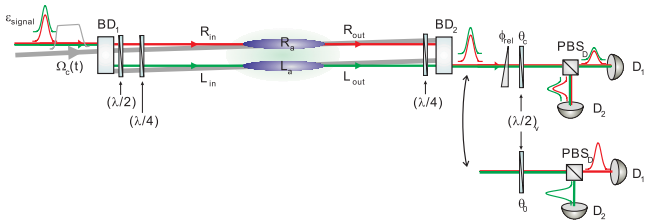

FIG. 17. (Color online) Two memory ensembles store two components of an entangled state which are later retrieved and analyzed by two pairs of coincidence detectors $D_{1,2}$.

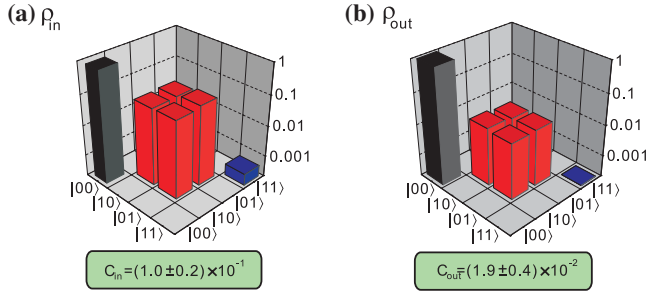

FIG. 18. (Color online) Characterization of the retrieved entangled state. The reconstructed density matrices of the input (a) and the output (b) states of the light. From Choi *et al.*, 2008.

mation of $E_{oF}=0.025$ ebits. (A concurrence of unity corresponds to $E_{oF}=1$ ebits, i.e., to a maximally entangled Bell state.) The input state was linearly polarized at 45° with respect to the polarizing beam splitter (Fig. 17). The photonic state of the two outputs of the beam splitter conditioned on the successful preparation of the single photon state is $\Psi_{in}=(|0_L\rangle|1_R\rangle+e^{i\varphi}|1_L\rangle|0_R\rangle)/\sqrt{2}$. The two components of this state have been directed into two atomic ensembles. The two ensembles were two groups of atoms within a MOT. Rb atoms were optically pumped into a particular magnetic sublevel of the ground state $F=4$, $m_F=0$ which contributed to a better performance of the memory.

After the EIT storage and retrieval steps similar to those described earlier the two retrieved components were combined on a polarizing beam splitter. With a suitable choice of the phase the state recreated from an ideal memory would make the single linearly polarized photon, just like the input one. Changing the phase between the two components of the state stored in the two ensembles by adjusting the $\lambda/2$ wave plate Choi *et al.* (2008) performed tomography of the entangled state and obtained the density matrix of it. The results of this procedure are shown in Fig. 18. From these results the concurrence of the retrieved state of 0.017 ($E_{oF}=0.001$ ebit) has been inferred demonstrating that the retrieved state has retained entanglement after the storage process.

The overall efficiency of the storage and retrieval of entanglement measured by the ratio of the concurrence of the output to the concurrence of the input is 20% after the storage time of 1.1 μsec. It is limited by the finite optical depth of the sample and can be improved by optimization of the pulse shapes.

These experiments represent exciting experimental progress; however, a higher efficiency is still desirable for future applications. Higher efficiency can be achieved with an increased optical depth, but also by optimizing the shape of the classical driving field $\Omega(t)$. This optimization problem is discussed by Gorshkov, André, Fleischhauer, *et al.* (2007), Gorshkov *et al.* (2007a, 2007b, 2007c, 2008) [see also Dantan and Pinard (2004), Dantan *et al.* (2005), Dantan, Cviklinski, Pinard, and Grangier (2006), and Nunn *et al.* (2007)]. These studies showed that for any slowly varying pulse of duration T such that $Td\gamma\gg 1$ (bandwidth $BW\ll d\gamma$) the optimal storage and retrieval efficiency is the same and is independent of the detuning from the excited atomic state. Furthermore, the optimized inefficiency depends only on the optical depth d and scales as $1/d$. These results can be understood from a new "universal" physical picture of the storage and retrieval process: First, for a given stored spin wave, the retrieval process is essentially a constructive interference effect similar to super radiance, where the radiated fields from all atoms interfere constructively in a certain direction. As a result there is a fixed branching ratio between the decay into the desired quantum field mode and the decay into all other modes, which is independent of the control field shape as long as sufficient optical power is used. Second, the optimal storage procedure is the time reversal of the retrieval procedure, and, by time reversal symmetry, the optimal storage efficiency is identical to the retrieval efficiency.

The retrieval efficiency does, however, depend on the spin wave mode, and for optimal storage the classical drive field $\Omega(t)$ has to be chosen so that it maps an incoming field mode into the optimal spin wave. This optimal field shape $\Omega(t)$ can be found by a direct calculation but an alternative experimental procedure for finding optimal shapes is demonstrated by Novikova *et al.* (2007). In this experiment which worked in the classical regime with many photons in the signal beam, the shape of the pulse to be stored was optimized for a given classical drive field. Novikova *et al.* (2007) first stored a given pulse and recorded the shape of the retrieved pulse. Then the time reverse of the recorded pulse was used as an input for the next round of storage, retrieval, and measurement. This procedure rapidly converges and yields the optimal efficiency (Gorshkov *et al.*, 2007b), which in the experiment was in the range 42–45 %. Novikova *et al.* (2008), on the other hand, used the full theoretical optimization of the classical field shape $\Omega(t)$ to store arbitrary field shapes and retrieve them into a possibly differently shaped mode with a similar efficiency.

Because the optimal strategy for storage and retrieval is based on time reversal, higher efficiency can actually be achieved if the excitation is read out in the backward direction compared to the direction of storage (Gorshkov *et al.*, 2007b). This change of direction, however, requires a redefinition of the atomic operators (29). The mode functions $u_m(z;\vec{r}_\perp)$ in Eq. (29) are solutions to the 3D Maxwell equation in the forward direction but may not be so in the backward direction. This will complicate the dynamics unless the mode function can be chosen real, which requires a Fresnel number much larger than unity [for a discussion of a related problem see André (2005)]. Furthermore a finite energy difference ω_{01} between the two ground states introduces a momentum difference $\Delta k=\omega_{01}/c$ which reduces the achievable memory efficiency unless $\Delta kL\lesssim 1$ (Gorshkov *et al.*, 2007b). A way to cope with this problem is presented by Surmacz *et al.* (2008).

For applications in a quantum network, stored excitations will have to be processed in the quantum memory. A first step in this direction was performed in recent experiments by Simon, Tanji, Ghosh, *et al.* (2007) and Simon, Tanj, Thompson, *et al.* (2007). The latter experiment involved two atomic ensembles in a medium finesse ($\mathcal{F}=240$) cavity. It demonstrated adiabatic transfer of a single excitation stored in one ensemble to the other ensemble with the cavity mode serving as a quantum bus, as well entanglement of the two ensembles by a partial transfer. First, a single excitation is generated in one ensemble by driving a weak parametic-gain interaction with subsequent detection of a Stokes photon, as described above. Conditioned on the successful generation of a single excitation in ensemble 1, beam-splitter interactions are switched on and couple both ensembles to a common cavity mode, as shown in Fig. 14(b). This is done adiabatically, first for the "empty" ensemble 2 and then for ensemble 1, in a counterintuitive sequence generating an adiabatic dark state passage $|1\rangle_1|0\rangle_2 \rightarrow |0\rangle_1|1\rangle_2$. After the transfer, the single excitation was read out from ensemble 2, demonstrating a transfer efficiency between 10% and 25%, depending on the optical depth. Simon, Tanji, Ghosh, *et al.* (2007) also demonstrated a partial swap of the excitation, generating in the ideal case an entangled state of the ensembles, $|1\rangle_1|0\rangle_2 \rightarrow \cos\theta|1\rangle_1|0\rangle_2+\exp(i\phi)\sin\theta|0\rangle_1|1\rangle_2$, where θ is controlled via the intensities and ϕ by the relative phase of the laser fields Ω_i in Fig. 14(b). Reading out the collective excitations and measuring photon correlation functions, similar to what was done by Chou *et al.* (2005), a lower bound on the entanglement of the ensembles was determined, giving a concurrence larger than 0.0046 corresponding to an entanglement of formation of $E_{\mathrm{of}} \geqslant 0.0001$ ebit (Wootters, 1998).

E. Photon echo

It has long been known that the photon echo technique (Kurnit *et al.*, 1964) could be used to store classical light pulses. Recently it has been realized that one can extend these techniques into the quantum interface domain (Moiseev and Kröll, 2001; Kraus *et al.*, 2006). If a light pulse is absorbed by an ensemble of two-level atoms, the quantum properties of light will be stored in atoms as shown in the early experiment by Hald *et al.* (1999). The problem is that for a meaningful memory the coherence time of the optical transition should be longer than the duration of the pulse. However, this means that the bandwidth of the interaction which is set by the inverse coherence time is narrower than the bandwidth of the light set by its inverse duration, so that the entire pulse cannot be stored. A solution of this problem is to use a medium with inhomogeneous broadening. Then different frequency components of the light pulse will be effectively stored in different subgroups of atoms. To avoid the dephasing of the stored state caused by the broadening a photon echo technique is used which also allows one to control the release of the stored excitation.

The essence of the photon echo approach is to have an inhomogeneously broadened line which is then reversed. In the original approach an incoming light field is absorbed by a two-level system with a broadened optical transition. Due to the inhomogeneous broadening the optical coherence from each atom precesses at different frequencies $\exp(-i\omega_i t)$. These different precession frequencies dephase the optical polarization such that it does not radiate because the radiation from different atoms interfere destructively. In the simplest version of the photon echo, a strong π pulse, which interchanges the ground and excited states, is applied after a time $T/2$. This strong π pulse effectively reverses the phase acquired by each atom such that the subsequent time evolution causes a rephasing of the optical coherence. At time T the atomic polarizations are again in phase causing an echo signal to be emitted.

A modification of the photon echo technique called controlled reversible inhomogeneous broadening (CRIB) which in principle allows an ideal memory efficiency was introduced by Moiseev and Kröll (2001) and Nilsson and Kröll (2005) and further developed by Kraus *et al.* (2006). Moiseev and Kröll (2001) considered a Λ system similar to Fig. 1(b). The photon is absorbed while an applied electric field broadens the $|0\rangle$-$|e\rangle$ absorption line. A π pulse traveling in the same (forward) direction is applied, which takes the population from the excited state to the initially empty state $|1\rangle$ for long term storage. Later on another π pulse traveling in the opposite (backward) direction is applied, which releases the excitation. During the retrieval process the broadening with the applied electric field is reversed, which reverses the time evolution resulting in an ideal retrieved signal in the backward direction, provided that the excited-state decoherence is negligible. Experimentally this scheme was realized by Alexander *et al.* (2006). Staudt *et al.* (2007) demonstrated that similar photon echo techniques can preserve the coherence of time bin qubits conditioned on having an outgoing photon. There are by now many versions of this CRIB approach, differing, e.g., by whether the broadening arises from differences in the response of the atoms to a homogeneous field (transverse broadening) or from spatially dependent broadening (longitudinal broadening). A full account of all different types is beyond the scope of this review [see, e.g., Longdell *et al.* (2008) for theoretical discussion of several different schemes].

In a recent experiment (Hétet, Longdell, *et al.*, 2008) CRIB has been implemented in a particularly elegant and simple way. A similar technique was also considered theoretically by Sangouard *et al.* (2007). In contrast to most other techniques considered here, no strong classical control pulse is required in this scheme. Hétet, Longdell, *et al.* (2008) applied a gradient electric field to the crystal used for the memory. Light interacted with Pr^{3+} ions which were doped into a Y_2SiO_5 host. Due to the gradient field the resonance frequencies of the ions at different parts of the crystal were distributed by the Stark effect within the 2 MHz bandwidth. The homoge-

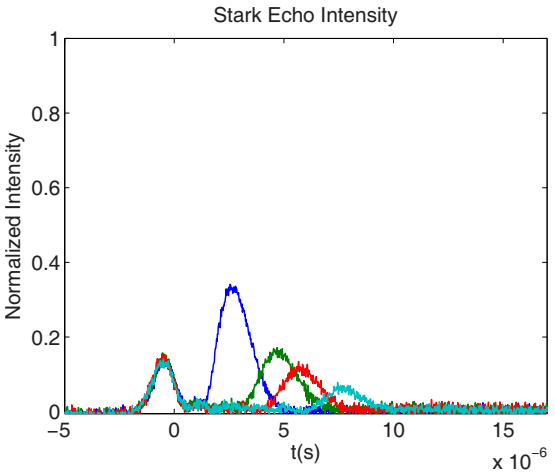

FIG. 19. (Color online) Transmitted and retrieved pulses for different storage times for an echo based memory [private communication from Hétet, Longdell, *et al.* (2008)]. The small peak at $t \approx 0$ represents a small leakage (nonstored component) of the incoming field, whereas the later peaks are the retrieved field. The emission time of these light pulses is controlled by reversing the sign of an applied electric field halfway during the storage period.

neous linewidth of the ions is 100 kHz. Hence the ions should have been in principle capable of storing a pulse of light for this time, which is 20 times longer than the pulse duration. The stored light has been released by reversing the sign of the electric field gradient. In the experiment a classical pulse of 2 μsec duration was stored for 2 μsec. An overall efficiency of the storage and retrieval of 15% has been achieved. The results for the echo memory for classical pulses are shown in Fig. 19. The figure shows the transmitted part of the input pulses (centered around zero) and stored and retrieved pulses for different storage times. All pulses are normalized to the amplitude of the input pulse.

An important question is to which extent the addition and reversal of broadening improves the memory performance compared to the other approaches considered here. For the approaches of Sangouard *et al.* (2007) and Hétet, Longdell, *et al.* (2008) a major practical advantage is that it does not rely on any classical laser fields. This, however, limits the attainable storage time to the coherence time of the optical transition, which is typically shorter than for the ground states. The advantage of reversible broadening for the storage of a single mode in the ground-state coherence was investigated by Gorshkov *et al.* (2007c, 2008) where it was found that little was gained. The situation is, however, different for the storage of multiple modes. In particular, it was found by Simon, Tanji, Ghosh, *et al.* (2007) and Nunn *et al.* (2008) that CRIB changes the scaling of the number of modes which can be stored from $\sqrt{d}$ to d, thus significantly increasing the multimode capacity. Furthermore a novel type photon echo approach using atomic frequency combs was proposed (Afzelius *et al.*, 2009). This proposal takes advantage of a large inhomogeneous broadening in a solid state system. By exploiting atoms with different resonance frequencies one can increase the effective number of atoms participating in the memory and thereby achieve an efficient quantum memory with high multimode capacity. Using this approach de Riedmatten *et al.* (2008) demonstrated the coherent mapping of light at the single photon level onto a neodymium ion doped crystal, and collective release of the stored light at a predetermined time. Moreover, this experiment demonstrated the storage of pulses in different temporal modes, proving the multimode capacity of this approach.

VI. QUANTUM TELEPORTATION BETWEEN LIGHT AND ATOMS

A. Quantum teleportation

Quantum teleportation is a means for sending quantum states from A to B in a disembodied fashion using two separate channels: a quantum channel connecting A and B and a classical one. It makes use of entanglement shared via the quantum channel and classical communication. Apart from being one of the most surprising and mind-boggling discoveries in quantum information theory, quantum teleportation has become an essential primitive in quantum computation and quantum communication.

Shortly after the first theoretical layout for quantum teleportation of states of a qubit (Bennett *et al.*, 1993) the protocol was extended to states of continuous variables (Vaidman, 1994; Braunstein and Kimble, 1998). Both sorts of protocols were first demonstrated with light, utilizing either probabilistically generated Bell states of photon pairs (Bouwmeester *et al.*, 1997) or deterministically generated EPR beams (Furusawa *et al.*, 1998), both obtained from parametric down conversion. The first teleportation involving massive particles was performed recently in the ion trap experiments at Innsbruck (Riebe *et al.*, 2004) and NIST (Barrett *et al.*, 2004). For a recent review on teleportation of states of continuous variables see Furusawa and Takei (2007).

Our focus here is on teleportation protocols involving both matter and light. In such a scenario, quantum states carried by traveling pulses of light are teleported onto a stationary quantum memory, for example, an ensemble of neutral atoms, using the quantum interface. The first realization of teleportation involving matter and light utilized the entangled state created via the quantum Faraday-QND interaction of a pulse of light with the collective spin of an atomic ensemble (Sherson, Krauter, *et al.*, 2006). In this experiment deterministic teleportation with the fidelity higher than any classical state transfer can achieve has been demonstrated. Recently probabilistic teleportation between light and matter has also been demonstrated using parametic-gain and Λ-type interactions (Chen *et al.*, 2008) and has been extended to entanglement swapping, which is the teleportation of entanglement (Yuan *et al.*, 2008).

In a nutshell, a teleportation protocol involves three steps: First, an entangled state is created and shared as a resource between two stations (usually termed "Alice"

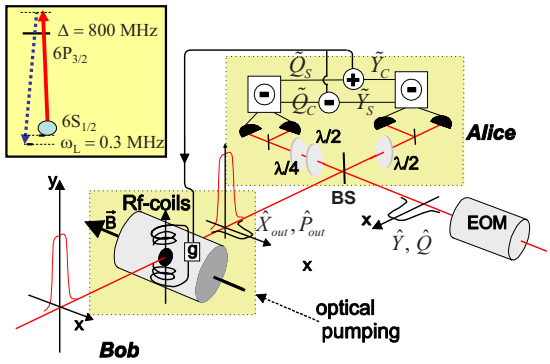

FIG. 20. (Color online) Experimental setup for the teleportation of light to atoms. Strong y-polarized pulse interacts with atoms and generates an entangled x-polarized mode at the upper sideband frequency (inset). This entangled light is overlapped with the pulse to be teleported on a 50/50 beam splitter BS after which the Bell measurements are performed. The results of the Bell measurements are fed back onto atoms via rf magnetic coils. From Sherson, Krauter, *et al.*, 2006.

and "Bob"). In the cases considered below, the entanglement between atoms (Bob) and light is generated by sending a strong driving pulse through atoms. As a result of this interaction the forward scattered photons of the orthogonal polarization sent to Alice become entangled with atoms kept by Bob as shown in Fig. 20. The ideal continuous variable EPR entanglement corresponds to $\Delta(X_A+X_L)^2=\Delta(P_A-P_L)^2\to 0$. Alice also receives another unknown quantum state described by canonical variables Y,Q sent by a hypothetical sender "Victor," which is to be teleported to Bob. For this, Alice performs a joint measurement of X_L+Y and P_L-Q, called a Bell measurement, on the photonic part of the entangled state that she has received and the unknown quantum state of light to be teleported. This measurement is performed by mixing two light pulses on a beam splitter as in Fig. 20. The results of this measurement are communicated to Bob. Bob uses this classical information to perform a correcting operation on his quantum system, atoms, by shifting $X_{A,\mathrm{fin}}=X_A+(X_L+Y)\to Y$ and $P_{A,\mathrm{fin}}=P_A-(P_L-Q)\to Q$, thereby recovering the original unknown state.

We see that in the hypothetical case of vanishing EPR variances, first and second moments and thus any Gaussian state (i.e., a state with Gaussian wave function or Wigner function) are transmitted perfectly. This in turn implies that any (non-Gaussian) state, including a qubit of the form $\alpha|0\rangle+\beta|1\rangle\in L^2(\mathbb{R})$, would be teleported faithfully, as the set of coherent states is a subset of all Gaussian states and provides a basis for the full Hilbert space $L^2(\mathbb{R})$ [for the proof of this in the Schrödinger picture and for the Wigner function, see Braunstein and van Loock (2005)]. In this sense the distinction between teleportation protocols for qubits and continuous variables is superficial. For realistic cases of imperfect teleportation where fidelity is not perfect, performance of each teleportation protocol should be evaluated in detail having in mind a particular application.

If EPR variances do not vanish, as is necessarily the case due to energy restrictions, teleportation will not be perfect, and it is necessary to evaluate the performance of the teleportation. The teleportation is essentially a protocol mapping the state of one system to another. We can therefore use the fidelity as the figure of merit as discussed in Sec. V.A, i.e., find out when the performance of the protocol becomes better than that of the best classical protocol for a given class of input states.

B. Teleportation based on Faraday interaction in magnetic field

Sherson, Krauter, *et al.* (2006) obtained the entangled state of light and atoms for teleportation via the Faraday interaction of light with a single collective atomic spin, precessing in an external magnetic field. The relevant level scheme is shown in Fig. 4 and in the inset to Fig. 20. The situation is described by the Hamiltonian and Maxwell-Bloch equations given in Sec. II.E. In this case, the Hamiltonian does not fulfil the QND criteria (Holland *et al.*, 1990; Poizat *et al.*, 1994) because the Faraday interaction H_F [cf. Eq. (34)] does not commute with the free Hamiltonian (63) describing the Zeeman splitting of ground states. In fact, as seen from the inset in Fig. 20, the interaction resembles the Raman process. The Maxwell-Bloch equations (65) were integrated by Hammerer *et al.* (2005, 2006) and the solutions are again conveniently expressed in terms of experimentally measurable cosine and sine modulation modes (66),

$$X_{A,\mathrm{out}}=X_{A,\mathrm{in}}+\frac{\kappa}{\sqrt{2}}P_{L_c,\mathrm{in}},$$

$$P_{A,\mathrm{out}}=P_{A,\mathrm{in}}+\frac{\kappa}{\sqrt{2}}P_{L_s,\mathrm{in}},$$

$$P_{L_c,\mathrm{out}}=P_{L_c,\mathrm{in}},$$

$$X_{L_c,\mathrm{out}}=X_{L_c,\mathrm{in}}+\frac{\kappa}{\sqrt{2}}P_{A,\mathrm{in}}+\left(\frac{\kappa}{2}\right)^2P_{L_s,\mathrm{in}}+\frac{1}{\sqrt{3}}\left(\frac{\kappa}{2}\right)^2P_{L_{s,back},\mathrm{in}},$$

$$P_{L_s,\mathrm{out}}=P_{L_s,\mathrm{in}},$$

$$X_{L_s,\mathrm{out}}=X_{L_s,\mathrm{in}}-\frac{\kappa}{\sqrt{2}}X_{A,\mathrm{in}}-\left(\frac{\kappa}{2}\right)^2P_{L_c,\mathrm{in}}-\frac{1}{\sqrt{3}}\left(\frac{\kappa}{2}\right)^2P_{L_{c,back},\mathrm{in}}.$$

The terms proportional to κ^2 are a new feature, specific for this setup, and represent atom-mediated backaction of light onto itself. This effect involves the previously defined cosine and sine modes as well as yet another pair of canonical independent "back-action modes" $P_{L_{c(s),back},\mathrm{in}}$, which can be treated as vacuum noise opera-

tors. To see that this interaction can be used for teleportation we inspect the EPR-type correlations between the atomic mode $X_{A,\mathrm{out}}$, $P_{A,\mathrm{out}}$ and the light mode of the upper sideband X_+, P_+ with the frequency $\omega+\omega_L$:

$$X_{L_+,\mathrm{out}} = \frac{1}{\sqrt{2}}(X_{L_s,\mathrm{out}} - P_{L_c,\mathrm{out}}),$$

$$P_{L_+,\mathrm{out}} = (1/\sqrt{2})(X_{L_c,\mathrm{out}} + P_{L_s,\mathrm{out}}).$$

One easily finds an EPR variance of

$$\Delta_{\mathrm{EPR}} = \Delta(X_{A,\mathrm{out}} + X_{L_+,\mathrm{out}})^2 + \Delta(P_{A,\mathrm{out}} - P_{L_+,\mathrm{out}})^2 = \frac{1}{2}\left[1 + \left(1 - \frac{\kappa}{2}\right)^2\right]^2 + \frac{1}{3}\left(\frac{\kappa}{2}\right)^4 \gtrsim 0.66, \tag{85}$$

where the lower bound is achieved for $\kappa \simeq 1.48$. Hence the modes of light and atoms are in an entangled state which can be used for teleportation.

The state to be teleported is encoded in the lower sideband $\omega-\omega_L$ with respect to the carrier frequency (Fig. 20), expressed in terms of measurable cosine and sine modulation modes as

$$Y = (1/\sqrt{2})(Y_\mathrm{s} + Q_\mathrm{c}), \quad Q = -(1/\sqrt{2})(Y_\mathrm{c} - Q_\mathrm{s}), \tag{86}$$

where $[Y,Q]=i$. The Bell measurement of the commuting observables after combining the entangled and the to-be-teleported states yields

$$\tilde{X}_\mathrm{c} = \frac{1}{\sqrt{2}}(X_{L_c,\mathrm{out}} + Y_\mathrm{c}), \quad \tilde{X}_\mathrm{s} = \frac{1}{\sqrt{2}}(X_{L_s,\mathrm{out}} + Y_\mathrm{s}),$$

$$\tilde{Q}_\mathrm{c} = \frac{1}{\sqrt{2}}(P_{L_c,\mathrm{out}} - Q_\mathrm{c}), \quad \tilde{Q}_\mathrm{s} = \frac{1}{\sqrt{2}}(P_{L_s,\mathrm{out}} - Q_\mathrm{s}). \tag{87}$$

Conditioned on these results the atomic state is then displaced in order to get in the ensemble average the final state

$$X_{A,\mathrm{fin}} = X_{A,\mathrm{out}} + \tilde{X}_\mathrm{s} - \tilde{Q}_\mathrm{c} = (X_{A,\mathrm{out}} + X_{L_+,\mathrm{out}}) + Y,$$

$$P_{A,\mathrm{fin}} = P_{A,\mathrm{out}} - \tilde{X}_\mathrm{c} - \tilde{Q}_\mathrm{s} = (P_{A,\mathrm{out}} - P_{L_+,\mathrm{out}}) + Q.$$

In the hypothetical case of vanishing EPR variances of $X_{A,\mathrm{out}}+X_{L_-,\mathrm{out}}$ and $P_{A,\mathrm{out}}-P_{L_-,\mathrm{out}}$ atoms would correctly display the statistics of the Y,Q mode, reproducing any input state (coherent, Fock, etc.) as desired. For the given minimal EPR variances of 0.66, that is for a variance of 0.33 in each EPR variable $X_{A,\mathrm{out}}+X_{L_+,\mathrm{out}}$ and $P_{A,\mathrm{out}}-P_{L_+,\mathrm{out}}$, teleportation will not be perfect, but still below the classical limit corresponding to the total EPR variance of 2. This discussion ignores atomic decay and light absorption which can be included as described in Sec. II.C.

The experimental implementation of this teleportation protocol by Sherson, Krauter, *et al.* (2006) was performed with a new generation of paraffin coated cells filled with cesium similar to those shown in Fig. 8. Atoms are initially prepared in a coherent spin state by a 4 msec circularly polarized optical pumping pulse propagating along the direction of the magnetic field, into the sublevel $F=4$, $m_F=4$ of the ground state (inset in Fig. 20). Then an entangled light-atom state is generated by sending a strong pulse polarized along the y axis (Fig. 20). The initially vacuum state of the x polarization of this pulse is populated after the interaction with the field $X_{L,\mathrm{out}}$, $P_{L,\mathrm{out}}$ which is entangled with the atomic variables $X_{A,\mathrm{out}}$, $P_{A,\mathrm{out}}$ according to Eq. (85). (Compared to the theoretical derivation of the Faraday interaction in Sec. II the polarizations of the classical and quantum fields are interchanged. This is of minor importance since it merely swaps the vertical and diagonal transitions in Fig. 2.)

The nearly optimal value of the coupling constant $\kappa \approx 1$ was achieved with 4×10^{13} photons in the strong pulse with the duration of 1 msec and a cross section of 4.4 cm^2 detuned by 825 MHz and a number of atoms on the order of 10^{12} corresponding to the Cs temperature of 25 °C. At Alice's location the mode of light entangled with atoms is combined with the input pulse to be teleported on a 50/50 beam splitter (Fig. 20). The strong y-polarized pulse which travels along with the entangled quantum field conveniently serves as the local oscillator for the polarization homodyne measurements of the Stokes operators S_y and S_z performed at two outputs of BS. The output $\cos(\omega_L t)$ and $\sin(\omega_L t)$ components of the photocurrent are processed by the lock-in amplifiers to produce the feedback signals $\tilde{Q}_{c,s}$, $\tilde{Y}_{c,s}$. The two feedback signals at $\omega_L=322$ kHz phase shifted by $\pi/2$ with respect to each other are fed into the rf magnetic coils surrounding the atoms with a variable electronic gain. The gain is chosen so that the atomic variables are shifted by one vacuum unit if the input light mode contains one vacuum unit of excitation. This condition corresponds to the "unity gain" teleportation.

To prove the success of the teleportation protocol a strong verifying pulse reads out the atomic operators (collective spin projections). The same homodyne polarization measurement setup is used. An example of the atomic state read out is shown in Fig. 21. A gain of 0.95 is found from the slope of the linear fit to the data, whereas variances of the final atomic state after teleportation $\Delta X_{A,\mathrm{out}}=\Delta P_{A,\mathrm{out}}=1.2$ are found from the variance of the distribution of the data. These variances are below the classical teleportation limit corresponding to three units of vacuum noise, that is to 3/2. Accordingly the fidelity of the teleportation calculated as

$$F = [\bar{n}(1-g)^2 + 1/2 + \Delta X^2_{A,\mathrm{out}}]^{-1/2}[\bar{n}(1-g)^2 + 1/2 + \Delta P^2_{A,\mathrm{out}}]^{-1/2} \tag{88}$$

for a distribution of coherent states with a width of $\bar{n}$ is greater than the best classical fidelity. Indeed the fidelities of, $F=0.60\pm0.02$ and 0.58 ± 0.02 have been obtained for sets of input states with $\bar{n}=5$ and 20, respectively, whereas best classical fidelities for these cases are 0.54 and 0.51.

As shown in the supplementary notes to Sherson, Krauter, *et al.* (2006) and in Hammerer (2006) the knowl-

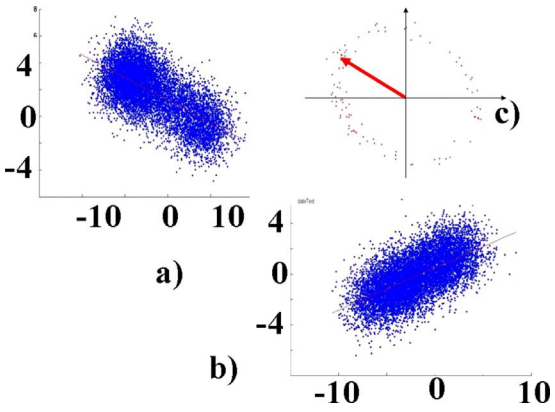

FIG. 21. (Color online) Teleportation results. (a), (b) Two canonical operators of the verifying pulse plotted as a function of the corresponding canonical operators of the input pulse for 2×10^3 realizations (vacuum units). The slope which is close to $1/2$ should be multiplied by 2 to account for the attenuation of the verifying pulse on the beam splitter. From the variances of the distributions along the vertical axis the atomic state variances and the fidelity are obtained. (c) A set of input states with $\langle n\rangle=5$ and random phases. From Sherson, Krauter, *et al.*, 2006.

edge of $\Delta X_{A,\mathrm{out}}$, $\Delta P_{A,\mathrm{out}}$ for the teleportation of the coherent states corresponds to the complete knowledge of the teleportation map and allows one to calculate the fidelity of the qubit teleportation as

$$F_q=[6+16s^2+24s^4+4(g-1)(1-2s^2)+(g-1)^2(1-6s^2)]/6(1+2s^2)^3, \quad (89)$$

where $s^2=2\Delta X^2_{A,\mathrm{out}}-1$. The quality of mapping for the two canonical operators is assumed to be equal $\Delta X_{A,\mathrm{out}}=\Delta P_{A,\mathrm{out}}$. Direct demonstration of the qubit teleportation under the conditions of Sherson, Krauter, *et al.* (2006) has not been possible due to the absence of a light qubit source with the pulse duration of 1 msec. As shown theoretically by Sherson, Krauter, *et al.* (2006), a qubit fidelity of $F_q=0.74$ is achievable for $\kappa=1$.

The protocol can in principle be improved by properly taking backaction modes, treated here simply as noise terms, into account. This is to a large extent a question of detector bandwidth and improved postprocessing of photocurrents. Hammerer, Polzik, and Cirac (2005) showed that in this way the fidelity can be increased up to 80% corresponding to half a unit of added vacuum noise. This noise stems from the initial vacuum fluctuations of light before the light-atom interaction which can in turn be reduced using a squeezed light for entanglement with atoms. One ends up with a similar situation as in the standard protocol (Vaidman, 1994; Braunstein and Kimble, 1998): the quality of teleportation is in the end limited by the amount of available squeezing, which emerges here again to be an irreducible resource (Braunstein, 2005).

A number of alternative proposals for deterministic teleportation involving light and atomic ensembles have been suggested. Horoshko and Kilin (2000) and Mišta and Filip (2005) studied the application of the state of light and atoms created in a QND interaction [cf. Eq. (40)] as a resource for teleportation and showed that the use of squeezing of light and atoms as well as unbalanced beam splitters in the Bell measurement can improve the fidelity. Teleporation of states of light to atoms, based on entanglement between motional degrees of freedom of a Bose-Einstein condensate and light, has been suggested by Paris *et al.* (2003) and Cola *et al.* (2004).

VII. ERRORS AND FIDELITY FOR DIFFERENT INTERFACES

Despite impressive successes the unconditional fidelity and/or efficiency of the quantum interfaces demonstrated so far does not exceed 70% and in many cases is at the level of 20%. Several factors, some more fundamental and some more technical, contribute to this.

A. Scaling with optical depth

In the theory section we showed that spontaneous emission can be avoided for large optical depth $d\gg1$. Here we discuss the errors due to a finite d for different approaches. In the entanglement section we showed that the single ensemble squeezing ΔP_A^2 or the two ensemble correlation Δ_{EPR} is $\sim1/\sqrt{d}$. This limit, however, depends on the exact decay mechanism, and a better scaling of single ensemble squeezing $1/d$ can be achieved if the QND interaction through phase shift measurements using two closed transitions (Sec. II.G) is used, since in this case spontaneous emission does not add noise to P_A.

For a quantum memory the inefficiency of storage with the beam-splitter interaction (Raman or EIT) scales as $1/d$ if suitably shaped spatial mode functions are used. If storing or reading out the spatially symmetric mode is preferable, as in the repeater case where the probabilistic entanglement is generated in this mode (Sec. IV.C), the scaling is again weak, $1/\sqrt{d}$ (Gorshkov, André, Fleischhauer, *et al.*, 2007; Gorshkov *et al.*, 2007b). However, a better performance can be achieved with ensembles in optical cavities (Gorshkov *et al.*, 2007a), where the scaling is $1/\mathcal{F}d$ ($\mathcal{F}$ is the cavity finesse), see in particular the experiments by Simon *et al.* (2007b, 2007c). The protocols based on the Faraday interaction naturally couple to the symmetric modes and may be better suited for this mode than the beam-splitter interaction. These memory protocols have a coupling constant $\kappa^2\sim1$, which yields $\sim1/d$ or $\sim\ln(d)/d$ (Sherson, Fiurasek, *et al.*, 2006) error due to spontaneous emission.

Different protocols are also characterized by different kinds of errors. The protocols based on the single-pass QND-Faraday interaction have variable gain, faithfully reproduce mean values of the input states, and thus give good fidelity over a large phase space. The error in the beam-splitter protocols corresponds to a loss on a beam splitter and thus gives bad fidelity for states with a large amplitude. On the other hand the low fidelity beam

splitter (Raman and EIT) protocols usually add only vacuum noise, whereas single pass QND-based protocols add multiphoton errors. Which kind of error is less harmful depends on a particular application. For instance, Brask and Sørensen (2008) showed that memories based on the single pass QND-Faraday interaction are not well suited for the DLCZ-repeater protocol (Duan *et al.*, 2001), because the repeater protocol is specifically designed to correct only for the photon loss errors. A full evaluation of the performance thus depends on the particular application one has in mind.

B. Optical losses

Losses of photons affect the performance of memory, and different memories are affected to a different extent. Clearly in the protocols insensitive to the vacuum component optical losses only lead to lower efficiency, that is to a lower probability of success. On the contrary, if the goal of a protocol is an unconditionally high fidelity, as in the case of protocols based on homodyning, optical losses directly affect the fidelity. Beside usual losses due to reflection on windows of cells and chambers which can be reduced by coating, there are losses due to absorption of light by atoms of the memory. These losses were included in our theoretical discussion in Sec. II.C, where we found that the decoherence of the quantum fields and the atoms vanished in the limit of large d. In addition one should also account for the damping of the classical fields. In Sec. II.C we also discussed that the probability of photon absorption η_L is linked to the probability of spontaneous emission of an atom η_A by $\eta_L = \eta_A N_A / N_L$, where N_L, N_A are the number of photons of the driving field and the number of atoms, respectively. If $N_L \gg N_A$ can be satisfied then the photon absorption can be made very small.

C. Inhomogeneous broadening

Another source of possible errors is inhomogeneous broadening of the optical transitions. Solid state systems have a strong inhomogeneous broadening because each of the emitters sits in a slightly different environment, while inhomogeneous broadening in room-temperature atomic ensembles is due to the Doppler broadening of the atomic lines. In the theoretical derivation we assumed only a homogeneous broadening of the optical transitions (the photon echo approach discussed in Sec. V.E is a notable exception). One therefore cannot just replace the optical depth d appearing in the formulas derived in the theory section by the measured optical depth in the presence of inhomogeneous broadening.

A detailed study of the effect of inhomogeneous broadening for a quantum memory using the beam-splitter interaction is presented by Gorshkov *et al.* (2007c) who showed that even far off resonance the inhomogeneous broadening of the line still plays a role. The reason is that the strong field leads to a considerable ac-Stark shift of the ground state $|1\rangle$ even far off resonance. The inhomogeneous broadening introduces energy shifts which are different for each atom and thus causes decoherence of the collective states. As a result the effect of inhomogeneous broadening is as severe off resonance as it is on resonance. Hence the total inefficiency of the memory protocol has two contributions. The first is the spontaneous emission which scales as $1/d_{\mathrm{hom}}$, where d_{hom} is the optical depth of the ensemble without the broadening. The second contribution is from the inhomogeneous broadening and scales as $1/d_{\mathrm{inhom}}^2$, where d_{inhom} is the actual optical depth in the presence of broadening (this scaling assumes that the broadened lines fall off sufficiently fast; for other profiles, e.g., Lorentzian, the scaling is $1/d_{\mathrm{inhom}}$). If one increases the length of the sample the system will eventually be dominated by the $1/d_{\mathrm{hom}}$ contribution and thus behaves as if it were homogeneously broadened.

The imperfections induced by inhomogeneous broadening discussed above can to some degree be reduced by taking a more *active* approach where one tries to engineer the broadening. In essence the photon echo approaches discussed in Sec. V.E provide examples of such engineering of inhomogeneous broadening, where the externally imposed inhomogeneous broadening becomes a useful resource. An interesting example of engineering of inhomogeneous broadening is presented by Afzelius *et al.* (2009), who considered engineering a frequency comb in the atomic line shape, using the hole-burning techniques discussed in Sec. III.C Essentially this allows for exploiting atoms in a solid state medium which have their resonance frequency shifted far away by inhomogeneous broadening (thus reducing the $1/d_{\mathrm{hom}}$ error discussed above), while avoiding the detrimental effects of inhomogeneous broadening (thus reducing the $1/d_{\mathrm{inhom}}^2$ error).

For the Faraday interaction the situation is different than for the beam-splitter interaction. The Faraday interaction is only employed far off resonance, and unlike the case of the beam-splitter interaction the ac-Stark shift does not cause decoherence. The strong classical light couples to both ground states and shifts them by the same amount. As a result the spin dynamics is not affected by a difference in the level shifts, and the Faraday interaction becomes insensitive to the inhomogeneous broadening for detunings much larger than the hyperfine structure of the excited state and the Doppler width.

In addition to broadening of the optical transitions, inhomogeneous broadening also affects the ground states, due to magnetic field gradients. This broadening is particularly bad because it leads to decoherence during the period when information is stored in the ground states of the ensemble, and is a major limitation for the coherence time in many experiments.

D. Atomic motion

As discussed in Sec. III the atomic motion in and out of the optical beam can severely affect the performance

of the interface. For the Faraday interaction a strong suppression of this effect is achieved in the experiments (Julsgaard *et al.*, 2001, 2004; Sherson, Krauter, *et al.*, 2006) because the light beams cover most of the atomic volume and the interaction time is much longer than the atomic transient time of flight. This suppression is, however, not perfect. As analyzed by Sherson, Krauter, *et al.* (2006) the fact that atoms move accros the interaction volume leads to extra spin noise which should be accounted for when the projection noise level is being established.

For experiments with cold atoms the atomic motion can still be of a problem, in particular when spin waves with very short wavelength are created in the memory.

E. Atomic collisions

For atomic gasses it is important also to consider the effect of atomic collisions. For experiments with paraffin coated cells atom-atom collisions contribute up to 20–40 Hz to the ground-state decoherence (Sherson, Julsgaard, and Polzik, 2006). In experiments where a buffer gas is used to suppress atomic motion, the alkali atom–buffer gas collisions often have little effect on the ground-state coherence of the atoms and the memory time. The buffer gas does, however, change the dynamics during the interaction with the light. The homogeneous broadening due to collisions with the buffer gas can be included in the theory by modifying the homogenous linewidth γ (Erhard and Helm, 2001). At the same time collisions change the velocity of the atoms and thereby their Doppler shift. The collisions thus change the phase spreading which causes decoherence of the collective states from being ballistic to diffusive, and this reduces the inefficiency from the inhomogeneous broadening.

For the write stage of the probabilistic entanglement protocol a different effect related to the collisional broadening has been observed by Manz *et al.* (2007) and discussed theoretically in a different context (Childress *et al.*, 2005). The collisions with buffer gas atoms cause the alkali atoms to emit photons at the resonance frequency of the atoms rather than at the anti-Stokes frequency. To observe the entanglement it is thus necessary to filter out these incoherent photons with a frequency filter. This effect, however, has little consequences for other protocols.

F. Geometry of the ensemble

In most cases the two ground states of the ensemble are nondegenerate, so there is an additional phase factor $\exp[i(k_0'-k_0)z]$ associated with the difference of the k vectors for the classical and quantum fields. This phase can be absorbed into the definition of the mode functions $u_m(\vec{r},t)$ in Eqs. (29) and (32), and does not play a role for the beam-splitter and parametric-gain interactions applied separately. However, if one reads out the memory in the backward direction, which is sometimes advantageous, or combines the two protocols, the atomic operators should be redefined and this phase can have a detrimental effect (Duan *et al.*, 2002; André, 2005; Gorshkov *et al.*, 2007b; Surmacz *et al.*, 2008), see also Sec. V.D. For the Faraday interaction on the other hand, the mode functions must have a constant phase and this means that the atomic ensemble must be much smaller than the wavelength corresponding to the ground-state splitting. In practice this wavelength varies from $\sim$100 m in case of Zeeman splitting with $B\simeq 1$ G to $\sim$3 cm in case of hyperfine splitting. In addition the Fresnel number corresponding to the shape of the atomic ensemble must be large in order to stay within a single transverse spatial mode approximation for the Faraday interaction.

G. Deviation from a two-level ground-state model

When the ground-state level used for the interface is magnetically degenerate with more than two states and the detuning of the strong field is not sufficiently larger than the hyperfine splitting of the excited state, the interaction of the Faraday type (a_1 vector term in Sec. II.D) is modified with the Raman interaction (a_2 tensor term). The Hamiltonian becomes $\hat{H}=\chi_{\mathrm{BS}}\hat{a}_L\hat{a}_A^\dagger+\chi_P\hat{a}_L\hat{a}_A$ +H.c. Various aspects of this effect have been considered by Julsgaard (2003), Kupriyanov *et al.* (2005), and Sherson, Julsgaard, and Polzik (2006), as well as by Geremia *et al.* (2006). Whereas in early work this effect was considered as a source of imperfections, lately it became a subject of intensive studies as a new resource for interfaces (Wasilewski *et al.*, 2009).

The beam-splitter interaction (EIT) experiments mostly use two ground hyperfine levels. Magnetic degeneracy leads to imperfections which can be reduced by careful optical pumping and polarization filtering (Choi *et al.*, 2008).

VIII. OUTLOOK

The light-matter quantum interface, a term coined in the end of 1990s, is one of the pillars of the field of quantum information processing and communication (Zoller *et al.*, 2005). In less than a decade since the first demonstrations of a quantum interface between light and an atomic ensemble the ensemble approach has become one of the most active areas of research in the field. The interactions which seem most promising for interfaces at the moment are discussed in this review: the QND-Faraday and Raman interactions, EIT, and photon echo.

Both fundamental and application driven aspects are obvious within this approach. One of the interesting fundamental issues concerns the multiparticle entanglement necessarily present in the ensemble-based approach. At the same time the interface is a kind of a quantum channel, hence its relation to the theory of quantum channel capacity should be explored in the future. This issue is connected to the fidelity of the interface since it is known that a quantum channel with $F>2/3$ for coher-

ent states has a nonzero quantum capacity (Grosshans and Grangier, 2001; Wolf *et al.*, 2007). Quantum interface also allows for storing optimal quantum clones of a state of light as proposed by Fiurasek *et al.* (2004). Another feature which is intrinsic for the ensembles of atoms is their multimode capacity. This multimode capacity comes in the form of different temporal light shapes which are mapped into different longitudinal or spectral atomic modes (Fleischhauer and Lukin, 2002; Simon, de Riedmatten, *et al.*, 2007; Nunn *et al.*, 2008; Afzelius *et al.*, 2009) as well as different transverse modes or "quantum holograms" (Surmacz *et al.*, 2008; Vasilyev *et al.*, 2008), see also Tordrup *et al.* (2008). Along the lines of the latter the first experiments demonstrating storage of classical images via the EIT approach have recently appeared (Shuker *et al.*, 2008; Vudyasetu *et al.*, 2008).

Long-distance quantum communication is one of the most actively pursued applications of the interface at the moment. It is based on the combination of probabilistic entanglement generation and deterministic entanglement swapping—a quantum repeater with atomic ensembles (Duan *et al.*, 2001)—which may serve as the basis for a "quantum internet" (Kimble, 2008). New applications for quantum memories and interfaces, such as, e.g., quantum voting and surveying (Hillery *et al.*, 2006; Vaccaro *et al.*, 2007), should be explored.

Advanced architectures for quantum computing may be enabled by highly efficient photon-based connections between small scale atomic processing nodes (Jiang *et al.*, 2007). An interesting direction in this respect is the combination of photon counting and QND-Faraday continuous variable measurement techniques. It allows one to combine the high efficiency of the homodyne measurement and the non-Gaussian states, such as Schrödinger cat states which can be generated by photon counting (Massar and Polzik, 2003; Genes and Berman, 2006). Progress along these lines depends critically on the development of highly efficient photon counters and photon number resolving detectors (Achilles *et al.*, 2004; Waks *et al.*, 2006).

For new applications of quantum interfaces a major challenge for experimentalists will be to improve the fidelity and efficiency of the interface, and for theorists to find protocols where atomic memories with the fidelity and efficiency at the level of 90–95 %—the likely levels to be achieved within the next few years—can help to achieve goals impossible with classical interfaces.

Besides the fiducial write and read processes and long storage times, a quantum interface between light and matter will likely have to show yet another key element: the possibility to process stored quantum information and to allow for quantum logical gate operations for active entanglement purification and error correction (Dür and Briegel, 2007). Theoretical studies of the requirements on gate operations in quantum repeater architectures have been performed in great detail by Briegel *et al.* (1998), Dür *et al.* (1999), Klein *et al.* (2006). Hartmann *et al.* (2007), and Dorner *et al.* (2008), recently investigated the usage of decoherence free subspaces in quantum communication. Proposals for ensemble-based implementations unifying an efficient light matter interface, stable quantum memory and reliable small scale quantum processors are rare. A number of theoretical studies suggest gate operations on stored collective excitations via a Rydberg blockade mechanism (Lukin *et al.*, 2001; Brion *et al.*, 2007; Petrosyan and Fleischhauer, 2008; Pedersen and Mølmer, 2009), via an EIT enhanced optical nonlinearity (Lukin and Imamoglu, 2001; Ottaviani *et al.*, 2003; André *et al.*, 2005; Wang *et al.*, 2006), or in hybrid systems, such as in Rabl *et al.* (2006), where a Cooper pair box serves as a saturable, nonlinear element. Initial experiments along those lines are in progress.

Efficient ensemble-based quantum memories and matter-light interfaces—small scale quantum processors for error correction, repeaters, possibly satellite-based quantum communication (Aspelmeyer *et al.*, 2003; Pfennigbauer *et al.*, 2005), and even hybrid systems (Hammerer *et al.*, 2009)—are the goals of today. The research performed towards this end is both of fundamental interest for our understanding of quantum physics and of technological importance. Its highly interdisciplinary character encompasses a broad spectrum of fields in physics as well as in computer science and information theory.

ACKNOWLEDGMENTS

We are grateful to our colleagues with whom we have had collaboration and many useful discussions on the subject of quantum interfaces over the past years. In particular we would like to thank N. Cerf, J. I. Cirac, J. Fiurášek, M. Fleischhauer, A. V. Gorshkov, H. J. Kimble, D. Kupriyanov, A. Kuzmich, M. Lukin, S. Massar, K. Mølmer, J. H. Müller, I.V. Sokolov, R. Walsworth, and P. Zoller. E.S.P. would like to especially thank the enthusiastic and talented members of his experimental team for whom the quantum interface has been a buzz word for the last decade. We acknowledge the financial support by the Danish National Research Foundation, by the Sixth and the Seventh Framework Programmes for Research of the European Commission under Future and Emerging Technologies (FET) grant agreements COVAQUIAL, QAP, COMPAS, CONQUEST, EuroSQUIP, and HIDEAS (Grant No. FP7-ICT-221906), by the Austrian FWF through SFB FOQUS and by the Institute for Quantum Optics and Quantum Information of the Austrian Academy of Sciences.

APPENDIX A: ADIABATIC ELIMINATION

The effective ground-state Hamiltonian can be obtained by adiabatic elimination. We start with the dipole Hamiltonian $H_{\rm int}=-\vec{E}\cdot\vec{D}$. For magnetic sublevels $\{|g_m\rangle\}$ all matrix elements of the ground-state dipole operator vanish $\langle g_m|\vec{D}|g_{m'}\rangle=0$, and similarly for the excited state $\langle e_m|\vec{D}|e_{m'}\rangle=0$. Introducing positively and negatively oscillating components $\vec{D}=\vec{D}^{(+)}+\vec{D}^{(-)}$ and $\vec{E}=\vec{E}^{(+)}+\vec{E}^{(-)}$ we obtain in the rotating wave approximation

$$H_{\rm int} = -(\vec{E}^{(-)} \cdot \vec{D}^{(+)} + \vec{D}^{(-)} \cdot \vec{E}^{(+)}), \tag{A1}$$

where the first (second) term describe down (up) transitions. Expanding the Hamiltonian we obtain

$$H_{\rm int} = -\sum_{m,m'} \vec{E}^{(-)} \cdot \vec{D}^{(+)}_{mm'} |g_m\rangle\langle e_{m'}| + \text{H.c.} \tag{A2}$$

Using the Hamiltonian $H_{\rm A}+H_{\rm int}$ we obtain

$$\frac{d}{dt}|g_m\rangle\langle e_{m'}| = -i\Delta_{m'}|g_m\rangle\langle e_{m'}| + i\vec{E}^{(+)}\sum_{m''}(\vec{D}^{(-)}_{m',m''}|g_m\rangle\langle g_{m''}| - \vec{D}^{(-)}_{m'',m}|e_{m''}\rangle\langle e_{m'}|). \tag{A3}$$

For weak excitation (far below saturation) we can neglect the excited-state operator $|e_{m''}\rangle\langle e_{m'}|$. Next, assuming the dynamics is slow compared to the detuning Δ, we ignore the left-hand side compared to the first term on the right-hand side. These approximations are valid provided that $\vec{E}^{(+)} \cdot \vec{D}^{(-)}_{m,m'} \ll \Delta_{m'}$. In this limit we obtain

$$|g_m\rangle\langle e_{m'}| \approx +\sum_{m''} \frac{\vec{E}^{(+)} \cdot \vec{D}^{(-)}_{m',m''}}{\Delta_{m'}} |g_m\rangle\langle g_{m''}|. \tag{A4}$$

To obtain an effective ground-state Hamiltonian we substitute Eq. (A4) into the Hamiltonian $H_{\rm A}+H_{\rm int}$. Note that we have to choose normal ordering of the operators in Eq. (A2) when we insert Eq. (A3). A detailed discussion may be found in Barnett and Radmore (1997). Second, since the terms in H_A involve the excited-state population one could be tempted to ignore it since the population is proportional to $1/\Delta_m^2$. On the other hand, there is also a factor Δ_m in front of this term, so that in total this is on the order of $1/\Delta_m$ and we have to include it. To treat this term we introduce any intermediate state $|g_0\rangle$

$$|e_{m'}\rangle\langle e_{m'}| = |e_{m'}\rangle\langle g_0| \cdot |g_0\rangle\langle e_{m'}| \tag{A5}$$

and substitute the result (A4) for $|g_0\rangle\langle e_{m'}|$. By doing this we arrive at the effective Hamiltonian in Eq. (25).

APPENDIX B: THREE-DIMENSIONAL HAMILTONIANS

We present the general Eq. (27) for the full three-dimensional Hamiltonian. In this appendix we discuss the 3D Hamiltonians for the three-model system, beams-splitter, parametic-gain, and Faraday interaction.

First we consider the atomic beam-splitter interaction in Fig. 2(a). We assume that the state $|1\rangle$ is coupled to an excited state by a classical field, so that $\vec{E}(\vec{r}) = \langle \vec{E}(\vec{r}) \rangle$. Inserting the expression for the quantized electric field into Eq. (12) we obtain

$$H_{BS} = \int d^3\vec{r} \left[\frac{-|\Omega(\vec{r},t)|^2}{4\Delta} a_A^\dagger(\vec{r}) a_A(\vec{r}) - \frac{|g(\vec{r})|^2}{\Delta} \sum_m |u_m(\vec{r}_\perp;z)|^2 a^\dagger_{L,m}(z) a_{L,m}(z) - \sum_m \left(\frac{g^*(\vec{r})\Omega(\vec{r},t)}{2\Delta} u^*_m(\vec{r}_\perp;z) a^\dagger_{L,m}(z) a_A(\vec{r}) + \text{H.c.} \right) \right], \tag{B1}$$

where the coupling constant $g(\vec{r})$ and resonant Rabi frequency are defined as in Eq. (31) except with z replaced by $\vec{r}$. The first term in this Hamiltonian is the ac Stark of the ground state caused by the classical field, the second term is the change in the index of refraction that the quantum field experiences, and the last term represents the exchange of excitation between the light and ground-state coherence. We have here ignored the small ac-Stark shift caused by the weak quantum field.

In case of the parametic-gain interaction shown in Fig. 2(b), the fields interact to the transitions which are flipped compared to the case of the beam-splitter interaction. The emission of a photon is therefore coupled to an atomic transition in the opposite direction and we obtain the parametric Hamiltonian by making the replacement $a_A(\vec{r}) \leftrightarrow a_A^\dagger(\vec{r})$ in the coupling between atoms and light. In addition, the effective ac-Stark shift has the opposite sign. The Hamiltonian thus reads

$$H_G = \int d^3\vec{r} \left[\frac{|\Omega(\vec{r},t)|^2}{4\Delta} a_A^\dagger(\vec{r}) a_A(\vec{r}) - \sum_m \left(\frac{g^*(\vec{r})\Omega(\vec{r},t)}{2\Delta} u^*_m(\vec{r}_\perp;z) a^\dagger_{L,m}(z) a_A^\dagger(\vec{r}) + \text{H.c.} \right) \right]. \tag{B2}$$

There is no index of refraction here since now the quantum field couples to the almost empty transition. On the other hand, the classical field now sees the atomic population, and we should include the index of refraction in the propagation of the classical light, which enters through the phase of Ω.

For the Faraday interaction we assume a strong x-polarized classical field, and consider the quantum field in the y polarization as shown in Fig. 2(c). There are now two paths which lead to creation of a photon: photon creation (or absorption) can appear both through the creation and annihilation of an atomic excitation. As discussed in the main text the Faraday interaction is a combination of the two Hamiltonians in Eqs. (B1) and (B2) with equal weights. For the 1/2-1/2 transition shown in Fig. 2, however, the two paths leading to the creation of a photon have opposite signs due to the Clebsch-Gordon coefficients. The coupling constant g is defined for circularly polarized light, so we should include a factor of $\sqrt{2}$ coming from the expansion of the y-polarized quantum field in the circular polarization basis. The Hamiltonian is then given by $H_F = (H_{\rm BS} - H_G)/\sqrt{2}$.

For the spin 1/2 system classical and quantum fields experience the same index of refraction, so we can remove the index of refraction from $H_{\rm BS}$ if we also ignore it for the classical field. An important result for this Hamiltonian is that the ac-Stark shift of the ground state disappears, because the classical field shifts the two atomic states by the same amount.

APPENDIX C: PROPAGATION EQUATIONS FOR LIGHT

The light Hamiltonian (for a single transverse mode) is given by

$$H_L = \sum_k |k| c a_k^\dagger a_k, \tag{C1}$$

where the sum is over all longitudinal wave vectors. We now derive the time evolution of the operator $a_L(z)$ defined in Eq. (10). If we assume that the modes contributing to the slowly varying operator $a_L(z)$ are centered around a large positive value k_0, we can ignore the absolute value of the wave vector. Combining the time derivative caused by the explicit time dependence introduced in Eq. (10) with the time evolution caused by H_L we find the Heisenberg equation of motion

$$\frac{\partial a_L}{\partial t} = i\omega_0 a_L - i[a_L,(H_L + H_{\rm int})]$$

$$= -c\frac{\partial}{\partial z}a_L - i[a_L,H_{\rm int}]. \tag{C2}$$

To simplify the equations we introduce a rescaled time variable by defining new operators $\tilde{a}_L(z,\tau)=a_L(z,t=\tau+z/c)$ and $\tilde{a}_A(z,\tau)=a_A(z,t=\tau+z/c)$. The propagation equation for the light can then be simplified by using

$$\left(\frac{\partial}{\partial t} + c\frac{\partial}{\partial z}\right)a_L(z,t=\tau+z/c) = c\frac{\partial}{\partial z}\tilde{a}_L(z,\tau). \tag{C3}$$

We also take the classical field to be moving in the positive z direction, in which case the Rabi frequency is $\Omega(z,t)=\Omega(t-z/c)=\Omega(\tau)$. The equations of motion always use this rescaled time and we omit the tilde on the operators and simply denote the rescaled time τ by t.

For the parametic-gain the z dependence of the Rabi frequency does not disappear completely from the equations of motion since we should include the $\exp[i\int dz'|g(z')|^2/\Delta]$ dependence associated with the index of refraction for the classical field. For the Faraday interaction the same factor appears in the propagation of the quantum field and both factors can be omitted.

APPENDIX D: INCLUSION OF SPONTANEOUS EMISSION

In Sec. II.B we derived equations of motion ignoring spontaneous emission. To include spontaneous emission we should modify Eq. (A3) such that it contains a decay as well as the Langevin noise operators associated with the decay. The general treatment of the Langevin noise operators is quite complicated because they depend on details of the decay mechanism. In particular, the equations for the parametic-gain and Faraday interaction depend on whether the atoms end up in the states $|0\rangle$ and $|1\rangle$ or some auxiliary states $|a_m\rangle$ (Fig. 2). For the beamsplitter interaction, on the other hand, the precise state that the atoms decay to is less important (Gorshkov *et al.*, 2007a, 2007b). Here for simplicity we only consider the decay to some auxiliary states $|a_m\rangle$.

To describe spontaneous emission we assume that each of the excited states $|e_m\rangle_j$ of the jth atom couples to some state $|a_m\rangle_j$ via a continuum of modes described by the annihilation operators $b_j(\omega)$. We assume that each atom couples to its own continuum. By doing so we ignore collective scattering effects such as superradiance and Bragg scattering, and we also ignore dipole-dipole interactions mediated by other than forward modes. Whether this is a suitable approximation should be evaluated for each particular realization, but to our knowledge little work has been done on this subject. The decay of the jth atom may then be described as

$$H^j_{\rm decay} = \int d\omega \Big[b_j^\dagger(\omega) b_j(\omega) + \rho(\omega)\sum_m [g_m(\omega)|e_m\rangle_j\langle a_m|b_j(\omega) + \text{H.c.}]\Big], \tag{D1}$$

where $g_m(\omega)$ is the coupling constant of the mth excited state and $\rho(\omega)$ is the density of states of the continuum. To arrive at the equations of motion for the atomic operators we first derive the equations of motion for $b_j(\omega)$ using the Hamiltonian (D1). We then formally solve this equation by integrating over time and substitute the result into the equation for $|g_m\rangle_j\langle e_m|$. In the Markov approximation (Barnett and Radmore, 1997) Eq. (A3) acquires the additional terms

$$\frac{d}{dt}|g_m\rangle_j\langle e_{m'}| = \cdots - \frac{\gamma_{m'}}{2}|g_m\rangle_j\langle e_{m'}| + \sqrt{\gamma_m}F^j_{gm,em'}(t), \tag{D2}$$

where we have ignored the Lamb shift. The decay and noise operators are given by

$$\gamma_m = 2\pi|g_m(\omega_m)|^2\rho(\omega_m) \tag{D3}$$

and

$$F^j_{gm,em'}(t) = \frac{-i|g_m\rangle_j\langle a_{m'}|}{\sqrt{\gamma_{m'}}} \times \int d\omega g_{m'}(\omega) b_j(\omega,t=0)e^{-i(\omega-\omega_{m'})t} \tag{D4}$$

with ω_m being the transition frequency for the $|e_m\rangle$ to $|a_m\rangle$ transition. Note that if there is a difference between the population decay rate and twice the decay rate of the polarization, e.g., due to collisional broadening, the decay rate $\gamma_m/2$ appearing here should be the polarization decay rate. The correlation functions within the Markov approximation are

$$\langle F^{j\dagger}_{gm,em'}, F^{j'}_{gm'',em'''}\rangle \approx 0,$$
$$\langle F^{j}_{gm,em'}, F^{j'\dagger}_{gm'',em'''}\rangle \approx \delta(t-t')\delta_{m',m'''}\delta_{j,j'}\langle |g_m\rangle\langle g_{m''}|\rangle. \tag{D5}$$

Since most of the atoms are always in the state $|0\rangle$ the only important noise operators are $F_{g0,em}$.

The equations of motion derived in Sec. II.B are due to the time evolution of a_L and the time evolution of $j_+(\vec{r})$ used in the definition of a_A in Eq. (21). Because the decay simply adds a term in Eq. (D2) which is similar to the detuning term in Eq. (A3) we can obtain the equations of motion for these operators using the replacement in Eq. (42). Note that for operators $|g_m\rangle\langle e_{m'}|$ the detuning and decay appears in the combination $\Delta - i\gamma/2$ so that for the ground-state operators $|g_m\rangle\langle g_{m'}|$ coupling to $|g_m\rangle\langle e_{m''}|$ one should use the minus sign in the substitution. On the other hand, if the coupling is to operators $|e_{m''}\rangle\langle g_{m'}|$, one should use the plus sign. In order to conserve the commutation relation for the operators a_A and a_L one should also include the Langevin noise operators and the time derivative of $\langle j_x(\vec{r})\rangle$ used in the definition of a_A (21).

For the beam-splitter interaction the time derivative of $\langle j_x(\vec{r})\rangle$ can be ignored because the strong classical field couples to an almost empty transition. The equation of motion can therefore be obtained simply by making the substitution (42). The equation of motion for the light (35) arises from the commutator of a_L with the Hamiltonian (A1). In the resulting equation of motion a_L couples to $|0\rangle\langle e|$ and we should therefore use the minus sign in Eq. (42). The atomic annihilation operator is proportional to $|0\rangle\langle 1|$, which couples to $|0\rangle\langle e|$ and $|e\rangle\langle 1|$. The contribution from $|e\rangle\langle 1|$ is, however, small and has been neglected in Eq. (35), and we should once again use the minus sign in the substitution (42). Ignoring the noise operators we arrive at the equations of motion (43). Including the noise operators gives the additional terms

$$\frac{\partial}{\partial z}a_L(z,t) = \cdots + \frac{\sqrt{\gamma}g^*}{\Delta - i\frac{\gamma}{2}}F(z,t),$$
$$\frac{\partial}{\partial t}a_A(z,t) = \cdots - \frac{\sqrt{\gamma}\Omega^*}{2\Delta - i\gamma}F(z,t). \tag{D6}$$

The noise $F(z,t)$ appearing here is defined by first defining with the rescaling

$$F(\vec{r},t) = \frac{1}{\sqrt{n(\vec{r},t)}}\sum_j F^j_{g0,e}(t)\delta(\vec{r}-\vec{r}_j). \tag{D7}$$

Integrating the equations of motion over the transverse coordinates we define $F(z,t)$ in analogy with Eq. (29) (ignoring the mode index m for a single mode). The resulting operator has the standard expectation value of vacuum noise $\langle F^\dagger(z,t)F(z',t')\rangle = 0$, $\langle F(z,t)F^\dagger(z',t')\rangle = \delta(z-z')\delta(t-t')$. The addition of these noise operators ensures that the atom and light operators retain the correct commutation relations.

For the parametic-gain the situation is a little different. The light operator a_L couples to the coherence $|1\rangle\langle e|$ and we should still use the substitution (42) with the minus sign. The atomic coherence $|0\rangle\langle 1|$ again couples to $|0\rangle\langle e|$ and $|e\rangle\langle 1|$, but now we can no longer neglect $|e\rangle\langle 1|$, which gives rise to the ac-Stark shift [the first term in the spin equation in Eq. (36)]. We should therefore use the plus sign in the substitution (42) for this term.

To include the change of the mean spin $\langle j_x(\vec{r},t)\rangle$ we include the decay of the densities n_0 and n_1 of atoms in states $|0\rangle$ and $|1\rangle$ given by

$$\frac{d}{dt}n_0(\vec{r},t) \approx -\frac{\gamma|\Omega(\vec{r},t)|^2}{4\Delta^2+\gamma^2}n_0(\vec{r},t),$$
$$\frac{d}{dt}n_1(\vec{r},t) \approx 0. \tag{D8}$$

Since we also assume that the decay takes the atoms to some auxiliary state $|a_m\rangle$, an initially fully polarized state will remain fully polarized so that $\langle j_x(\vec{r},t)\rangle \approx n_0(\vec{r},t)/2$ as long as the interaction with the quantum field is weak (note, however, that we are describing a situation leading to superradiant scattering so that this approximation may break down quickly). The contribution from the time derivative of the mean spin then exactly cancels the decay of $a_A(z,t)$ arising from the substitution (42). Since there is no longer any decay, one also finds that the resulting equations of motion (53) do not contain any noise.

Finally for the Faraday interaction the easiest way to proceed is to combine again the results for the beam-splitter interaction and the parametic-gain. Similar to the discussion in Appendix B the equations of motion for the Faraday interaction can therefore be obtained by subtracting the right-hand side of Eq. (53) from the right-hand side of Eq. (43) and dividing by $\sqrt{2}$. Furthermore, we again ignore the change of the propagation caused by the index of refraction because this is accompanied by a similar change in the propagation of the classical light. The resulting equations in terms of the x and p operators are given in Eq. (54) without the noise operators. The noise operators give the additional terms

$$\frac{\partial}{\partial z}x_L(z,t) = \cdots + \frac{g\sqrt{2\gamma}}{\sqrt{4\Delta^2+\gamma^2}}F_x(z,t),$$
$$\frac{\partial}{\partial z}p_L(z,t) = \cdots + \frac{g\sqrt{2\gamma}}{\sqrt{4\Delta^2+\gamma^2}}F_p(z,t),$$
$$\frac{\partial}{\partial t}x_A(z,t) = \cdots - \frac{\Omega\sqrt{\gamma}}{\sqrt{4\Delta^2+\gamma^2}}F_x(z,t),$$
$$\frac{\partial}{\partial t}p_A(z,t) = \cdots - \frac{\Omega\sqrt{\gamma}}{\sqrt{4\Delta^2+\gamma^2}}F_p(z,t). \tag{D9}$$

Here for simplicity we have assumed Ω and g to be real and have defined new noise operators

$$F_x(z,t) = \frac{1}{\sqrt{2}}[e^{i\phi}F(z,t) + e^{-i\phi}F^\dagger(z,t)],$$
$$F_p(z,t) = \frac{1}{\sqrt{2}i}[e^{i\phi}F(z,t) - e^{-i\phi}F^\dagger(z,t)], \tag{D10}$$

which have the standard commutation relation $[F_x(z,t),F_p(z',t')]=i\delta(z-z')\delta(t-t')$.

APPENDIX E: DIMENSIONLESS EQUATIONS OF MOTION

Casting the equations of motion for all three basic interactions in a dimensionless form allows to see that the constant κ, Eq. (56), naturally plays the role of the coupling constant for all protocols. We introduce the dimensionless position and time coordinates $s=z/L$ and $v=h(0,t)/h(0,T)$ running from 0 to 1. The rescaled time variable simplifies the equations because it is proportional to the total integrated intensity of the field. In the weak saturation limit the dynamics is completely controlled by the incident number of photons in the classical field. Changing the intensity will thus influence the temporal dynamics of the system, but the final state depends primarily on the total number of incident photons. When using such rescaled coordinates it is desirable to also change the field operators such that an incident light field operator which is normalized in time $[a_L(t),a_L^\dagger(t')]=\delta(t-t')$ is now normalized relative to the new time variable $[a_L(v),a_L^\dagger(v')]=\delta(v-v')$. This normalization is achieved with the rescaling

$$\tilde{a}_A(s=z/L) = \sqrt{L}a_A(z),$$
$$\tilde{a}_L(v(t)) = -\frac{\kappa\sqrt{4\Delta^2+\gamma^2}}{\sqrt{d\gamma}\Omega(t)}a_L(t), \tag{E1}$$

where we have used the dimensionless coupling constant $\kappa=\sqrt{h(0,T)}$, which appeared in the solution for the Faraday interaction [cf. Eq. (57)] in the far off-resonant limit $\Delta \gg \gamma$. Below we omit the tilde on the operators on the left-hand side. In these new rescaled variables the equations of motion for the beam-splitter interaction (43) become

$$\frac{\partial}{\partial s}a_L(s,v) = i\frac{\gamma d}{2(2\Delta - i\gamma)}a_L(s,v) - i\kappa\frac{e^{i\phi}}{2}a_A(s,v),$$
$$\frac{\partial}{\partial v}a_A(s,v) = i\kappa^2\frac{\Delta + i\frac{\gamma}{2}}{\gamma d}a_A(s,v) - i\kappa\frac{e^{i\phi}}{2}a_L(s,v). \tag{E2}$$

With the same rescaling for the parametic-gain interaction (53) we find

$$\frac{\partial}{\partial s}a_L(s,v) = -i\kappa\frac{e^{i\phi}}{2}a_A^\dagger(s,v),$$
$$\frac{\partial}{\partial v}a_A(s,v) = -i\frac{\kappa^2\Delta}{\gamma d}a_A(s,v) - i\kappa\frac{e^{i\phi}}{2}a_L^\dagger(s,v), \tag{E3}$$

where we have again assumed that g is real.

For the Faraday interaction the equations of motion (54) become

$$\frac{\partial}{\partial s}x_L(s,v) = \kappa p_A(s,v) - \frac{\gamma^2}{4\Delta^2+\gamma^2}\frac{d}{2}x_L(s,v),$$
$$\frac{\partial}{\partial s}p_L(s,v) = -\frac{\gamma^2}{4\Delta^2+\gamma^2}\frac{d}{2}p_L(s,v),$$
$$\frac{\partial}{\partial v}x_A(s,v) = \kappa p_L(s,v) - \frac{\kappa^2}{2d}x_A(s,v),$$
$$\frac{\partial}{\partial v}p_A(s,v) = -\frac{\kappa^2}{2d}p_A(s,v), \tag{E4}$$

where we have ignored small corrections which vanish in the far-detuned limit.

APPENDIX F: TENSOR DECOMPOSITION

The coefficients determining the strength of the irreducible tensor components are

$$a_k(\Delta) = (-)^{1+F}c_k(2k+1)\sqrt{\frac{2F+1}{3}} \times\left[\sum_{F'}\frac{(-)^{F'}}{1-\delta_{F'}/\Delta}(2F'+1) \times\begin{Bmatrix} J' & F' & I \\ F & J & 1\end{Bmatrix}^2\begin{Bmatrix} F & k & F \\ 1 & F' & 1\end{Bmatrix}\right],$$

where the expressions in curly brackets are 6j symbols, $\Delta=\Delta_{F+1}$, $\delta_{F'}=\Delta_{F+1}-\Delta_{F'}$ and

$$c_0 = 1, \quad c_1 = \sqrt{\frac{2}{F(F+1)}},$$
$$c_2 = -\frac{3}{\sqrt{10F(F+1)(2F-1)(2F+3)}}.$$

The last line is valid for $F>1/2$, that is nuclear spin $I\neq 0$, and has to be replaced by $c_2=0$ for $I=0$.

In the asymptotic limit of large (blue) detuning, $-\Delta \gg \delta_{F'}$, the sum in square brackets can be simplified by means of

$$\sum_{F'=F-1}^{F+1}(-)^{F'}(2F'+1)\begin{Bmatrix} J' & F' & I \\ F & J & 1\end{Bmatrix}^2\begin{Bmatrix} F & k & F \\ 1 & F' & 1\end{Bmatrix} = (-)^{(2J+2F+J'+I+k)}\begin{Bmatrix} J & I & F \\ F & k & J\end{Bmatrix}\begin{Bmatrix} J & J & k \\ 1 & 1 & J'\end{Bmatrix}$$

to get

$$a_k = \lim_{\Delta\to-\infty} a_k(\Delta) = (-)^{2J+F+J'+I+k+1} c_k(2k+1) \times \sqrt{\frac{2F+1}{3}} \begin{Bmatrix} J & I & F \\ F & k & J \end{Bmatrix} \times \begin{Bmatrix} J & J & k \\ 1 & 1 & J' \end{Bmatrix}.$$

From this expression it is evident that a_2 has to vanish because the triple $\{J,J,k\}=\{1/2,1/2,2\}$ does not satisfy the triangle inequality. For the particular case of the cesium ($I=7/2$) D_2 line at $F=4\to F'=3,4,5$ the asymptotic values of the nonvanishing coefficients are $a_0=1/6$, $a_1=1/24$.

REFERENCES

Achilles, D., C. Silberhorn, C. Sliwa, K. Banaszek, I. A. Walmsley, M. J. Fitch, B. C. Jacobs, T. B. Pittman, and J. D. Franson, 2004, J. Mod. Opt. **51**, 1499.

Adesso, G., and G. Chiribella, 2008, Phys. Rev. Lett. **100**, 170503.

Adesso, G., and F. Illuminati, 2007, J. Phys. A **40**, 7821.

Afzelius, M., C. Simon, H. de Riedmatten, and N. Gisin, 2009, Phys. Rev. A **79**, 052329.

Alexander, A. L., J. J. Longdell, M. J. Sellars, and N. B. Manson, 2006, Phys. Rev. Lett. **96**, 043602.

Alexandrov, E., 2003, Phys. Scr., T **105**, 27.

André, A., 2005, Nonclassical States of Light and Atomic Ensembles: Generation and New Applications, Ph.D. thesis (Harvard University).

André, A., M. Bajcsy, A. S. Zibrov, and M. D. Lukin, 2005, Phys. Rev. Lett. **94**, 063902.

Andre, A., L. M. Duan, and M. D. Lukin, 2002, Phys. Rev. Lett. **88**, 243602.

André, A., and M. D. Lukin, 2002, Phys. Rev. Lett. **89**, 143602.

Appel, J., E. Figueroa, D. Korystov, M. Lobino, and A. I. Lvovsky, 2008, Phys. Rev. Lett. **100**, 093602.

Appel, J., P. J. Windpassinger, D. Oblak, U. B. Hoff, N. Kjrgaard, and E. S. Polzik, 2009, Proc. Natl. Acad. Sci. U.S.A. **106**, 10960.

Arecchi, F. T., E. Courtens, R. Gilmore, and H. Thomas, 1972, Phys. Rev. A **6**, 2211.

Aspelmeyer, M., T. Jennewein, M. Pfennigbauer, W. R. Leeb, and A. Zeilinger, 2003, IEEE J. Sel. Top. Quantum Electron. **9**, 1541.

Atature, M., J. Dreiser, A. Badolato, and A. Imamoglu, 2007, Nat. Phys. **3**, 101.

Bajcsy, M., A. S. Zibrov, and M. D. Lukin, 2003, Nature (London) **426** 638.

Balić, V., D. A. Braje, P. Kolchin, G. Y. Yin, and S. E. Harris, 2005, Phys. Rev. Lett. **94**, 183601.

Barnett, S. M., and P. M. Radmore, 1997, *Methods in Theoretical Quantum Optics* (Oxford University Press, Oxford).

Barrett, M., J. Chiaverini, T. Schaetz, J. Britton, W. Itano, J. Jost, E. Knill, C. Langer, D. Leibfried, R. Ozeri, and D. Wineland, 2004, Nature (London) **429**, 737.

Bartlett, S. D., B. C. Sanders, S. L. Braunstein, and K. Nemoto, 2002, Phys. Rev. Lett. **88**, 097904.

Bennett, C., G. Brassard, C. Crépeau, R. Jozsa, A. Peres, and W. Wootters, 1993, Phys. Rev. Lett. **70**, 1895.

Black, A. T., J. K. Thompson, and V. Vuletić, 2005, Phys. Rev. Lett. **95**, 133601.

Boller, K.-J., A. Imamolu, and S. E. Harris, 1991, Phys. Rev. Lett. **66**, 2593.

Bouchoule, I., and K. Mølmer, 2002, Phys. Rev. A **66**, 043811.

Bouwmeester, D., J. Pan, K. Mattle, M. Eibl, H. Weinfurter, and A. Zeilinger, 1997, Nature (London) **390**, 575.

Bowen, W. P., N. Treps, B. C. Buchler, R. Schnabel, T. C. Ralph, H.-A. Bachor, T. Symul, and P. K. Lam, 2003a, Phys. Rev. A **67**, 032302.

Bowen, W. P., N. Treps, B. C. Buchler, R. Schnabel, T. C. Ralph, T. Symul, and P. K. Lam, 2003b, IEEE J. Sel. Top. Quantum Electron. **9**, 1519.

Braginsky, V. B., and F. Y. Khalili, 1996, Rev. Mod. Phys. **68**, 1.

Braje, D. A., V. Balić, S. Goda, G. Y. Yin, and S. E. Harris, 2004, Phys. Rev. Lett. **93**, 183601.

Brask, J. B., and A. S. Sørensen, 2008, Phys. Rev. A **78**, 012350.

Braunstein, S., and H. Kimble, 1998, Phys. Rev. Lett. **80**, 869.

Braunstein, S. L., 2005, Phys. Rev. A **71**, 055801.

Braunstein, S. L., C. A. Fuchs, and H. J. Kimble, 2000, J. Mod. Opt. **47**, 267.

Braunstein, S. L., C. A. Fuchs, H. J. Kimble, and P. van Loock, 2001, Phys. Rev. A **64**, 022321.

Braunstein, S. L., and P. van Loock, 2005, Rev. Mod. Phys. **77**, 513.

Briegel, H.-J., W. Dür, J. I. Cirac, and P. Zoller, 1998, Phys. Rev. Lett. **81**, 5932.

Brion, E., K. Mølmer, and M. Saffman, 2007, Phys. Rev. Lett. **99**, 260501.

Camacho, R. M., C. J. Broadbent, I. Ali-Khan, and J. C. Howell, 2007, Phys. Rev. Lett. **98**, 043902.

Carman, R. L., F. Shimizu, C. S. Wang, and N. Bloembergen, 1970, Phys. Rev. A **2**, 60.

Cerf, N. J., O. Krüger, P. Navez, R. F. Werner, and M. M. Wolf, 2005, Phys. Rev. Lett. **95**, 070501.

Chaikin, P. M., and T. C. Lubensky, 1995, *Principles of Condensed Matter Physics* (Cambridge University Press, Cambridge, U.K.).

Chaneliere, T., D. Matsukevich, S. Jenkins, S.-Y. Lan, T. A. B. Kennedy, and A. Kuzmich, 2005, Nature (London) **438**, 833.

Chaneliere, T., D. N. Matsukevich, S. D. Jenkins, S.-Y. Lan, R. Zhao, T. A. B. Kennedy, and A. Kuzmich, 2007, Phys. Rev. Lett. **98**, 113602.

Chaudhury, S., G. A. Smith, K. Schulz, and P. S. Jessen, 2006, Phys. Rev. Lett. **96**, 043001.

Chen, S., Y.-A. Chen, T. Strassel, Z.-S. Yuan, B. Zhao, J. Schmiedmayer, and J.-W. Pan, 2006, Phys. Rev. Lett. **97**, 173004.

Chen, S., Y.-A. Chen, B. Zhao, Z.-S. Yuan, J. Schmiedmayer, and J.-W. Pan, 2007, Phys. Rev. Lett. **99**, 180505.

Chen, Y.-A., S. Chen, Z.-S. Yuan, B. Zhao, C.-S. Chuu, J. Schmiedmayer, and J.-W. Pan, 2008, Nat. Phys. **4**, 103.

Chen, Z.-B., B. Zhao, Y.-A. Chen, J. Schmiedmayer, and J.-W. Pan, 2007, Phys. Rev. A **76**, 022329.

Childress, L., J. M. Taylor, A. S. Sørensen, and M. D. Lukin, 2005, Phys. Rev. A **72**, 052330.

Choi, K. S., H. Deng, J. Laurat, and H. J. Kimble, 2008, Nature (London) **452**, 67.

Chou, C., S. Polyakov, A. Kuzmich, and H. Kimble, 2004, Appl. Phys. Lett. **92**, 213601.

Chou, C. W., H. de Riedmatten, D. Felinto, S. V. Polyakov, S. J. van Enk, and H. J. Kimble, 2005, Nature (London) **438**, 828.

Chou, C.-W., J. Laurat, H. Deng, K. S. Choi, H. de Riedmat-

ten, D. Felinto, and H. J. Kimble, 2007, Science **316**, 1316.
Chuu, C.-S., T. Strassel, B. Zhao, M. Koch, Y.-A. Chen, S. Chen, Z.-S. Yuan, J. Schmiedmayer, and J.-W. Pan, 2008, Phys. Rev. Lett. **101**, 120501.
Cola, M., M. Paris, N. Piovella, and R. Bonifacio, 2004, J. Phys. B **37**, S187.
Dantan, A., A. Bramati, and M. Pinard, 2005, Phys. Rev. A **71**, 043801.
Dantan, A., J. Cviklinski, E. Giacobino, and M. Pinard, 2006, Phys. Rev. Lett. **97**, 023605.
Dantan, A., J. Cviklinski, M. Pinard, and P. Grangier, 2006, Phys. Rev. A **73**, 032338.
Dantan, A., and M. Pinard, 2004, Phys. Rev. A **69**, 043810.
de Echaniz, S. R., M. Koschorreck, M. Napolitano, M. Kubasik, and M. W. Mitchell, 2008, Phys. Rev. A **77**, 032316
de Riedmatten, H., M. Afzelius, M. U. Staudt, C. Simon, and N. Gisin, 2008, Nature (London) **456**, 773.
Deutsch, I. H., and P. S. Jessen, 1998, Phys. Rev. A **57**, 1972.
Dorner, U., A. Klein, and D. Jaksch, 2008, Nature (London) **8**, 0468.
Du, S., P. Kolchin, C. Belthangady, G. Y. Yin, and S. E. Harris, 2008, Phys. Rev. Lett. **100**, 183603.
Duan, L. M., J. I. Cirac, and P. Zoller, 2002, Phys. Rev. A **66**, 023818.
Duan, L.-M., J. I. Cirac, P. Zoller, and E. S. Polzik, 2000, Phys. Rev. Lett. **85**, 5643.
Duan, L.-M., G. Giedke, J. I. Cirac, and P. Zoller, 2000, Phys. Rev. Lett. **84**, 2722.
Duan, L.-M., M. D. Lukin, J. I. Cirac, and P. Zoller, 2001, Nature (London) **414**, 413.
Dür, W., and H. J. Briegel, 2007, Rep. Prog. Phys. **70**, 1381.
Dür, W., H.-J. Briegel, J. I. Cirac, and P. Zoller, 1999, Phys. Rev. A **59**, 169.
Eckert, K., O. Romero-Isart, M. Rodriguez, M. Lewenstein, E. S. Polzik, and A. Sanpera, 2008, Nat. Phys. **4**, 50.
Edmonds, A., 1964, *Drehimpulse in der Quantenmechanik* (Bibliographisches Institut, Mannheim).
Einstein, A., B. Podolsky, and N. Rosen, 1935, Phys. Rev. **47**, 777.
Eisaman, M., A. Aandre, F. Massou, M. Fleischhauer, A. Zibrov, and M. Lukin, 2005, Nature (London) **438**, 837.
Eisert, J., and M. B. Plenio, 2003, Int. J. Quantum Inf. **1**, 479.
Eisert, J., S. Scheel, and M. B. Plenio, 2002, Phys. Rev. Lett. **89**, 137903.
Erhard, M., and H. Helm, 2001, Phys. Rev. A **63**, 043813.
Felinto, D., C. W. Chou, J. Laurat, E. W. Schomburg, H. de Riedmatten, and H. J. Kimble, 2006, Nat. Phys. **2**, 844.
Fernholz, T., H. Krauter, K. Jensen, J. F. Sherson, A. S. S. Rensen, and E. S. Polzik, 2008, Phys. Rev. Lett. **101**, 073601.
Fiurasek, J., 2002, Phys. Rev. Lett. **89**, 137904.
Fiurasek, J., 2003, Phys. Rev. A **68**, 022304.
Fiurasek, J., H. J. Cerf, and E. S. Polzik, 2004, Phys. Rev. Lett. **93**, 180501.
Fiurasek, J., J. Sherson, T. Opatrny, and E. S. Polzik, 2006, Phys. Rev. A **73**, 022331.
Fleischhauer, M., A. Imamoglu, and J. P. Marangos, 2005, Rev. Mod. Phys. **77**, 633.
Fleischhauer, M., and M. Lukin, 2002, Phys. Rev. A **65**, 022314.
Fleischhauer, M., and M. D. Lukin, 2000, Phys. Rev. Lett. **84**, 5094.
Fleischhauer, M., and T. Richter, 1995, Phys. Rev. A **51**, 2430.
Fraval, E., M. J. Sellars, and J. J. Longdell, 2005, Phys. Rev. Lett. **95**, 030506.
Furusawa, A., J. Sorensen, S. Braunstein, C. Fuchs, H. Kimble, and E. S. Polzik, 1998, Science **282**, 706.
Furusawa, A., and N. Takei, 2007, Phys. Rep. **443**, 97.
Genes, C., and P. R. Berman, 2006, Phys. Rev. A **73**, 013801.
Geremia, J. M., J. K. Stockton, and H. Mabuchi, 2006, Phys. Rev. A **73**, 042112.
Giedke, G., and J. I. Cirac, 2002, Phys. Rev. A **66**, 032316.
Giedke, G., M. M. Wolf, O. Krüger, R. F. Werner, and J. I. Cirac, 2003, Phys. Rev. Lett. **91**, 107901.
Gorshkov, A. V., A. André, M. Fleischhauer, A. S. Sørensen, and M. D. Lukin, 2007, Phys. Rev. Lett. **98**, 123601.
Gorshkov, A. V., A. André, M. D. Lukin, and A. S. Sørensen, 2007a, Phys. Rev. A **76**, 033804.
Gorshkov, A. V., A. André, M. D. Lukin, and A. S. Sørensen, 2007b, Phys. Rev. A **76**, 033805.
Gorshkov, A. V., A. André, M. D. Lukin, and A. S. Sørensen, 2007c, Phys. Rev. A **76**, 033806.
Gorshkov, A. V., T. Calarco, M. D. Lukin, and A. S. Sørensen, 2008, Phys. Rev. A **77**, 043806.
Groeger, S., G. Bison, J. Schenker, R. Wynands, and A. Weis, 2006, Eur. Phys. J. D **38**, 239.
Grosshans, F., and P. Grangier, 2001, Phys. Rev. A **64**, 010301.
Hald, J., J. L. Sørensen, C. Schori, and E. S. Polzik, 1999, Phys. Rev. Lett. **83**, 1319.
Hammerer, K., 2006, Quantum Information Processing with Atomic Ensembles and Light, Ph.D. thesis, (Technical University Munich).
Hammerer, K., M. Aspelmeyer, E. S. Polzik, and P. Zoller., 2009, Phys. Rev. Lett. **102**, 020501.
Hammerer, K., K. Mølmer, E. S. Polzik, and J. Cirac, 2004, Phys. Rev. A **70**, 044304.
Hammerer, K., E. S. Polzik, and J. I. Cirac, 2005, Phys. Rev. A **72**, 052313.
Hammerer, K., E. S. Polzik, and J. I. Cirac, 2006, Phys. Rev. A **74**, 064301.
Hammerer, K., M. M. Wolf, E. S. Polzik, and J. I. Cirac, 2005, Phys. Rev. Lett. **94**, 150503.
Hansel, W., P. Hommelhoff, T. W. Hansch, and J. Reichel, 2001, Nature (London) **413**, 498.
Happer, W., 1972, Rev. Mod. Phys. **44**, 169.
Happer, W., and B. S. Mathur, 1967, Phys. Rev. **163**, 12.
Hartmann, L., B. Kraus, H.-J. Briegel, and W. Dür, 2007, Phys. Rev. A **75**, 032310.
Hau, L. V., S. E. Harris, Z. Dutton, and C. H. Behroozi, 1999, Nature (London) **397**, 594.
Hemmer, P. R., A. V. Turukhin, M. S. Shahriar, and J. A. Musser, 2001, Opt. Lett. **26**, 361.
Herskind, P., A. Dantan, M. B. Langkilde-Lauesen, A. Mortensen, J. L. Sørensen, and M. Drewsen, 2008, Appl. Phys. B **93**, 373.
Hétet, G., J. J. Longdell, A. L. Alexander, P. K. Lam, and M. J. Sellars, 2008, Phys. Rev. Lett. **100**, 023601.
Hétet, G., A. Peng, M. T. Johnsson, J. J. Hope, and P. K. Lam, 2008, Phys. Rev. A **77**, 012323.
Hillery, M., M. Ziman, V. Buzek, and M. Bieliková, 2006, Phys. Lett. A **349**, 75.
Holland, M. J., M. J. Collett, D. F. Walls, and M. D. Levenson, 1990, Phys. Rev. A **42**, 2995.
Holstein, T., and H. Primakoff, 1940, Phys. Rev. **58**, 1098.
Honda, K., D. Akamatsu, M. Arikawa, Y. Yokoi, K. Akiba, S. Nagatsuka, T. Tanimura, A. Furusawa, and M. Kozuma, 2008, Phys. Rev. Lett. **100**, 093601.
Horoshko, D. B., and S. Y. Kilin, 2000, Phys. Rev. A **61**,

032304.
Jackson, J. D., 1975, *Classical Electrodynamics*, 2nd ed. (Wiley, New York).
Jiang, L., J. M. Taylor, and M. D. Lukin, 2007, Phys. Rev. A **76**, 012301.
Josse, V., A. Dantan, A. Bramati, M. Pinard, and E. Giacobino, 2004, Phys. Rev. Lett. **92**, 123601.
Julsgaard, B., 2003, Entanglement and Quantum Interactions with Macroscopic Gas Samples, Ph.D. thesis (University of Aarhus, Aarhus).
Julsgaard, B., A. Kozhekin, and E. S. Polzik, 2001, Nature (London) **413**, 400.
Julsgaard, B., J. Sherson, J. Fiurasek, J. Cirac, and E. S. Polzik, 2004, Nature (London) **432**, 482.
Julsgaard, B., J. Sherson, J. L. S. Sorenson, and E. S. Polzik, 2004, J. Opt. B: Quantum Semiclassical Opt. **6**, 5.
Keyl, M., D. Schlingemann, and R. Werner, 2003, Quantum Inf. Process. **3**, 281.
Keyl, M., and R. Werner, 1999, J. Math. Phys. **40**, 3283.
Kimble, H. J., 2008, Nature (London) **453**, 1023.
Kitagawa, M., and M. Ueda, 1993, Phys. Rev. A **47**, 5138.
Kittel, C., 1987, *Quantum Theory of Solids* (Wiley, New York).
Klein, A., U. Dorner, C. M. Alves, and D. Jaksch, 2006, Phys. Rev. A **73**, 012332.
Korbicz, J. K., J. I. Cirac, and M. Lewenstein, 2005a, Phys. Rev. Lett. **95**, 120502.
Korbicz, J. K., J. I. Cirac, and M. Lewenstein, 2005b, Phys. Rev. Lett. **95**, 259901.
Kozhekin, A. E., K. Mølmer, and E. S. Polzik, 2000, Phys. Rev. A **62**, 033809.
Kraus, B., K. Hammerer, G. Giedke, and J. I. Cirac, 2003, Phys. Rev. A **67**, 042314.
Kraus, B., W. Tittel, N. Gisin, M. Nilsson, S. Kröll, and J. I. Cirac, 2006, Phys. Rev. A **73**, 020302.
Kupriyanov, D. V., O. S. Mishina, I. M. Sokolov, B. Julsgaard, and E. S. Polzik, 2005, Phys. Rev. A **71**, 032348.
Kurnit, N. A., I. D. Abella, and S. R. Hartmann, 1964, Phys. Rev. Lett. **13**, 567.
Kurucz, Z., and M. Fleischhauer, 2008, Phys. Rev. A **78**, 023805.
Kuzmich, A., N. P. Bigelow, and L. Mandel, 1998, Europhys. Lett. **42**, 481.
Kuzmich, A., W. P. Bowen, A. D. Boozer, A. Boca, C. W. Chou, L.-M. Duan, and H. J. Kimble, 2003, Nature (London) **423**, 731.
Kuzmich, A., and T. A. B. Kennedy, 2004, Phys. Rev. Lett. **92**, 030407.
Kuzmich, A., L. Mandel, and N. P. Bigelow, 2000, Phys. Rev. Lett. **85**, 1594.
Kuzmich, A., K. Molmer, and E. S. Polzik, 1997, Phys. Rev. Lett. **79**, 4782.
Kuzmich, A., and E. S. Polzik, 2000, Phys. Rev. Lett. **85**, 5639.
Kuzmich, A., and E. S. Polzik, 2003, *Quantum Information with Continuous Variables* (Kluwer, Dordrecht), pp. 231–265.
Leonhardt, U., 2003, Rep. Prog. Phys. **66**, 1207.
Liu, C., Z. Dutton, C. H. Behroozi, and L. V. Hau, 2001, Nature (London) **409**, 490.
Lloyd, S., and S. L. Braunstein, 1999, Phys. Rev. Lett. **82**, 1784.
Longdell, J. J., E. Fraval, M. J. Sellars, and N. B. Manson, 2005, Phys. Rev. Lett. **95**, 063601.
Longdell, J. J., G. Hétet, P. K. Lam, and M. J. Sellars, 2008, Phys. Rev. A **78**, 032337.
Louchet, A., Y. L. Du, F. Bretenaker, T. Chaneliére, F. Goldfarb, I. Lorgeré, J.-L. L. Gouët, O. Guillot-Noël, and P. Goldner, 2008, Phys. Rev. B **77**, 195110.
Loudon, R., 2004, *The Quantum Theory of Light* (Oxford University Press, Oxford).
Lukin, M. D., 2003, Rev. Mod. Phys. **75**, 457.
Lukin, M. D., M. Fleischhauer, R. Cote, L. M. Duan, D. Jaksch, J. I. Cirac, and P. Zoller, 2001, Phys. Rev. Lett. **87**, 037901.
Lukin, M. D., and A. Imamoglu, 2001, Nature (London) **413**, 273.
Lukin, M. D., S. F. Yelin, and M. Fleischhauer, 2000, Phys. Rev. Lett. **84**, 4232.
Lvovsky, A. I., and M. G. Raymer, 2009, Rev. Mod. Phys. **81**, 299.
Madsen, L. B., and K. Mølmer, 2004, Phys. Rev. A **70**, 052324.
Mandel, O., M. Greiner, A. Widera, T. Rom, T. W. Hansch, and I. Bloch, 2003, Nature (London) **425**, 937.
Manz, S., T. Fernholz, J. Schmiedmayer, and J.-W. Pan, 2007, Phys. Rev. A **75**, 040101.
Massar, S., and E. S. Polzik, 2003, Phys. Rev. Lett. **91**, 060401.
Massar, S., and S. Popescu, 1995, Phys. Rev. Lett. **74**, 1259.
Matsukevich, D. N., T. Chanelière, S. D. Jenkins, S.-Y. Lan, T. A. B. Kennedy, and A. Kuzmich, 2006, Phys. Rev. Lett. **97**, 013601.
Matsukevich, D. N., and A. Kuzmich, 2004, Science **306**, 663.
Menicucci, N. C., P. van Loock, M. Gu, C. Weedbrook, T. C. Ralph, and M. A. Nielsen, 2006, Phys. Rev. Lett. **97**, 110501.
Mewes, C., and M. Fleischhauer, 2005, Phys. Rev. A **72**, 022327.
Milonni, P. W., and J. H. Eberly, 1988, *Lasers* (Wiley, New York).
Mishina, O., D. Kupriyanov, and E. S. Polzik, 2006, in *Quantum Information Processing from Theory to Experiment*, Proceedings of the NATO Advanced Research Workshop (IOS, Amsterdam), Vol. 199, pp. 346–352.
Mishina, O. S., D. V. Kupriyanov, J. H. Müller, and E. S. Polzik, 2007, Phys. Rev. A **75**, 042326.
Mišta, L. J., and R. Filip, 2005, Phys. Rev. A **71**, 032342.
Moiseev, S., 2003, Opt. Spectrosc. **94** 788.
Moiseev, S. A., and S. Kröll, 2001, Phys. Rev. Lett. **87**, 173601.
Müller, J. H., P. Petrov, D. Oblak, C. L. G. Alzar, S. R. de Echaniz, and E. S. Polzik, 2005, Phys. Rev. A **71**, 033803.
Muschik, C. A., I. de Vega, D. Porras, and J. I. Cirac, 2008, Phys. Rev. Lett. **100**, 063601.
Muschik, C. A., K. Hammerer, E. S. Polzik, and J. I. Cirac, 2006, Phys. Rev. A **73**, 062329.
Neergaard-Nielsen, J. S., B. M. Nielsen, C. Hettich, K. Mølmer, and E. S. Polzik, 2006, Phys. Rev. Lett. **97**, 083604.
Nielsen, M., and I. Chuang, 2000, *Quantum Computation and Qauntum Information* (Cambridge University Press, Cambridge).
Nilsson, M., and S. Kröll, 2005, Opt. Commun. **247**, 393.
Nilsson, M., L. Rippe, S. Kroll, R. Klieber, and D. Suter, 2004, Phys. Rev. B **70**, 214116.
Novikova, I., A. V. Gorshkov, D. F. Phillips, A. S. Sørensen, M. D. Lukin, and R. L. Walsworth, 2007, Phys. Rev. Lett. **98**, 243602.
Novikova, I., D. F. Phillips, and R. L. Walsworth, 2007, Phys. Rev. Lett. **99**, 173604.
Novikova, I., N. B. Phillips, and A. V. Gorshkov, 2008, Phys. Rev. A **78**, 021802.
Nunn, J., K. Reim, K. C. Lee, V. O. Lorenz, B. J. Sussman, I. A. Walmsley, and D. Jaksch, 2008, Phys. Rev. Lett. **101**,

260502.
Nunn, J., I. A. Walmsley, M. G. Raymer, K. Surmacz, F. C. Waldermann, Z. Wang, and D. Jaksch, 2007, Phys. Rev. A **75**, 011401(R).
Oblak, D., P. G. Petrov, C. L. G. Alzar, W. Tittel, A. K. Vershovski, J. K. Mikkelsen, J. L. Sørensen, and E. S. Polzik, 2005, Phys. Rev. A **71**, 043807.
Ottaviani, C., D. Vitali, M. Artoni, F. Cataliotti, and P. Tombesi, 2003, Phys. Rev. Lett. **90**, 197902.
Ourjoumtsev, A., R. Tualle-Brouri, J. Laurat, and P. Grangier, 2006, Science **312**, 83.
Owari, M., M. B. Plenio, E. S. Polzik, A. Serafini, and M. Wolf, 2008, New J. Phys. **10**, 113014.
Paris, M., M. Cola, N. Piovella, and R. Bonifacio, 2003, Opt. Commun. **227**, 349.
Pedersen, L. H., and K. Mølmer, 2009, Phys. Rev. A **79**, 012320.
Petrosyan, D., and M. Fleischhauer, 2008, Phys. Rev. Lett. **100**, 170501.
Petrov, P. G., D. Oblak, C. L. G. Alzar, N. Kjærgaard, and E. S. Polzik, 2007, Phys. Rev. A **75**, 033803.
Pfennigbauer, M., M. Aspelmeyer, W. R. Leeb, G. Baister, T. Dreischer, T. Jennewein, G. Neckamm, J. M. Perdigues, H. Weinfurter, and A. Zeilinger, 2005, J. Opt. Netw. **4**, 549.
Phillips, D. F., A. Fleischhauer, A. Mair, R. L. Walsworth, and M. D. Lukin, 2001, Phys. Rev. Lett. **86**, 783.
Pittman, T. B., and J. D. Franson, 2002, Phys. Rev. A **66**, 062302.
Poizat, J. P., J. F. Roch, and P. Grangier, 1994, Ann. Phys. (Paris) **19**, 265.
Polzik, E. S., B. Julsgaard, J. Sherson, and J. L. Sørensen, 2003, Philos. Trans. R. Soc. London, Ser. A **361**, 1391.
Pu, H., and P. Meystre, 2000, Phys. Rev. Lett. **85**, 3987.
Rabl, P., D. DeMille, J. M. Doyle, M. D. Lukin, R. J. Schoelkopf, and P. Zoller, 2006, Phys. Rev. Lett. **97**, 033003.
Ralph, T. C., and P. K. Lam, 1998, Phys. Rev. Lett. **81**, 5668.
Raymer, M. G., and J. Mostowski, 1981, Phys. Rev. A **24**, 1980.
Riebe, M., H. Haffner, C. Roos, W. Hansel, J. Benhelm, G. Lancaster, T. Korber, C. Becher, F. Schmidt-Kaler, D. James, and R. Blatt, 2004, Nature (London) **429**, 734.
Sangouard, N., C. Simon, M. Afzelius, and N. Gisin, 2007, Phys. Rev. A **75**, 032327.
Sangouard, N., C. Simon, J. Minar, H. Zbinden, H. de Riedmatten, and N. Gisin, 2007, Phys. Rev. A **76**, 050301.
Sangouard, N., C. Simon, B. Zhao, Y.-A. Chen, H. de Riedmatten, J.-W. Pan, and N. Gisin, 2008, Phys. Rev. A **77**, 062301.
Schleier-Smith, M. H., I. D. Leroux, and V. Vuletic, 2010, Phys. Rev. Lett. **104**, 073604.
Schneider, S., A. Kasper, C. vom Hagen, M. Bartenstein, B. Engeser, T. Schumm, I. Bar-Joseph, R. Folman, L. Feenstra, and J. Schmiedmayer, 2003, Phys. Rev. A **67**, 023612.
Schnorrberger, U., J. D. Thompson, S. Trotzky, R. Pugatch, N. Davidson, S. Kuhr, and I. Bloch, 2009, Phys. Rev. Lett. **103**, 033003.
Sherson, J., J. Fiurasek, K. Mølmer, A. Sørensen, and E. S. Polzik, 2006, Phys. Rev. A **74**, 011802.
Sherson, J., B. Julsgaard, and E. S. Polzik, 2006, Adv. At. Mol. Phys. **54**, 81.
Sherson, J. F., H. Krauter, R. K. Olsson, B. Julsgaard, K. Hammerer, I. Cirac, and E. S. Polzik, 2006, Nature (London) **443**, 557.
Shuker, M., O. Firstenberg, R. Pugatch, A. Ron, and N. Davidson, 2008, Phys. Rev. Lett. **100**, 223601.
Simon, C., H. de Riedmatten, M. Afzelius, N. Sangouard, H. Zbinden, and N. Gisin, 2007, Phys. Rev. Lett. **98**, 190503.
Simon, J., H. Tanji, S. Ghosh, and V. Vuletic, 2007, Nat. Phys. **3**, 765.
Simon, J., H. Tanji, J. K. Thompson, and V. Vuletić, 2007, Phys. Rev. Lett. **98**, 183601.
Simon, R., 2000, Phys. Rev. Lett. **84**, 2726.
Sørensen, A., L. M. Duan, J. I. Cirac, and P. Zoller, 2001, Nature (London) **409**, 63.
Sørensen, A., and K. Mølmer, 1999, Phys. Rev. Lett. **83**, 2274.
Sørensen, A. S., and K. Mølmer, 2001, Phys. Rev. Lett. **86**, 4431.
Sørensen, M. W., and A. S. Sørensen, 2008, Phys. Rev. A **77**, 013826.
Staudt, M. U., S. R. Hastings-Simon, M. Nilsson, M. Afzelius, V. Scarani, R. Ricken, H. Suche, W. Sohler, W. Tittel, and N. Gisin, 2007, Phys. Rev. Lett. **98**, 113601.
Surmacz, K., J. Nunn, F. C. Waldermann, K. C. Lee, Z. Wang, I. A. Walmsley, and D. Jaksch, 2008, Phys. Rev. A **78**, 033806.
Surmacz, K., J. Nunn, F. C. Waldermann, Z. Wang, I. A. Walmsley, and D. Jaksch, 2006, Phys. Rev. A **74**, 050302.
Takano, T., M. Fuyama, R. Namiki, and Y. Takahashi, 2008, Phys. Rev. A **78**, 010307.
Takano, T., M. Fuyama, R. Namiki, and Y. Takahashi, 2009, Phys. Rev. Lett. **102**, 033601.
Takeuchi, M., S. Ichihara, T. Takano, M. Kumakura, and Y. Takahashi, 2007, Phys. Rev. A **75**, 063827.
Takeuchi, M., S. Ichihara, T. Takano, M. Kumakura, T. Yabuzaki, and Y. Takahashi, 2005, Phys. Rev. Lett. **94**, 023003.
Takeuchi, M., T. Takano, S. Ichihara, Y. Takasu, M. Kumakura, T. Yabuzaki, and Y. Takahashi, 2006, Appl. Phys. B: Lasers Opt. **83**, 107.
Thompson, J. K., J. Simon, H. Loh, and V. Vuletic, 2006, Science **313**, 74.
Thomsen, L. K., S. Mancini, and H. M. Wiseman, 2002a, J. Phys. B **35**, 4937.
Thomsen, L. K., S. Mancini, and H. M. Wiseman, 2002b, Phys. Rev. A **65**, 061801.
Tordrup, K., A. Negretti, and K. M. Mølmer, 2008, Phys. Rev. Lett. **101**, 040501.
Tóth, G., C. Knapp, O. Gühne, and H. J. Briegel, 2007, Phys. Rev. Lett. **99**, 250405.
Vaccaro, J. A., J. Spring, and A. Chefles, 2007, Phys. Rev. A **75**, 012333.
Vaidman, L., 1994, Phys. Rev. A **49**, 1473.
van der Wal, C. H., M. D. Eisaman, A. Andre, R. L. Walsworth, D. F. Phillips, A. S. Zibrov, and M. D. Lukin, 2003, Science **301**, 196.
van Enk, S. J., N. Lütkenhaus, and H. J. Kimble, 2007, Phys. Rev. A **75**, 052318.
Vasilyev, D. V., I. V. Sokolov, and E. S. Polzik, 2008, Phys. Rev. A **77**, 020302.
Vudyasetu, P. K., R. M. Camacho, and J. C. Howell, 2008, Phys. Rev. Lett. **100**, 123903.
Waks, E., E. Diamanti, and Y. Yamamoto, 2006, New J. Phys. **8**, 4.
Wang, X. G., and B. C. Sanders, 2003, Phys. Rev. A **68**, 033821.
Wang, Z.-B., K.-P. Marzlin, and B. C. Sanders, 2006, Phys. Rev. Lett. **97**, 063901.
Wasilewski, W., T. Fernholz, K. Jensen, L. S. Madsen, H. Krauter, C. Muschik, and E. S. Polzik, 2009, Opt. Express **17**,

14444.
Windpassinger, P. J., D. Oblak, P. G. Petrov, M. Kubasik, M. Saffman, C. L. G. Alzar, J. Appel, J. H. Müller, N. Kjærgaard, and E. S. Polzik, 2008, Phys. Rev. Lett. **100**, 103601.
Wineland, D. J., J. J. Bollinger, W. M. Itano, and D. J. Heinzen, 1994, Phys. Rev. A **50**, 67.
Wineland, D. J., J. J. Bollinger, W. M. Itano, F. L. Moore, and D. J. Heinzen, 1992, Phys. Rev. A **46**, R6797.
Wolf, M. M., G. Giedke, O. Kruger, R. F. Werner, and J. I. Cirac, 2004, Phys. Rev. A **69**, 052320.
Wolf, M. M., D. Perez-Garcia, and G. Giedke, 2007, Phys. Rev. Lett. **98**, 130501.
Wootters, W. K., 1998, Phys. Rev. Lett. **80**, 2245.
Yuan, Z.-S., Y.-A. Chen, S. Chen, B. Zhao, M. Koch, T. Strassel, Y. Zhao, G.-J. Zhu, J. Schmiedmayer, and J.-W. Pan, 2007, Phys. Rev. Lett. **98**, 180503.
Yuan, Z.-S., Y.-A. Chen, B. Zhao, S. Chen, J. Schmiedmayer, and J.-W. Pan, 2008, Nature (London) **454**, 1098.
Zare, R., 1988, *Angular Momentum* (Wiley, New York).
Zhao, B., Y.-A. Chen, X.-H. Bao, T. Strassel, C.-S. Chuu, X.-M. Jin, J. Schmiedmayer, Z.-S. Yuan, S. Chen, and J.-W. Pan, 2009, Nat. Phys. **5**, 95.
Zhao, B., Z.-B. Chen, Y.-A. Chen, J. Schmiedmayer, and J.-W. Pan, 2007, Phys. Rev. Lett. **98**, 240502.
Zhao, R., Y. O. Dudin, C. J. Campbell, D. N. Matsukevich, T. A. B. Kennedy, A. Kuzmich, and S. D. Jenkins, 2009, Nat. Phys. **5**, 100.
Zoller, P., *et al.*, 2005, Eur. Phys. J.: Appl. Phys. **36**, 203.